



Developing Poly(Polyol Sebacate)-Based Elastomeric Biomaterials for Soft Tissue Engineering

Yuan Li

Thesis submitted to the Monash University in conformity with the requirements of the degree of Doctor of Philosophy

Department of Materials Engineering

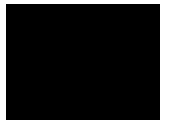
Monash University

Australia

March 2014

Declaration

I declare that this thesis contains no material which has been accepted for the award of any other degree or diploma at any university or any other institution. To the best of my knowledge, this thesis contains no materials published or written by another person previously, except where due reference is made in the thesis.



Yuan Li

01/03/2014

Notice 1

Under the Copyright Act 1968, this thesis must be used only under the normal conditions of scholarly fair dealing. In particular no results or conclusions should be extracted from it, nor should it be copied or closely paraphrased in whole or in part without the written consent of the author. Proper written acknowledgement should be made for any assistance obtained from this thesis.

Notice 2

I certify that I have made all reasonable efforts to secure copyright permissions for third-party content included in this thesis and have not knowingly added copyright content to my work without the owner's permission.

ACKNOWLEDGEMENTS

I am grateful to all the collaborators during my PhD research. Special thanks must go to Dr. Matteo Altissimo for his patient training of operating SEM at Melbourne Centre for Nanofabrication, Mr. Peter Nichols of the Monash School of Chemistry for his training and advice in operation and planning of the NMR experiments, and Ms. Karla Contreras for training me to do cell culture and absolutely excellent technical support in the tissue culture lab of the Division of Biological Engineering.

I would also like to acknowledge many members of the department, in particular Dr. Cornelis Moorhoff for his help and teaching in NMR techniques and advice in chemistry aspect, Mr. Silvio Mattievich for training me on Mini Instron and constantly world-class technical assistance, Prof. Yibing Cheng for his encouragement and invitation for attending a conference, Ms. Edna Tan for helping order chemicals and applying conference scholarships and Dr. Tara Schiller, Dr Jack Wang, Dr. Kun Wang, Mr. Ling Qiu, Dr. Jana Habsuda, for their patient training and technical assistance in the usage of various instruments. In addition, I would like to extend my thanks to my group mates for their tremendous help and wonderful friendships, especially Ms SL. Liang for her great help in my early PhD study and continuous contact and encouragement after her graduation. Mr. WC Huang, Ms. HN Shi for their great contribution and helps in my project, Mr. Bing Xu for training me to operate an electrospinner, his valuable experience and his helps in my study and life, Ms. XY Yang and Mr. CH Zhu for their patient discussions in study and kind helps.

I would like to thank A/Professor Qizhi Chen, Professor Wayne Cook and Dr. George A Thouas for their invaluable supervision, patient guidance, encouragement and critical support throughout my PhD study.

Lastly and most importantly, my deepest gratitude goes to my parents, Tao Li and Xiufang Xiong, for their unconditional love, great encouragement, truly understanding and endless support.

ABSTRACT

Biodegradable soft elastomeric biomaterials are desired in the application of soft tissue engineering and a new family of crosslinked elastomers, poly (polyol sebacate) (PPS), have shown promises in applications of nerve, vascular and myocardial tissue engineering. However, a number of problems remain with these novel polymers, including the poor reproducibility in the synthesis and properties of PPS, the toxicity of very soft versions of the PPS family, and too rapid degradation rates. Therefore, this PhD thesis project aims to address these issues and develop soft, degradable elastomers with improved reliability, biocompatibility and satisfactory degradation rates. The major results include:

- (1) The poor reproducibility of poly(glycerol sebacate) (PGS) was caused by the evaporation of small molecule, glycerol; and the satisfactory biocompatibility and reasonable slow degradation rate of PGS could only be achieved by a long curing time with a compromise of mechanical elasticity.
- (2) In order to achieve a satisfactory combination of mechanical flexibility and degradation rate, a larger monomer, xylitol, was used to replace glycerol to synthesize poly(xylitol sebacate) (PXS). A comparative study on PXS and PGS demonstrated that PXS polymers had better mechanical elasticity (twice elongation) than PGS of the same crosslink density, whilst their degradation rate and biocompatibility were similar to those of PGS counterparts.
- (3) The degradation mechanisms of PGS and PXS was further investigated *in vitro* and it demonstrated that all the materials underwent esterase enzymatic and free radical synergistically degradation.
- (4) In order to achieve nonlinear elasticity of soft tissue, an elastomeric PXS scaffold was fabricated by core/shell electrospinning technique using PXS as the core material and polyvinyl alcohol (PVA) as the shell polymer, with PVA shell being washed off after PXS curing. The newly fabricated PXS scaffold exhibited softer and remarkably higher rupture elongation than PXS sheet in aqueous conditions.

In conclusion, soft, degradable elastomeric biomaterial with improved reliability, biocompatibility and satisfactory degradation rates could be achieved from the elastomer PXS using the core/shell electrospinning technique. The produced PXS fibrous scaffold demonstrated a high potential in soft tissue engineering in terms of biocompatibility, mechanical properties and degradation kinetics. Further work shall focus on *in vivo* evaluation of the PXS fibrous scaffold.

CONTENTS

LIST OF TABLES	5
LIST OF FIGURES	7
CHAPTER ONE INTRODUCTION	12
CHAPTER TWO LITERATURE REVIEW: BIODEGRADABLE SOFT ELASTOMERS: SYNTHESIS/PROPERTIES OF MATERIALS AND FABRICATION OF SCAFFOLDS	14
2.1. Introduction biomaterials	14
2.2. Overview of elastomeric biomaterials.....	15
2.2.1. Naturally occurring elastomers.....	18
2.2.2. Synthetic elastomers	18
2.3. Thermoplastic elastomers.....	20
2.4. Poly (polyol sebacate) (PPS).....	22
2.4.1. Poly (glycerol sebacate) (PGS).....	23
2.4.1.1. Synthesis of PGS.....	23
2.4.1.2. Biocompatibility of PGS.....	25
2.4.1.3. Biodegradation of PGS	26
2.4.1.4. Mechanical properties of PGS	26
2.4.2. Poly(xylitol sebacate) (PXS) and other PPS elastomers	27
2.4.2.1. Synthesis of PPS	27
2.4.2.2. Mechanical properties, degradation and compatibility of PPS	27
2.4.3. Photopolymerised poly(glycerol sebacate-co-acrylate) (PGSA).....	29
2.4.4. Poly(glycerol sebacate)-co-poly(ethylene glycol)(PGS-co-PEG).....	31
2.4.4. PGS-based elastomeric composites	32
2.4.4.1. Bioglass PPS composite.....	33
2.4.4.2. multi-walled carbon nanotubes PGS composite	33
2.4.5. Applications of PPS-based elastomers	34
2.5. Citric acid	34
2.5.1. Synthesis	34
2.5.2. Mechanical properties, degradation and compatibility of PDC	34
2.5.3. Applications of POCs in tissue engineering	35

2.6. Other biodegradable soft elastomers	35
2.6.1. Polyester Amides	35
2.6.1.1. Synthesis	35
2.6.1.2. Mechanical properties, biocompatibility and degradability.....	35
2.6.2. Cross-linked Poly (1,3-trimethylene carbonate).....	36
2.7. Fabricate of soft elastomeric scaffolds.....	36
2.7.1. Solvent casting and particle leaching	36
2.7.2. Melt-based replica moulding and lamination technique.....	37
2.7.3. Electrospinning	38
2.7.4. Rapid-prototyping.....	39
2.7.5. Summary of PPS scaffolding techniques.....	43
2.8. Objectives of this project.....	43
CHAPTER THREE MATERIALS AND EXPERIMENTS.....	45
3.1. Materials.....	45
3.2. Synthesis of PGS and PXS.....	45
3.3. Fabricate PVA/PXS electrospun fibres	46
3.3.1. Preparation of core and shell solutions.....	46
3.3.2. Core/shell electrospinning	46
3.4. Characterisation.....	48
3.4.1. Determination of the degree of esterification in PGS and PXS	48
3.4.2. Gel point determination	49
3.4.3. NMR analysis	49
3.4.4. Water and THF swelling of PGS and PXS.....	50
3.5. Mechanical properties	50
3.6. Cytocompatibility <i>in vitro</i> (ISO 10993).....	51
3.7. Proliferation <i>in vitro</i> : MTS.....	52
3.8. Degradation test.....	53
3.8.1. PPS degradation test <i>in vitro</i> with esterase.....	53
3.8.2. Enzymatic and oxidation degradation of PGS and PXS materials.....	53
3.9. pH measurements of culture medium after incubation with PPS samples.....	54
3.10. SEM characterisation	55
3.11. Statistical analysis	55

CHAPTER FOUR SYNTHESIS, CHARACTERISATION AND PROPERTIES OF PGS PRE-POLYMER AND GEL	56
4.1. Introduction	56
4.2. Results and discussion.....	59
4.2.1. Esterification degree	59
4.2.2. Analysis of PGS structure by NMR	61
4.2.3. Mechanical properties of PGS	72
4.2.4. Biocompatibility of PGS	76
4.3. Conclusions	79
CHAPTER FIVE A COMPARATIVE STUDY ON PGS AND PXS: MECHANICAL PROPERTIES, BIODEGRADATION AND CYTOCOMPATIBILITY	81
5.1. Introduction	81
5.2. Results and Discussion.....	82
5.2.1. Degree of Esterification.....	82
5.2.2. Mechanical properties of PGS and PXS.....	85
5.2.2.1. Effects of curing time on mechanical properties	85
5.2.3. Diffusion rates of water and THF molecules in PGS and PXS	89
5.2.4. Enzymatic degradation of PGS and PXS	90
5.2.5. Biocompatibility of PGS and PXS	92
5.3. Conclusions	96
CHAPTER SIX ENZYMATIC AND OXIDATIVE DEGRADATION OF PPS.....	97
6.1. Introduction	97
6.2. Results and discussion.....	99
6.2.1. Mechanical properties and crosslink density	99
6.2.2. Mediation of degradation by enzymatic and oxidative action.....	100
6.2.2.1. Influence of polymer network structure.....	100
6.2.2.2 Effects of esterase, oxidase or hydroxyl radical	101
6.2.3. Secondary effects of oxidative chemicals	103
6.2.4. Changes in pH value in media before and during the degradation test	105
6.2.5. SEM examination	107
6.2.6. Cytotoxicity of degradation product.....	109
6.3. Conclusions	113

CHAPTER SEVEN ELASTOMERIC PXS/PVA FIBROUS SHEETS PRODUCED BY CORE/SHELL ELECTROSPINNING: FABRICATION, CHARACTERISATION AND PROPERTIES	114
7.1. Introduction	114
7.2. Results and discussion.....	116
7.2.1. Optimisation of PXS/PVA core/shell electrospinning conditions.....	116
7.2.2. Removal of PVA shell from the PXS/PVA spun mats.....	121
7.2.3. Mechanical properties of core/shell spun mesh materials	123
7.2.4. Cytocompatibility <i>in vitro</i>	133
7.3. Conclusions	133
CHAPTER EIGHT SUMMARY AND FUTURE WORK	135
8.1. Summary	135
8.1.1. Synthesis, characterisation and properties of PGS	135
8.1.2. A comparative study of PXS and PGS: mechanical properties, biodegradation and cytocompatibility.....	136
8.1.3. Enzymatic and oxidative degradation of PPS.....	137
8.1.4. Elastomeric PXS/PVA fibrous sheets produced by core/shell electrospinning: fabrication, characterisation and properties	137
8.2. Limitations	138
8.3. Future Work	139
8.3.1. Developing PPS-based copolymers.....	139
8.3.2. Surface modification of PPS.....	139
8.3.3. Improvement of the PVA/PXS electrospun scaffolds	140
8.3.4. <i>In vitro</i> and <i>in vivo</i> studies.....	140
8.4. Conclusions	141
REFERENCES.....	142
LIST OF PUBLICATIONS	152

LIST OF TABLES

CHAPTER TWO

Table 2.1 Biomedical elastomers[1, 5, 6, 9, 18]	16
Table 2.2 Important elastomers and their properties and tissue engineering applications	17
Table 2.3 Selected properties of some biomedical elastomers	20
Table 2.4 Advantages and disadvantages of thermoplastic and crosslinked elastomers [2, 56]	20
Table 2.5 The degradation rates of PGS <i>in vitro</i> and <i>in vivo</i>	25
Table 2.6 Synthesis and mechanical properties of PPS [1, 23, 130]	28
Table 2.7 Advantages and disadvantages of different PPS synthesis processes.....	31
Table 2.8 3D fabrication technologies of polymer scaffolds [18, 142-144, 148, 150, 151].....	42
Table 2.9 Advantages and disadvantages of PPS fabrication techniques [18]	43

CHAPTER THREE

Table 3.1 PVA polymers used in the work, optimal concentrations of solutions that produce satisfactory electrospun fibres	47
Table 3.2 Process of samples. All samples were heat treated at 130°C for 3 days in vacuum after fabrication.....	47

CHAPTER FOUR

Table 4.1 Thermal synthesis conditions of PGS in previous studies	57
Table 4.2 Conversion estimated by weight loss of the water by-product and by acid group titration. ..	60
Table 4.3 The percentage of glyceride esters units in PGS samples measured from the integrated areas of the methine carbon peaks of the ¹³ C NMR spectra of the polymers in acetone-d ₆ at 30°C, with the reference peak of acetone, C=O, at 205.87 ppm. The chemical shifts beneath the structures refer to the carbon atoms above them. These are compared with those calculated from the statistical distribution of species assuming the fractional conversion of hydroxyl groups (q) is the same for primary and secondary alcohols.	71

CHAPTER FIVE

Table 5.1 Degrees of esterification estimated by mass loss of the water by-product and the titration of acid groups. PPS materials were pre-polymerised at 130 °C for 1 day and cured at 130 °C for up to 12 days.....	84
--	----

CHAPTER SIX

Table 6.1 The mechanical properties of PGS and PXS and strand density ν calculated from Eq. 3.4...99

CHAPTER SEVEN

Table 7.1 PVA polymers used in this work, optimal concentrations of solutions that produced satisfactory electrospun fibres, and subsequent diameters of PVA and PXS/PVA fibres* .118

Table 7.2 Mechanical properties PXS sheet, PVA fibres, PXS/PVA core-shell fibres and washed PXS/PVA core-shell fibres.....125

LIST OF FIGURES

CHAPTER TWO

- Fig. 2.1 Elastomeric heart patches attached to the pericardium of rat hearts. Premature failure of a thermoplastic rubber patch (a), and maintenance of the physical integrity of a chemically cross-linked elastomer patch (b) [96].22
- Fig. 2.2 Reaction scheme for poly(glycerol sebacate), R=H or polymer chain.....23
- Fig. 2.3 Cross-linking scheme between two PGS polymer chains.23
- Fig. 2.4 General synthetic scheme of polyol-based polymers. Xylitol (1), sorbitol (2), mannitol (3) and maltitol (4) were polymerised with sebacic acid (5) in different stoichiometries, yielding PXS (6), PSS (7), PMS(8) and PMtS (9) [23].27
- Fig. 2.5 (a) Modification of poly(glycerol sebacate) pre-polymer with acrylate moieties for photo-initiated curing; (b) PGSA after polymerisation under UV light.30
- Fig. 2.6 The synthesis PGS-co-PEG polymer firstly involves polycondensation of PEG and sebacic acid to obtain a linear polymer chain then the glycerol was added to obtain a block copolymer of PGS-co-PEG [59].32
- Fig. 2.7 Overview of fabrication strategy for PGS microfluidic devices: A) Replica moulding of PGS layers. PGS pre-polymer is cured into micro-patterned sheets and delaminated in water. B) Multiple layers are bonded by physically adhering individual sheets and curing the films together [8]......38
- Fig.2.8 Fabrication of 3D designed PGS scaffolds involves creating wax moulds that are cast into hydroxyapatite to create an inverse mould and then cast into a PGS pre-polymer and cured, resulting in a PGS scaffold [149]......40
- Fig. 2.9 Accordion-like honeycomb scaffolds for myocardium.(a, b). Computer-designed image of the scaffolds. Scale bars: 1mm (a) and 200 μm (b). (c) Scanning electron micrographs demonstrating the fidelity of excimer laser micro-ablation in rendering an accordion-like honeycomb design in PGS. Scale bar: 200 μm [113]41

CHAPTER FOUR

- Fig. 4.1 The apparent percentage of esterification, calculated from mass loss and acid-group titration, in PGS samples prepared by different pre-polymerisation conditions: PGS treated for different pre-conditioning at 130 °C/24 hours or 150 °C/8 hours followed by post curing at 130 °C for different times. Samples postcured less than 20 hours were fully soluble in THF. After postcuring for 20h or more the PGS sample were not soluble in THF and formed crosslinked gel.61
- Fig. 4.2 a) Full ^1H -NMR spectrum, in acetone- d_6 , of the pre-polymer synthesized at 150°C for 8h. The resonance assignments of the polyester are given in the structure. The peak at 2.1 ppm is due to ^1H acetone impurities. b) Close up of the methine hydrogens of glycerol due to the 1-, 1,2- and 1,2,3-glycerides.....62

Fig. 4.3	¹³ C-NMR spectra. a) Full spectrum of the PGS pre-polymer polymerized at 150°C for 8h. b) Full spectrum of cross-linked polymer gel of poly(glycerol sebacate) prepared at 150°C for 8h, then 130°C for 48 hours. The peak at 205.9 ppm is due to deuterated acetone solvent.	64
Fig. 4.4	¹³ C NMR spectra in the of glyceride region. a) PGS pre-polymer polymerized at 150°C for 8h. b) Gel prepared at 150°C for 8h, then 130°C for 48 hours.	65
Fig. 4.5	DEPT ¹³ C NMR spectra differentiating the methine (downward point peaks) and methylene carbons (upward pointing peaks). a) Spectrum of PGS pre-polymer polymerized at 150°C for 8h. b) Spectrum of the polymer gel cross-linked 150°C for 8h, then 130°C for 48 hours.	66
Fig. 4.6	Proton-carbon correlation spectrum of (a) PGS pre-polymerized at 150 °C for 8 hours and (b) PGS gel at 150 °C for 8 hours and cured 48 hours at 130°C	67
Fig. 4.7	(a) Typical tensile stress-strain curves PGS treated at 150 °C/8 hours but crosslinked at 130 °C for different times; (b) Mechanical properties of PGS treated at 150 °C/8 hours or 130 °C/24h, but crosslinked at 130 °C for different times: Ultimate tensile strength (UTS), Young’s modulus (E) and strain at break (ε) of materials versus crosslinking time. The error bars represent one standard error.....	74
Fig 4.8	(a) Ultimate tensile strength (UTS), and (b) maximum strain (ε _{max}) at break of PGS samples versus the strand density calculated from Equation 3.4. The data was fitted to theoretical curves of Eq. 4.3 and Eq. 4.4 (the latter by use of the non-linear Solver method in Microsoft Excel 2007).....	75
Fig. 4.9	Images of SNL cells cultured in extracts prepared with different samples after 24h (a-d): (a) free culture medium; (b) PDLLA; (c) PGS treated at 150 °C for 8 h, but crosslinked at 130 °C for 48 h; (d) PGS treated at 150 °C for 8 h, but crosslinked at 130 °C for 96 h.	76
Fig. 4.10	Effect on lactic dehydrogenase (LDH) evolution of extract-free medium (the negative control), PDLLA, PGS cured for 48 h or 96 h, indicating the viability of SNL mouse fibroblasts. After 48h culture, the percentage of dead cells was significantly higher in the cultures containing the extracts of PGS cured for 48 h than in the other three cultures (p < 0.001), while PGS cured for 96 h did not show significant differences from the negative control and PDLLA (p >0.05).	78
Fig. 4.11	SNL cell proliferation kinetics measured by the AlamarBlue™ technique. The initial plating density was 5000 cells per well in a 48-well plate (n=5). The difference between negative control PDLLA and PGS cured at 130°C/96h material were not significant (p>0.05). The cells proliferated significantly more slowly on PGS cured at 130°C/48h, compared with those on negative control, PDLLA and PGS cured at 130°C/96h (p<0.01).	78

CHAPTER FIVE

Fig.5.1	Typical stress-strain curves of the PGS and PXS polymer sheets. Both PPS were pre-polymerised at 130 °C for 1 day, but PGS and PXS were treated for crosslink at 130 °C for up to 7 and 12 days, respectively. The specimen of PXS cured at 130 °C for 1 day did not break due to the tension limit of the tensile tester used.	85
---------	--	----

Fig.5.2 (a) Ultimate tensile strength (UTS), Young's modulus (E), and (b) strain at break (ϵ) of the PGS and PXS versus curing time	86
Fig. 5.3 Plots of (a) UTS and (b) elongation at break versus strand density (calculated from E) and linear fit analysis using the Origin software. The PGS and PXS materials were pre-polymerised at 130 °C for 1 day, and treated for crosslinking at 130 °C for up to 7 and 12 days, respectively.	87
Fig. 5.4 Swelling ratios of PGS and PXS v _z swelling time in (a) THF and (b) water vapours. The PGS and PXS materials were pre-polymerised at 130 °C for 1 day, and treated for crosslinking at 130 °C for up to 1.5 and 2 days, respectively. The strand densities in the two polymers were ~ 25 mole/ m ³	90
Fig. 5.5 The weight loss of the PGS and PXS polymers after incubation at 37 °C in the tissue culture medium with the addition of esterase (0.3 units of enzyme per mg of biomaterial) for up to 35 days. The PGS and PXS materials were pre-polymerised at 130 °C for 1 day and treated for crosslinking at 130 °C for 7 and 9 days, respectively.....	91
Fig 5.6 Schematic illustrations of (a) the PGS and (b) the PXS networks. G = Glycerol, S = Sebasic acid, X = Xylitol	92
Fig 5.7 Images of SNL cells cultured in extracts prepared with different samples after 24 h, without any pre-conditioning treatments. (a) Negative control (free culture medium); (b) positive control with PDLLA; PGS were polymerised at 130 °C for one day and cured at 130 °C for (c) 2 or (d) 4 days; PXS polymerised at 130 °C for one day and cured at 130 °C for (e) 2 or (f) 7 days.	94
Fig. 5.8 (a) Cytotoxicity of the PGS and PXS, determined by measuring the release of lactate dehydrogenase (LDH) after 2 days culture. The positive control group was PDLLA. The percentages of dead cells were significantly higher in the cultures containing the extracts of PGS and PXS cured for 2 days than those of other five cultures ($p < 0.001$), whereas the PGS and PXS specimens cured for longer time (4 or 7 days respectively) did not show significant differences from the either negative or positive control (PDLLA) group ($p > 0.05$), (b) plote the cytotoxicity with the esterification percentage of PGS and PXS cured for 2 days or longer time (4 or 7 days respectively).....	95
Fig. 5.9 SNL cell proliferation kinetics measured by the AlamarBlue™ technique. The initial plating density was 2500 cells per well in a 48-well plate ($n = 5$). Overall, there were no significant differences between any two of the four groups that were analysed ($p > 0.05$).	96

CHAPTER SIX

Fig. 6.1 Percentage weight changes of PGS and PXS during incubation at 37 °C in (a) blank medium, medium added with (b) esterase, (c) FeSO ₄ /H ₂ O ₂ , or (d) xanthine oxidase/xanthine (XOX), individually. The PGS material was treated for crosslinking at 130 °C for 2 or 7 days. The PXS material was treated for crosslinking at 130 °C for 2 or 12 days.* significant difference ($p < 0.01$).	101
--	-----

Fig. 6.2 Percentage thickness reductions of the present PGS and PXS materials after 35 days incubation in blank medium, or medium added with esterase, FeSO ₄ /H ₂ O ₂ , or XOX, separately. The PGS material was treated for crosslinking at 130 °C for 2 or 7 days. The PXS material was treated for crosslinking at 130 °C for 2 or 12 days.	102
Fig. 6.3 The weight loss of the present PGS and PXS materials incubated in tissue culture medium added with (a) FeSO ₄ /H ₂ O ₂ and esterase; (b) XOX and esterase. The PGS material was treated for crosslinking at 130 °C for 2 or 7 days. The PXS material was treated for crosslinking at 130 °C for 2 or 12 days.	104
Fig. 6.4 The reduction in thickness after 35 days incubation in media added with esterase; esterase plus FeSO ₄ /H ₂ O ₂ ; and esterase plus XOX. The PGS material was treated for crosslinking at 130 °C for 2 or 7 days. The PXS material was treated for crosslinking at 130 °C for 2 or 12 days...	104
Fig. 6.5 Decrease in pH value in DEMEN tissue culture medium after soaking with PGS and PXS specimens for (a) one and (b) two days. The media were blank, or added with esterase, FeSO ₄ /H ₂ O ₂ , XOX, esterase plus FeSO ₄ /H ₂ O ₂ , or esterase plus XOX.	106
Fig. 6.6 SEM surface morphologies of PGS and PXS samples after incubation for 35 days in (a) blank tissue culture medium, or media added with (b) esterase, (c) FeSO ₄ /H ₂ O ₂ , (d) esterase plus FeSO ₄ /H ₂ O ₂ , (e) XOX, and (d) esterase plus XOX. The PGS was cured at 130°C for 7 days, and PXS was cured at 130°C for 12 days.	108
Fig. 6.7 Live imaging of SNL cells cultured in the DMEM media which were soaked with PPS samples for one day. (a) DMEM alone, DMEM added with, (b) esterase, (c) XOX, (d) esterase plus XOX, (e) FeSO ₄ /H ₂ O ₂ , or (f) esterase plus FeSO ₄ /H ₂ O ₂ . The PGS was cured at 130°C for 2 days. Other PPS showed similar phenotypes of SNL cells in the above media.	110
Fig. 6.8 Representative morphologies of SNL cells cultured in the DMEM media which were soaked with PPS samples for two days. (a) blank DMEM, DMEM added with (b) esterase, (c) XOX, or (d) esterase plus XOX. PXS was cured at 130°C for 2 days.	111
Fig. 6.9 Lactic dehydrogenase (LDH) based evaluation on the effect of extractant media soaked with PPS samples for (a) one or (b) two days, on the viability of SNL mouse fibroblasts, extract-free (blank) medium being the negative control. The PGS material was treated for crosslinking at 130 °C for 2 or 7 days. The PXS material was treated for crosslinking at 130 °C for 2 or 12 days. (a) the four materials within each group did not exhibit a significant difference (p > 0.05); the differences between the groups of blank medium, medium added with esterase, XOX or esterase plus XOX were not significant (p > 0.05). The cell death percentages in the media added with FeSO ₄ /H ₂ O ₂ with or without esterase were significantly higher than other groups (p < 0.001). (b) The degradation of PGS-7days and PXS-12days materials in blank medium, medium added with esterase, XOX, or esterase plus XOX, showed a significantly lower toxicity than other PPS polymers and than in other media (p < 0.001).	112

CHAPTER SEVEN

Fig. 7.1 SEM images of PVA fibre mats after heating at 130°C for 24h. (a) PVA 31,000-50,000 g/mole, (b) 89,000-98,000 g/mole and (c) 146,000-186,000 g/mole; (a'-c') are higher magnification SEM images of (a-c). Circled areas show the fusion of PVA shells between fibres.....	119
Fig. 7.2 SEM images of PXS/PVA core/shell fibre mats after curing at 130°C for 3 days. (a) PVA 31,000-50,000 g/mole, (b) 89,000-98,000 g/mole and (c) 146,000-186,000 g/mole, $[\eta]C$ value are about 9, 10, 9 respectively. (a'-c') are higher magnification SEM images of (a-c) which shows fusing occurred between fibres at contacting points which impede the sliding between fibres.	120
Fig. 7.3 SEM images of PXS/PVA core/shell fibre mats after curing then washed in distilled water (a) spun mat with PVA 31,000-50,000 g/mol washed at 80°C for 24h. (b) spun mat with PVA 89,000-98,000 g/mol washed at 90°C for 4h. (a') and (b') are higher magnification SEM images of (a) and (b).....	122
Fig. 7.4 Typical tensile stress-strain curves of PXS sheets, PVA fibre mats, PXS/PVA fibre mats and PXS/PVA-washed fibre mats.	123
Fig. 7.5 Mechanical properties of PXS sheets, PVA fibre mat, PXS/PVA fibre mats and PXS/PVA-washed fibre mats. (a) Young's modulus (E), (b) Ultimate tensile strength (UTS) and (c) elongation at break. The error bars represent one standard error. * $p < 0.01$, # $p < 0.05$. NS stands for 'not significant'	124
Fig. 7.6 (a) The typical tensile stress-strain curves for the materials which show the effect of water on the mechanical properties of PVA fibre mats, PXS/PVA fibre mats and PXS/PVA-washed fibre mats. The fibres were tested under dry and hydrated conditions after immersion of mats in water (b) J-shaped tensile stress-strain curves of PXS/PVA-ww fibrous mats at the wet conditions.....	127
Fig. 7.7 The effect of water on the mechanical properties of fibre mats made from PVA, PXS/PVA and PXS/PVA-washed. The fibres were tested at dry condition and wet fibres after immersed in water, with values of (a) Young's modulus (E), (b) UTS and (c) elongation at break. The error bars represent one standard error. For those three materials the differences of all mechanical properties at dry and wet conditions are significant ($p < 0.01$).	128
Fig. 7.8 A 50-cycle tensile stress-strain curve of (a) PXS sheet, (b) PXS/PVA-washed fibre mat and (c) PXS/PVA-ww fibre mat.	130
Fig. 7.9 Images of SNL cells cultured in media with evaluated materials direct placed in for 24 h. (a) Negative control (free culture medium); (b) positive control with PLLA fibre; (c) PXS sheet; (d) PXS/PVA core/shell fibrous mesh (e) electrospun fibre mat of PXS/PVA, with PVA being washed off.....	132
Fig. 7.10 Cytotoxicity of the PXS sheet, electrospun fibre mat PXS/PVA and PXS/PVA-washed, determined by measure the release of LDH after two days of culture. The positive control group was PLLA electrospun fibre. The percentages of dead cells in test material's group were not significantly different from either the negative control (medium alone) or positive control (PLLA) groups.	133

CHAPTER ONE

INTRODUCTION

Tissue engineering uses biomaterial scaffolds to promote tissue regeneration of injured organ. Ideally, biomaterials should have minimised toxicity, desirable biocompatibility and satisfactory mechanical and physical performance. Despite many early successes, there are few synthetic biomaterials available for the repair of soft, mechanically functional tissues such as muscle and connective tissue. To engineer a soft tissue that works in a dynamic environment in the body, the biomaterial is required to sustain and recover from various deformations without mechanical irritations to the surrounding tissues. Unfortunately, currently dominant synthetic biomaterials, e.g. polyglycolide, polylactide and their copolymers, undergo plastic deformation and failure when exposed to long-term deformation, and thus their performance is often disappointing in tissue engineering of dynamic types.

In the last two decades, synthetic biodegradable elastomers have gained increasing attentions as transplantable biomaterials to provide the mechanical properties resembling soft tissues. Poly (polyol sebacate) (PPS) is a relatively new family of biodegradable crosslinked polyester elastomers [1, 2]. These biomaterials possess elastic strength similar to the level of soft tissues. Poly (glycerol sebacate) (PGS) is the most well studied member. However, PGS has some drawbacks. First, very soft PGS materials tend to be cytotoxic, Second, the fast degradation rates of soft PGS hamper their application in engineering of most soft types, such as muscle and tendon, which recover slowly. In addition, the reproducibility of PGS is rather poor due to the evaporation of volatile monomer, glycerol, during synthesis. We hypothesize that to change the synthesis conditions and use polyols of more hydroxyl groups, such as xylitol, could achieve a satisfactory combination of mechanical properties and biocompatibility, as well as an improved reproducibility. The primary objective of this project is, therefore, to systematically explore the synthesis conditions and properties of two PPS members, PGS and poly(xylitol sebacate) (PXS). To this end, the microstructure, mechanical properties, cytocompatibility and enzymatic degradation of PGS and PXS have been thoroughly investigated. The final goal of this project is to achieve a very soft elastomeric scaffold which is cyto- and mechano-compatible to the host organ and thus can deliver cells in the cellular therapy and provide a proper mechanical support to injured tissues that are exposed to cyclic deformation, such as cardiac, tendon, smooth muscle and lung epithelium.

This thesis is organised as follows. Chapter 2 provides a literature survey, aiming at identify the most promising elastomeric biomaterials used to for soft tissue engineering and rationalising techniques and fabrication strategies adopted in this project. Following the description of the experimental procedures (Chapter 3), Chapter 4-7 present the research work carried out. These chapters are focussed on the synthesis, characterisation and properties of PGS (Chapter 4), the comparison of PGS and PXS (Chapter 5), enzymatic and oxidative degradation of PPS (Chapter 6) and PXS/PVA core/shell electrospinning scaffold fabrication (Chapter 7), respectively. To maintain the relative independency of these four chapters such that they are readable without referring to other chapters, Chapter 4-7 begin with an introduction to the research background of their specific topics, then go on to describe and discuss results in detail and end with conclusions. At the end of this thesis a summary is presented and future work is recommended (Chapter 8).

CHAPTER TWO

LITERATURE REVIEW:

BIODEGRADABLE SOFT ELASTOMERS: SYNTHESIS/PROPERTIES OF MATERIALS AND FABRICATION OF SCAFFOLDS

Recently there has been increasing research efforts in the development of elastomeric biomaterials with desirable biocompatibility, degradation profile and mechanical properties for use in soft tissue engineering. This review provides an update on the progresses of developing biodegradable, soft elastomeric biomaterials and their tissue engineering scaffolding techniques. Following a brief review on traditional thermoplastic elastomers, including polyurethane (PU), polyhydroxyalkanoates (PHA) and aliphatic copolymers, detailed review is devoted to the synthesis, properties and scaffold fabrication of recently developed soft biodegradable elastomers, including PPS, PPS-based elastomers and citric-acid based elastomers. Although biodegradable soft elastomeric biomaterials have advantages (compliant and biodegradable), this review also identified a number of issues associated with the PPS family, including cytotoxicity, rapid *in vivo* degradation rates, and poor reproducibility. Future research directions are highlighted.

2.1. Introduction biomaterials

A common strategy in tissue engineering is to use a three-dimensional (3D) scaffold for proper cell growth and differentiation [3]. Existing evidence suggests that the mechanical conditioning regimens of elastomeric scaffolds promote improved tissue formation and allow gradual stress transfer from the degrading synthetic matrix to the newly formed tissue [4, 5]. However, the biodegradable thermoplastics currently dominantly being used in tissue engineering, e.g. polyglycolide (PGA), polylactide (PLA) and their copolymers, do not provide satisfactory performance in soft tissue engineering due to their high stiffness, plastic deformation and mechanical failure when exposed to long-term cyclic strain. In the last decade, synthetic biodegradable elastomers have increasingly become a popular option for soft tissue engineering, and researchers have explored a wide range of scaffolds having mechanical properties resembling those of natural tissues [1, 2, 6-10]. This review aims to provide an update on the biodegradable elastomers currently used in soft tissue engineering, with a focus on a new family of elastomers, PPS, which are the most promising biomaterials for use in soft tissue engineering.

2.2. Overview of elastomeric biomaterials

An elastomer is a polymer with a glass transition temperature (T_g) below room temperature and that has the ability to undergo elastic deformations; that is, to stretch and return to its original shape in a reversible way [11]. In order to work with mechanically dynamic tissues such as muscle, an elastomer must have the following characteristics: good biocompatibility with the host tissue and a glass transition temperature (T_g) lower than body temperature (i.e., 37°C) so as to recover from various deformations at the body temperature.

Biomedical elastomers can be classified into two categories according to the polymer sources: naturally occurring biological elastomers and chemically synthesised elastomers. Synthetic elastomers can further be divided into thermoplastic elastomers and crosslinked elastomers based on the type of “crosslink” used to join their chains. Table 2.1 provides important biomedical elastomers reported up to now, and more detailed reviews on their biomedical applications are available in the literature [2, 9, 10, 12-15].

The use of elastomers for medical devices is neither new nor recent, which can actually be traced back to as early as the mid 1890s, when the rubber industry began to expand [16]. Vulcanised natural rubber was used in medical devices (such as surgical gloves) soon after the discovery of the vulcanisation process [16]. Elastomeric materials have since been used in many medical products for their biocompatibility, durability, design adaptability, mechanical compliance and economy of cost. Both natural and synthetic rubbers (e.g., silicones, polyurethanes, polyolefins and polydienes) have been used in a range of implantables including cardiovascular devices, prosthetic devices, catheters, transdermal therapeutic systems, orthodontics and ophthalmological materials [17], as listed in Table 2.2.

Table 2.1 Biomedical elastomers[1, 5, 6, 9, 18]

Elastomers	Abbreviations	Ref
1. Synthetic elastomer		
<u>Thermoplastic elastomer</u>		
Poly(hydroxyalkanoate)	PHA	[19]
Poly(4-hydroxybutyrate)	P4HB	[20]
Poly(3-hydroxybutyrate-co-3-hydroxyvalerate)	PHBV	[19]
Polyurethane	PU	[10]
Poly(phosphazene)	PPHOS	[21]
Poly(ether/ester)	PEE	[21]
Poly(ethyleneglycol)/Poly(butylene terephthalate)	PEG/PBT	[21]
Poly(ϵ -caprolactone)copolymer		[21]
Poly(glycolide-co-caprolactone)	PGCL	[21]
Poly(caprolactone-co-lactide)	PCLA	[21]
Poly(<i>p</i> -dioxanone-co- ϵ -caprolactone)	PDSCL	[22]
Poly(1,3-trimethylene carbonate)	PTMC	[21]
<u>Crosslinked elastomer</u>		
Poly(polyolsebacate)	PPS	[23]
Poly(glycerol sebacate)	PGS	[1]
Poly(xylitol sebacate)	PXS	[24]
Poly(glycerol sebacate acrylate)	PGSA	[25]
Poly(diols citrate)	PDC	[6]
Poly(1,8-octanediol-co-citric acid)	POC	[6]
Poly(1,8-octanediol-co-citric acid)-cysteine	POC-Cys	[26]
Poly(1,10-decanediol-co-citric acid)	PDC	[6]
poly((1,2-propanediol-sebacate)-citrate)	PPSC	[27]
Poly(octamethylene maleate (anhydride) citrate)	POMaC	[28]
Poly (ethylene glycol) maleate citrate	PEGMC	[29]
Star-poly(esters) copolymer	SCP	
Poly(ϵ -caprolactone-D,L-lactide-glycerol-co-2,2-bis(ϵ -CL-4-yl)-propane)	SCP-co-BCP	[30]
Poly(ϵ -caprolactone-D,L-lactide-glycerol-acrylate)	ASCP	[31]
Poly (ester amide)		
Poly(1,3-diamino-2-hydroxypropane-co-polyolsebacate)	APS	[32]
2. Natural degradable polymers		
Polysaccharides		
Alginate		[33], [34], 35]
Elastic Proteins		
Collagen		[35]
Gelatin		[36]
Fibrin		[35]
Elastin		[37]
Elastin-like polypeptides	ELPs	[38]
Silk-elastinlike protein polymers	SELPs	[39]

Table 2.2 Important elastomers and their properties and tissue engineering applications

Elastomers	Advantages or disadvantages	Medical devices (current and potential)	Reviews
Polyurethanes (PU) (Physically crosslinked)	Enormous diversity of chemical compositions and physical-mechanical properties. Tissue-specific biocompatibility. Widely tuneable biodegradability. Mechanical flexibility. Moderate blood compatibility. Tuneable rate of moisture transmission.	Wound dressings and scaffolds for tissue engineering could permit new developments.	[13, 17]
Polyhydroxyalkanoate (PHA) (Physically crosslinked)	Excellent biocompatibility. A wide range of mechanical properties and biodegradability Expensive.	Scaffolds or template for tissue engineering	[40]
Polyesters and copolyesters (Physically crosslinked)	Natural softness, good contact to surfaces Pleasant feeling, comparable to that of dry human skin No contamination to wounds, no plasticizers used Excellent resistance to a wide range of solvents and chemicals High tear strength Low-friction surfaces - no problems of adhering to wound areas, clothing, or bedding Extremely good breathability. Good processability. Good sterilisability. Low toxicity.	Wound care dressings	[17]
Polyolefin and polydiene (Chemically crosslinked)	Excellent biostability Functionality Biocompatibility	Hexsyn™: Ethylene-Propylene rubber: Finger joint prostheses	[17, 41]
Poly(polyol sebacate) (PPS) (Chemically crosslinked)	Soft elasticity. Moderate biocompatibility. Tuneable degradability. Mild cytotoxicity.	Scaffolds or template for tissue engineering	[18, 23, 42]
Biological polymers (elastic proteins) (hydrogen bonding or chemically crosslinked, such as elastins)	Excellent biocompatibility. Concerns of disease transfer.	Templates or scaffolds for tissue engineering and regeneration	[43]

2.2.1. Naturally occurring elastomers

The natural extracellular matrices (ECMs) of soft tissues are composed of various collagens; thus, collagens have been widely used in soft tissue engineering [44, 45]. They provide a natural substrate for cellular attachment, proliferation and differentiation. Collagen, gelatine, fibrin and alginate have been extensively investigated in tissue engineering of almost all types, including bone [46], cartilage [47], skin [48], ligaments [49], vessels [50], heart muscles [51], the liver [52] and nerves [53]. Selected properties of them are listed in Table 2.3. Although natural polymers have advantages such as biodegradability and cytocompatibility as well as unique chemical, physical and mechanical properties (e.g. non-linear elasticity), they are subject to tedious purification techniques, processing variability and regulatory issues [2, 54]. In addition, they have unreliable mechanical properties and variable physical properties with different sources of protein matrices [18]. These shortcomings of natural materials form the motivation for developing synthetic biodegradable polymers for use in tissue engineering.

2.2.2. Synthetic elastomers

From a biological and clinical standpoint, synthetic elastomers should exhibit both biocompatibility and mechano-compatibility with natural ECM proteins. From a polymer perspective, these materials should be able to be synthesized in large batches and exhibit tuneable properties that could be realized by altering synthetic schemes and polymer processing conditions. To satisfy these criteria, the design of these materials should follow certain principles, including: (1) incorporation of ester bonds in polymer chains to promote degradation by hydrolysis and enzymatic activity; (2) tuneable elastomeric mechanical properties; and (3) use of non-toxic monomers that can be metabolized or excreted by the host[2]. There are two types of synthetic elastomers: thermoplastic elastomers (physical cross-linked) and crosslinked elastomers (chemically cross-linked) [55]. In thermoplastic elastomers, hard and rigid block segments alternate with block segments of a soft and flexible segments [55]. At ambient temperatures, the soft, amorphous segments impart the rubbery, elastic behaviour to the material. At temperatures below T_g or melting temperature (T_m) of the hard segments, the hard chain segments from numerous adjacent chains aggregate together to form rigid amorphous or crystalline domains. These domains are ‘physical cross-links’ that act as anchor points that restrict soft chain segment motions; they function in much the same way as ‘chemical cross-links’ in crosslinked elastomers [55].

The major advantage of thermoplastic elastomers over crosslinked elastomers is that upon heating above T_g or T_m of the hard phase, they soften and flow (i.e., the physical cross-links disappear) and can thus be processed easily. Unlike thermoplastic elastomers, cross-linked elastomers gain their elasticity from a chemical cross-linking process that occurs when the compound is subjected to heat or radiation, a process often called ‘curing’. Once cured, these compounds obtain the necessary physical properties. Reheating chemically cross-linked polymers will not cause them to flow as thermoplastics do consequently, conventional reforming is normally difficult or impossible with chemically crosslinked elastomers [55].

Thermoplastic elastomers have good processability while crosslinked elastomers will not flow once cured [55]. However, they often contain crystalline regions that cause heterogeneous degradation and a non-linear loss of mechanical strength with time. Moreover, the 3D geometry of a thermoplastic scaffold is commonly lost during the hydrolysis period. In this regard, crosslinked elastomers offer advantages for biomedical applications over thermoplastic materials [2, 56], as listed in Table 2.4.

In contrast, crosslinked elastomeric polyesters undergo a combination of bulk and surface erosion degradation, which results in the maintenance of the 3D structure throughout the hydrolytic process [56]. In addition, crosslinked elastomeric polyesters, which can breakdown to natural metabolic products by simple hydrolysis, have potential to be tailed in their degradation rates to match the healing kinetics of injured tissue. The rest of this article is thus devoted to synthetic crosslinked elastomers.

Table 2.3 Selected properties of some biomedical elastomers

Polymers	Young's modulus (MPa)	Tensile strength (MPa)	Elongations (%)	Refs
Synthetic elastomers				
PU _s (PEUU ^a)	7-70	4-60	100-950	[57]
PHAs (P3HB ^b -co-P4HB ^c)	50-300	20-50	400-1000	[2]
PCL-co-LA	30	32	120	[58]
PGS	0.05-1.5	0.2-0.7	120- 270	[1, 2, 7, 18]
Other PPS	0.4 -380		10- 200	[23]
PGSA	0.05-1.4	0.05-0.5	40-190	[25]
PGS-co-PEG	0.013-2.2	0.026-0.388	55-108	[59]
Naturally occurring				
Elastin (bovine ligament)	1.1	2	150	[60, 61]
Resilin (dragonfly tendon)	2	4	190	[60]
Knee articular cartilage	2.1-11.8			[56]
Smooth muscle (relaxed)	0.006		300	
Smooth muscle (contracted)	0.01		300	
Human bladder	0.25	0.27	0.7	
Heart muscle (At the end of diastole)				[18]
Myocardium of rat	0.14	0.03-0.07		
Myocardium of human	0.2-0.5	0.003-0.015		

^aPEUU= polyester urethane urea. ^bP3HB= Poly(3-hydroxybutyrate). ^cP4HB= Poly(4-hydroxybutyrate).

Table 2.4 Advantages and disadvantages of thermoplastic and crosslinked elastomers [2, 56]

Materials	Advantages	Disadvantages
Thermoplastic elastomers (e.g. PU, PHA)	<ul style="list-style-type: none"> • Good processability • Tuneable mechanical properties and • Tuneable degradation rate through modification of the soft and hard segments. 	<ul style="list-style-type: none"> • Heterogeneous degradation • non-predictable loss of mechanical strength • 3D geometry lost during the hydrolysis period
Crosslinked elastomers (e.g. PPS)	<ul style="list-style-type: none"> • Retention of the 3D structure • Predictable degradation rates and a linear loss of mechanical strength with time 	<ul style="list-style-type: none"> • Poor processability • Curing conditions limit the application of crosslinked elastomers as drug-delivery vehicles

2.3. Thermoplastic elastomers

PU (e.g. PEUU) and PHA (e.g. P3HB-co-P4HB and P4HB) represent two dominant thermoplastic rubbers. Their typical mechanical properties are provided in table 2.3. An immediate and frequently utilised strategy for achieving biodegradation of PU elastomers is to incorporate a polyester macrodiol soft segment that hydrolyses *in vitro* and *in vivo*, such as poly(lactic acid) (PLA) or poly(glycolic acid) (PGA)[62]. In general, PUs and PHAs degrade more slowly than PGA/PLA/PLGA, with degradation rates being typically 2-3 years. From the degradation point of view, PUs and

PHAs could be useful in tissue engineering for implants that require a longer retention time or a higher stability in the surrounding environment, but which are eventually absorbed. This might be useful in tissue engineering for implants that require a longer retention time or a higher stability in the surrounding environment, but which are eventually absorbed. This might be useful for tissues with slower healing and remodelling times, or with an inability to maintain innate structure integrity (e.g. large wound). In addition to cardiovascular tissue engineering [63, 64], PUs and PHAs have proven highly versatile, having been investigated for the repair of soft tissue (e.g., nerve [59, 65-71], blood vessel [70], intestine [72],) as well as harder load-bearing tissue (e.g., bone [73-78], cartilage [79], meniscus [80-85] and ligament [86, 87]).

Polycaprolactone (PCL) has been copolymerized with PGA and PLA to produce thermoplastic rubber-like biomaterials [58, 70, 88, 89]. Most of these copolymers are synthesized by ring-opening polymerization in presence of an initiator such as stannous (II) octoate [$\text{Sn}(\text{Oct})_2$]. Their mechanical properties are listed in table 3. PLA, PGA, PCL and their copolymers remain popular for a variety of reasons, but primarily their biocompatibility and biodegradability [35]. The degradation rates of the PCL-based ratio of co-monomers. In general, the copolymers degrade faster than the homopolymer alone. PGA-co-CL (PGACL) scaffolds lost 50% after 6 week incubation, whereas it took 6-12 months for PGA to degrade [90].

PGACL and PLACL copolymers have both been investigated for potential applications in tissue engineering [12]. In an *in vivo* work, cell-seeded scaffolds were implanted subcutaneously in nude mice. After three weeks, the PGACL scaffolds were found to provide adequate physical characteristics to induce new tissue formation [90]. PLACL scaffolds have shown encouraging results as vascular graft both in canine [91, 92] and human experimental subjects [58, 92].

As summarised in table 2.4, the thermoplastic elastomers have advantages, being biocompatible and having a good processibility. One of major drawbacks of thermoplastic elastomers is their heterogeneous degradation properties [93, 94]. This heterogeneous degradation is presented as a localised loss of structure integrity of the materials with time (Fig. 2.1) such as that the loss of mechanical strength is less predictable [95]. This becomes more critical when thermoplastic materials are used to build a three-dimensional (3D) structure. The 3D geometry of a thermoplastic is lost during degradation of foam struts and the architecture of the network is difficult to maintain [96]. Chemically cross-linked elastomers, on the other hand, provide more consistent degradation rates and predictable decline in mechanical properties due to their homogeneity (Fig. 2.1). Over the

past decade, chemically cross-linked biodegradable elastomers have gained increasingly attention in the field of tissue engineering, as discussed in Section 2.4-2.6. Among them, poly (polyol sebacate) (PPS) is a family of soft elastomers showing great potential in organ engineering of soft types [1, 8, 97].

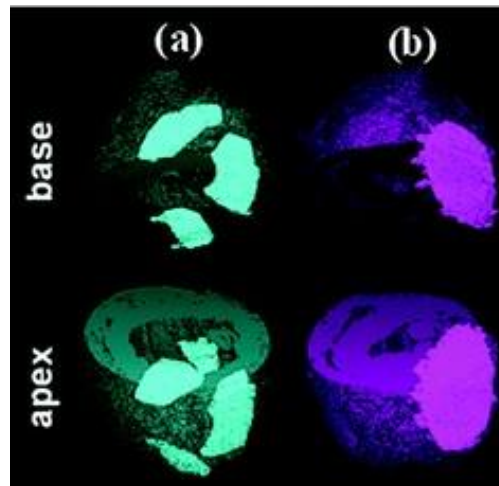


Fig. 2.1 Elastomeric heart patches attached to the pericardium of rat hearts. Premature failure of a thermoplastic rubber patch (a), and maintenance of the physical integrity of a chemically cross-linked elastomer patch (b) [95].

2.4. Poly (polyol sebacate) (PPS)

PPS is a new family of cross-linked elastomers that were recently developed for medical applications by Langer's group at MIT [1, 8, 97]. These polymers are biocompatible and inexpensive [98], and they have already shown potential applications in nerve [99] and vascular tissue engineering [100-103]. A polyol is a sugar alcohol containing multiple hydroxyl groups (e.g., glycerol, mannitol, sorbitol and xylitol). Sebacic acid, a dicarboxylic acid with structure $(\text{HOOC})(\text{CH}_2)_8(\text{COOH})$, is a naturally occurring chemical derived from castor oil which has been proven safe *in vivo* [104-106]. Polyol and sebacic acid are both endogenous monomers found in human metabolism.

2.4.1. Poly (glycerol sebacate) (PGS)

2.4.1.1. Synthesis of PGS

The synthesis of PGS can be presented by the polymerisation process of PGS (Fig. 2.2), which is the first and most-studied member of the PGS family. It was pioneered by Langer's group in 2002 [107], and it was later developed further by a number of research groups worldwide [102, 108]. PGS has been synthesised by an either equimolar amounts or different molar ratios of monomers, glycerol and sebacic acid, which are polymerised through step growth addition polycondensation. Glycerol is tri-functional, and it provides the hydroxyl groups for the formation of ester groups which link the sebacic acid and polyol together (Fig. 2.2).

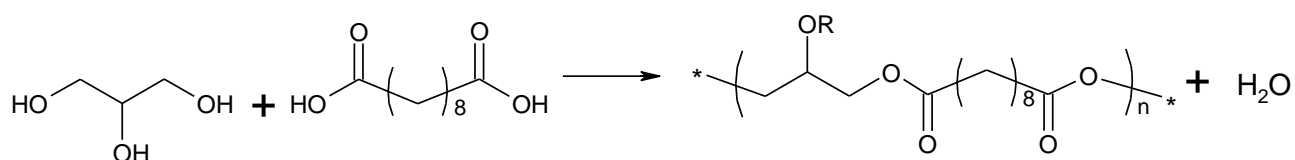


Fig. 2.2 Reaction scheme for poly(glycerol sebacate), R=H or polymer chain.

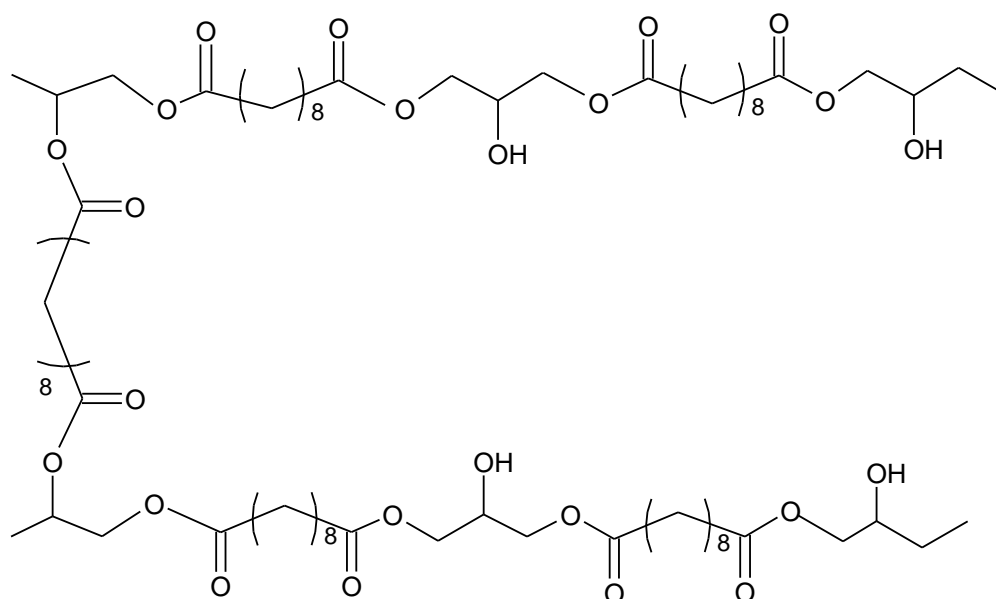


Fig. 2.3 Cross-linking scheme between two PGS polymer chains.

Thermal-treatment is a common method of synthesising PGS due to the ease of processing, and it is typically conducted in two steps: pre-polymerisation and crosslinking. The prepolymer is formed by heating a mixture of glycerol and sebacic acid under a purge of inert gas through the reacting chamber to prevent reactants' oxidation and at atmospheric pressure to minimize evaporation of the

volatile polyol monomers. The pre-polymerisation conditions vary from 110 to 150 °C for 1 to 12 hrs.

The level of linear versus cross-linking depends on the reaction kinetics of primary and secondary hydroxyl (–OH) groups of glycerol (Figs. 2.2 and 2.3). The primary –OH groups react much faster than the secondary ones at 100-150°C [109], and form PGS polymer chains. The cross-linking process, which involves the secondary –OH groups (Fig. 2.3), becomes prominent only when there is a severe lack of primary –OH groups in the reactant system. The PGS pre-polymer can be dissolved in organic solvent (e.g., tetrahydrofuran (THF), 1,3-dioxolane and ethanol), which can subsequently be processed into various forms of tissue engineering substitutes, including porous scaffold [110], thin film or sheet[102] and even fibre. The final resultant polymer material is a transparent elastomer, which is a covalently cross-linked 3D network of random coils with hydroxyl groups attached to the backbone.

PGS has been synthesised over a range of temperatures and durations [1, 7, 8, 102, 110-112]. It must be mentioned that the polymerisation kinetics of PGS reported from various studies have not proven to be consistent [113]. In the work on surgical sealants [114], a non-cross-linked pre-polymer, which can either dissolve in THF or flow at a temperature around 40-50 °C, was produced after synthesis at 110 °C for three days, whereas a crosslinked PGS solid was formed under the same synthesis conditions in another work [113]. Similar discrepancies can also be found in studies produced by other research groups. In the work of Wang and co-workers [42], for instance, a cross-linked PGS elastomer was produced after synthesis at 120 °C for three days, while in Yi and Lavan's work [115], an uncrosslinked PGS pre-polymer was synthesised under the same conditions, and the pre-polymer was subsequently dissolved into THF for the production of PGS fibres.

The above discrepancy was potentially caused by a number of factors. On the one hand, the cross-link kinetics of PGS are influenced by the synthesis conditions, especially temperature and the molar ratio of glycerol and sebacic acid. On the other hand, the synthesis conditions can vary significantly from one research laboratory/group to another. Firstly, the temperature uniformity of a vacuum oven is ± 1 °C at best, typically 2.5 °C for most ovens. A difference of 5 °C can greatly change the cross-link kinetics of PGS, according to our experience. Secondly, the loss of volatile glycerol monomer is inevitable, and both the flow rate of the (nitrogen) gas purge and the capacity of the vacuum pump can greatly affect the loss of glycerol during synthesis. Consequently, different research groups report different cross-link kinetics for the 'same' PGS polymers under the 'same'

conditions. Hence, the reproducibility of PGS materials remains to be improved.

2.4.1.2. Biocompatibility of PGS

PGS has consistently been reported to have good biocompatibility *in vivo*. Animal studies have showed that PGS has a similar acute inflammatory response to that of PLGA, with less fibrous capsule formation and absence of chronic inflammation [1, 116]. However, controversial results have been reported on the biocompatibility of PGS *in vitro*. The NIH 3T3 fibroblast cells were viable on highly crosslinked PGS samples and showed normal morphology with a higher growth rate than the control (PLGA), as tested by MTT assay [1]. In another series of studies, soft PGS, which was prepared from equimolar monomers and crosslinked for a short time, was shown to be toxic to mouse fibroblasts [108, 117, 118]. Apparently, the degree of cytotoxicity is associated with the crosslink density. It is possible that a highly crosslinked network degrades (via hydrolysis of ester bonds) slowly, and thus the concentration of potentially toxic degradation products in the environmental medium is sufficiently low to cause little cellular death.

Table 2.5 The degradation rates of PGS *in vitro* and *in vivo*

Experiment conditions	Materials	Experiment conditions	Experiment period	Degradation	Ref
<i>In vitro</i>	PGS	Phosphate buffered saline (PBS) solution	60 days	Weight loss 17± 6%	[1]
	PGS and PGS/Bioglass [®] composites	Standard tissue culture medium	60 days	Weight loss 10-25%	[119]
<i>In vitro</i> enzymatic degradation	PGS (curing time 42, 66, 90, 114 h)	Lipase-containing solutions	3-12h	0.05mm/3h	[120]
	PGS and PGS/Bioglass [®] composites	Lipase- and esterase-containing solutions		0.5-0.8 mm/month	[121]
<i>In vivo</i>	PGS	Implanted subcutaneously in rats	60 days	Completely 0.2 or 1.5 mm/month	[111]
	PGS	Grafted onto rat hearts	6 weeks	Completely resorbed	[116]
	PGS (curing time 42, 66, 90, 114 h)	Implanted on backs of rats	7 weeks	Completely resorbed	[120]

2.4.1.3. Biodegradation of PGS

The degradation rates of PGS have been investigated both *in vitro* and *in vivo*, as listed in Table 2.5. The degradation is much faster *in vivo* than *in vitro* [1, 111, 119]. The *in vivo* degradation kinetics indicates that aqueous enzymatic action may catalyse the breakdown of ester bonds in PGS and thus facilitate the hydrolytic weakening of this material *in vivo*. This has been supported by subsequent work in which the *in vitro* degradation behaviour of PGS was studied in lipase [120] and esterase [121] containing solutions, which catalysed the hydrolysis of ester bonds.

PGS has an advantage over other elastomers in terms of degradation behaviour. PGS predominantly degrades through surface erosion, which means the rate of degradation is predictable [122]. Both mechanical strength and mass decrease almost linearly with time as the polymer degrades. During *in vivo* degradation, it maintains its original shape, with relatively low swelling. The water content of PGS implants rises and reaches 15% in 35 days, at which point the polymer degrades > 70 wt % [111]. This manner of degradation is desired in many biomedical applications such as drug-delivery devices [123], scaffolding [8, 102] and soft tissue engineering [7, 112, 124-126].

However, the rapid degradation of PGS materials tend cause cytotoxicity [124] due to either excess non-reacted carboxylic acid groups or excessive amount of carboxylic acids produced by the aqueous hydrolysis of the PGS ester groups, which lowers the local extracellular pH to below physiological values (7.2-7.4). Another drawback is that the rapid degradation rate of PGS is believed to limit their application as a scaffold material in engineering tissues that have a healing rate of several months or years (e.g., the cardiac muscle). Hence, alternative chemical approaches are needed to decrease the enzymatic hydrolysis rate of the ester bonds in PGS polymers [120]. Nonetheless, its fast degradation kinetics match the healing rate of bone (typically 4-6 weeks [127]), and it is thus desired in bone tissue engineering.

2.4.1.4. Mechanical properties of PGS

PGS exhibits a tensile Young's modulus of 0.05-1.5MPa, an ultimate tensile strength (UTS) of 0.4 to 0.7 MPa and a maximal elongation of 120-300% [1, 124]. The typical mechanical properties of PGS are within the range of common soft tissue shown in Table 2.3. The mechanical properties of PGS can be tuned by varying curing temperature and time, which influence the cross-link density of materials [128].

2.4.2. Poly(xylitol sebacate) (PXS) and other PPS elastomers

2.4.2.1. Synthesis of PPS

The PGS elastomers mentioned above cover a modest range of mechanical properties and degradation rates. To expand the properties spectrum and suitable for more application, new members of the PPS family have been explored through polycondensation of other polyols with sebacic acid (Fig. 2.4) [23, 24]. The reaction rate systematically decreases with increasing numbers of –OH group polyols. PXS, for example, has to be polymerised at a higher temperature for pre-polymerisation and/or longer curing time than PGS to achieve similar mechanical properties to PGS, as shown in Table 2.6.

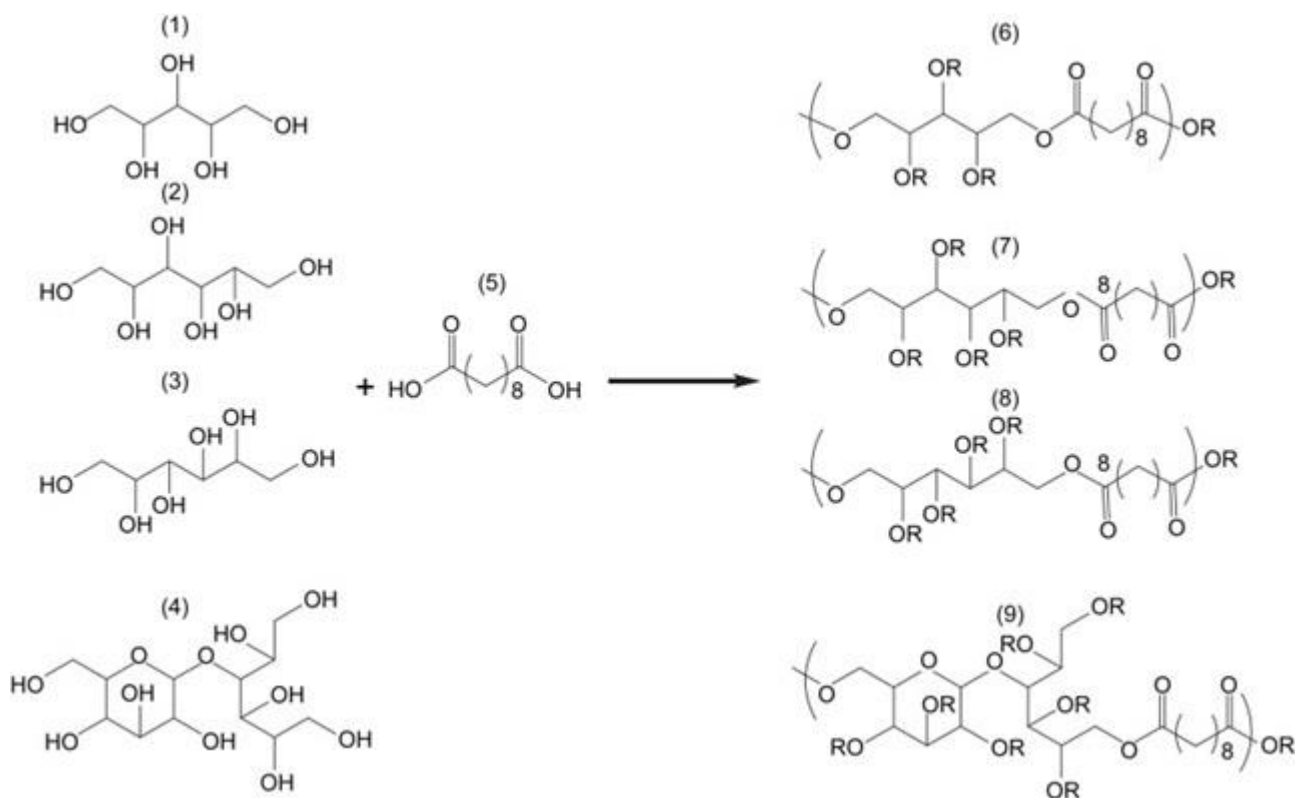


Fig. 2.4 General synthetic schemes of polyol-based polymers. Xylitol (1), sorbitol (2), mannitol (3) and maltitol (4) were polymerised with sebacic acid (5) in different stoichiometries, yielding PXS (6), PSS (7), PMS(8) and PMtS (9) [23].

2.4.2.2. Mechanical properties, degradation and compatibility of PPS

Collectively, PPS elastomers exhibit a tensile Young's modulus ranging from 0.05 to 400 MPa, maximal elongation at break ranging from 10 to 500 % [23]. The mechanical properties of PPS can

be tuned by a number of viable, including synthetic conditions, type of polyols and the mole ratio of monomers [23].

The biocompatibility of the PPS polymers is similar to that of PLGA [23, 129]. Similar to PGS, all PPS members show fast degradation kinetics *in vivo* than *in vitro* under physiological conditions, compared with PLGA. A most recent study has demonstrated that the enzymatic-mediated degradation rate of PXS is significantly slower, approximately half of that of PGS [130].

Table 2.6 Synthesis and mechanical properties of PPS [1, 23, 129]

	Synthesis pre-polymer	Curing condition	E (MPa)	UTS (MPa)	Ultimate elongation (%)
PGS 1:1	1120 °C-24h inert gas, then 120 °C-5h, 40mTorr	120 °C - 48h, 40mTorr	0.282±0.03	> 0.5	267±59
PXS1:1#	150 °C 2h inert gas, then 2 to 12h , 50 mTorr	120 °C 2Pa 4 days	0.82±0.15	0.61±0.19	205 ± 56
PXS1:2			5.33±0.40	1.43±0.15	33 ± 5
PSS1:1		120 °C 2Pa 5 days	0.37±0.08	0.57±0.15	192 ± 60
PSS1:2		120 °C 2Pa 4 days	2.67±0.12	1.16±0.33	66 ± 25
PMS 1:1		120 °C 2Pa 5 days	2.21±0.21	0.79±0.10	51 ± 9
PMS 1:2			12.82±2.9	3.32±0.76	45 ± 12
PMtS 1:4			378.0±33	17.64±1.3	11 ± 1
PES 1:1	145 °C 2h inert gas then 7h 50 mTorr	120 °C 3 days	0.08±0.01	0.14±0.03	446 ± 41
		140 °C 3days	1.92±0.12	1.03±0.19	85 ± 14

polyol : sebacic acid mole ratio

PSS poly(sorbitol sebacate), PMS poly(mannitol sebacate), PMtS poly(maltitol sebacate), PES poly(erythritol sebacate)

2.4.3. Photopolymerised poly(glycerol sebacate-co-acrylate) (PGSA)

One limitation to the thermal cross-linking procedure of the PGS system is the harsh processing conditions (long-term high-temperature curing), which could limit its ability to polymerise directly in a tissue or incorporate cells or temperature-sensitive molecules. To overcome this shortcoming, photo-crosslinkable elastomers were developed by Nijst et al., and they demonstrated the ability to form an elastomeric network from poly(glycerol sebacate-co-acrylate) (PGSA) under mild conditions while preserving a wide range of physical properties [25]. The advantages and disadvantages of both synthesis methods are presented in Table 2.7.

Photo-crosslinkable PGSA has been synthesised by reacting PGS precursors with acryloyl chloride (deprotonating free hydroxyl groups and appending acrylate groups) to form PGSA pre-polymer (in Fig. 2.5). A PGSA pre-polymer was cast into its final form and then cross-linked using a photo-initiator and UV light by photo-induced free radical polymerisation at room temperature. By deprotonating free hydroxyl groups and appending acrylate groups, the PGS pre-polymer was modified with acrylate moieties that participate in chemical cross-linking between polymer chains. The materials were rapidly polymerised at room temperature after UV light irradiation [25].

By varying the degree of acrylation of PGSA, these elastomers exhibited a Young's modulus, UTS and elongation at break ranging from 0.05 to 1.4MPa, 0.05 to 0.50 MPa, and 40 to 190 %, respectively [25]. The spectrum of PGSA properties could be expanded by the copolymerisation of PGSA with other acrylated molecules such as PEG-diacrylate. Increasing the concentration of PEG-diacrylate of this polymer system increases the Young's modulus and the UTS, while decreasing the maximum elongation, the swelling ratio and degradation rate [25]. *In vitro* assessments showed that photo-cured PGSA films supported human primary cell adherence and subsequent proliferation [25]. However, a mild to moderate inflammatory response of implanted PGSA was observed *in vivo* [131].

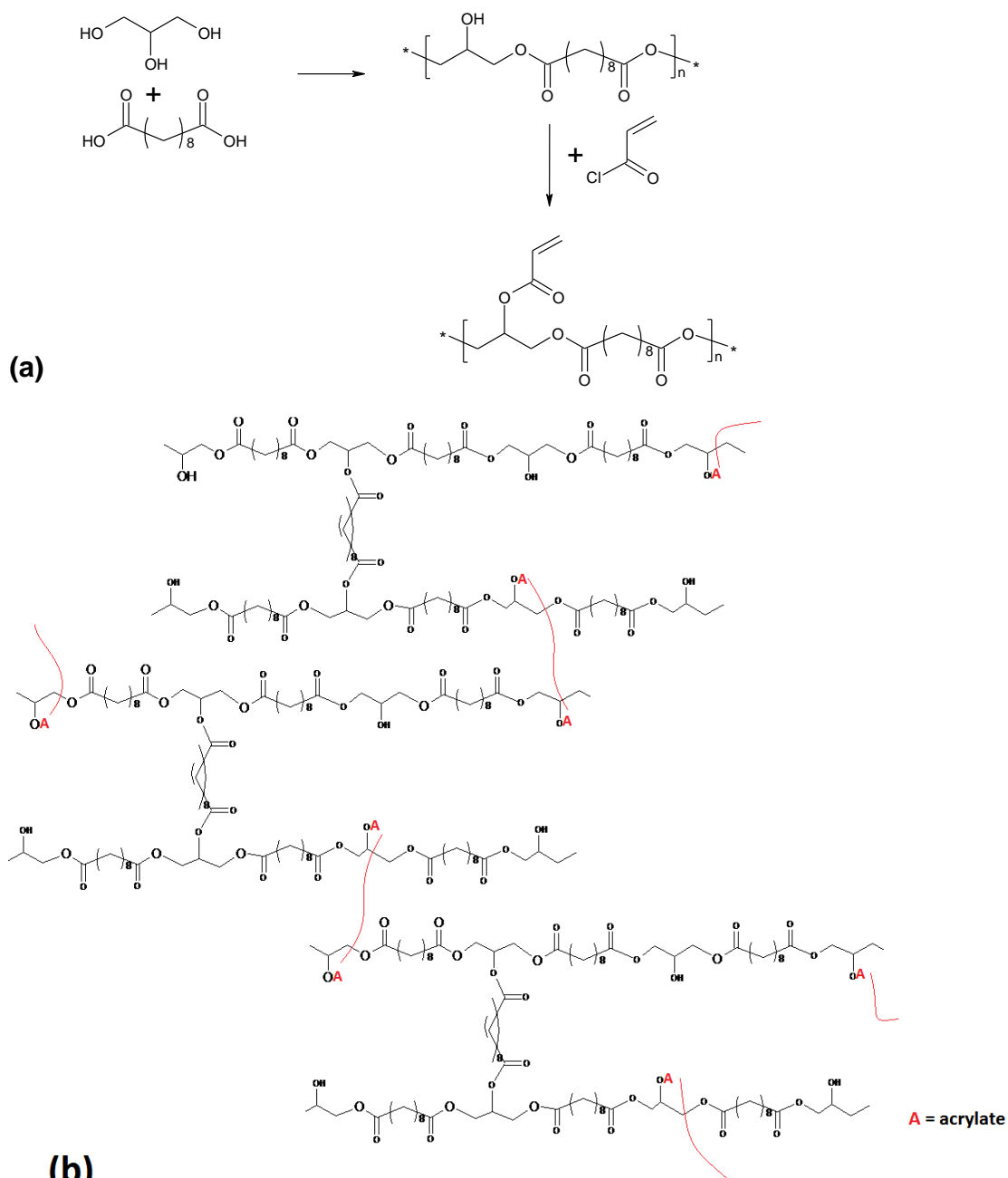


Fig. 2.5 (a) Modification of poly(glycerol sebacate) pre-polymer with acrylate moieties for photo-initiated curing; (b) PGSA after polymerisation under UV light.

Table 2.7 Advantages and disadvantages of different PPS synthesis processes

PPS synthesis processes	Advantages	Disadvantages
Thermal crosslinking	<ul style="list-style-type: none"> • Properties can be easily controlled by varying temperature and time • Cheap and easy to produce large batches of elastomers • Various shapes can be cast from pre-polymers 	<ul style="list-style-type: none"> • Harsh processing condition (long-term high-temperature curing, vacuum condition)
Photo crosslinking	<ul style="list-style-type: none"> • Short reaction time • Mild reaction condition (room temperature) • <i>In situ</i> curing • Properties tuneable by varying degree of acrylation and combination with other acrylated molecules 	<ul style="list-style-type: none"> • UV light required for polymerisation • Long-term UV light exposure may damage cell • Non-polymerised PGSA may be toxic to cells

2.4.4. Poly(glycerol sebacate)-co-poly(ethylene glycol)(PGS-co-PEG)

To enhance the water uptake capacity of PGS (about 2%) and improve its hydrophilic properties for the utility in soft tissue engineering, Ali Khademhosseini and co-workers [59] developed poly(glycerol sebacate)-co-poly(ethylene glycol)(PGS-co-PEG), which is a biodegradable polyester soft elastomer. PGS-co-PEG prepolymers have been synthesised by two steps condensation. First, sebacic acid and polyethylene react at 130 °C under argon for 2h, which is followed by further reaction under vacuum for 24h. Second, a specific amount of glycerol is added, and the mixture is heated for 96h at 130 °C under vacuum [59].

PGS-co-PEG polymer can achieve almost 15-fold higher water uptake capacity, compared with PGS. The PGS-co-PEG materials showed elastomeric properties and can be subjected to severe deformation such as bending, knotting and stretching without structure fracture. Their Young's modulus, ultimate stress and elongation can be altered from 13 kPa to 2.2MPa, 26 kPa to 3.8 MPa, and 55-108%, respectively, by altering the amount of PEG within the copolymer network [59]. However, the degradation rate was accelerated by increasing the PEG concentration in the PGS-co-PEG polymer and the material showed 15% to 81% weight loss at 21 days. *In vitro* cell proliferation test demonstrated that PGS-co-PEG polymers can support NIT 3T3 fibroblasts proliferation and there is no significant difference in cell proliferation due to the addition of PEG in the copolymer network.

PGS-co-PEG Synthesis

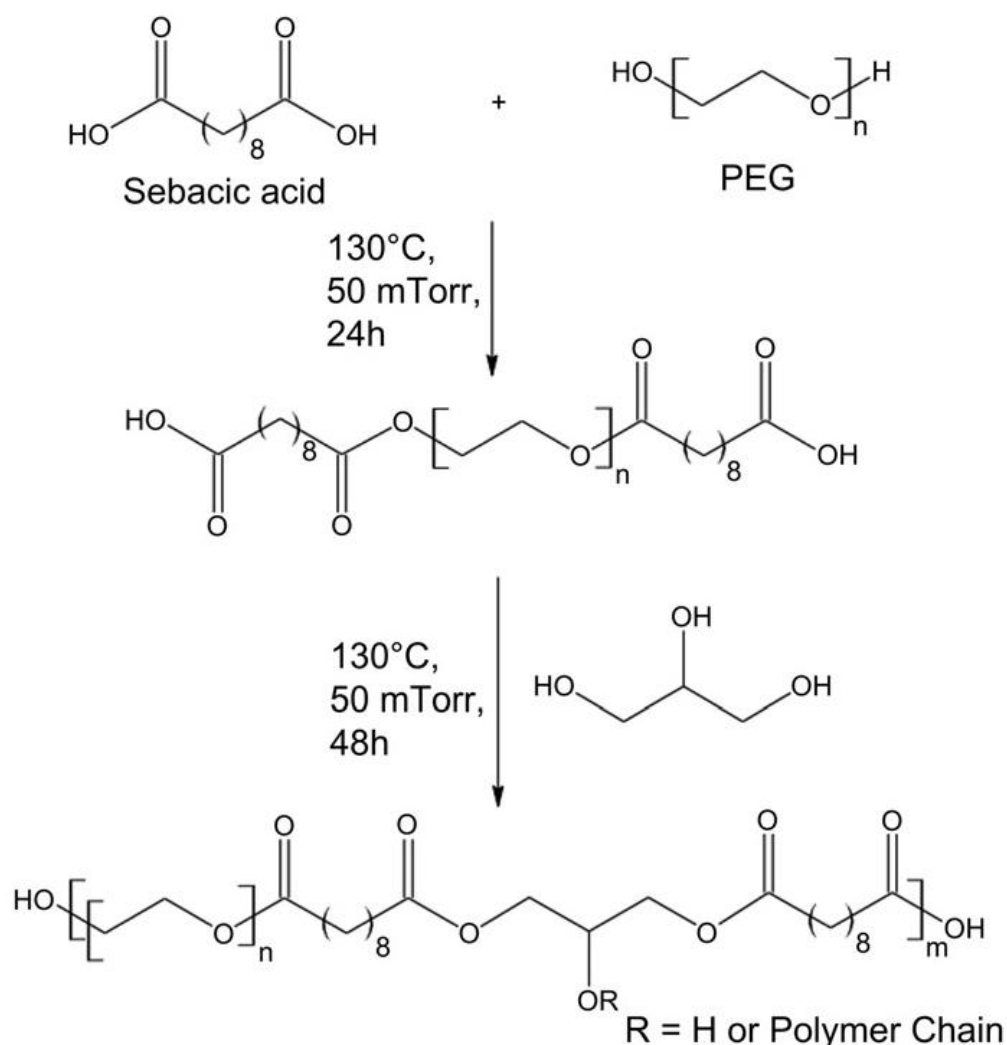


Fig. 2.6 The synthesis PGS-co-PEG polymer firstly involves polycondensation of PEG and sebacic acid to obtain a linear polymer chain then the glycerol was added to obtain a block copolymer of PGS-co-PEG [59].

2.4.4. PGS-based elastomeric composites

One strategy to expand the properties of a class of materials is to develop a composite. Although PPS has a wide range of properties, the spectrum can be further increased by developing a PPS composite [119, 132, 133]. A PPS-based bioactive glass/ceramic-filled composite was developed to simultaneously increase the PPS modulus and elongation and to minimise the drawbacks of PPS

(e.g., the cytotoxicity caused by the acidic degradation products of very soft PGS materials mentioned above) [119].

2.4.4.1. Bioglass PPS composite

The composites of PGS and alkaline Bioglass® filler have demonstrated both improved cytocompatibility and enhanced mechanical properties [117, 119]. Firstly, the addition of micro-sized Bioglass® to PGS increased the elongation at break from 160 to 550%. Secondly, the moduli of PGS/Bioglass® drops abruptly in a physiological environment (culture medium), and the level of the drop can be tuned such that Bioglass® does not harden the composite *in vivo* but rather maintains the desired compliance of biomaterials required for soft tissue engineering [117, 119]. The *in vitro* biodegradability of PGS/ Bioglass® with different concentrations of bioceramic filler were tested and have been found that the degradation rate of these materials in tissue culture medium were significant higher than in buffered solution at optimal pH 8 and esterase were added in both conditions [121]. The enzymatic mediated of PGS/ Bioglass® degradation rate (0.6-0.9mm/month) can be controlled by modifying the curing conditions and incorporating alkaline bioceramic filler [121].

2.4.4.2. multi-walled carbon nanotubes PGS composite

A potential electronically active PGS-based composite has been fabricated through incorporating multi-walled carbon nanotubes (MWCNTs) [133]. The motivation behind the work is that increasing the amount of MWCNTs may eventually leads to a percolating network of these conductive elements to form an electronically active PGS composite that may be utilised as a conducting biomaterial system in neural repair (e.g., nerve-bridging devices) or nerve-tissue engineering. Compared with pure poly(glycerol–sebacate–citrate)(PGSC), (PGSC)-based MWCNT-filled elastomeric composite exhibits increased mechanical properties with strength and modulus being 4.4 and 9.2 MPa, respectively. The composite materials demonstrated little cytotoxicity and slow degradation rates [133].

2.4.5. Applications of PPS-based elastomers

The major reason why PPS is of major interest in tissue engineering and regeneration is that PPS have been reported to be non-toxic based on *in vitro* cell-based outcomes [101] and *in vivo* findings using animal models [134, 135]. PGS is the most well studied PPS elastomer, with specific benefits shown in cardiovascular tissue engineering [100, 108] and small diameter nerve grafting [125].

2.5. Citric acid

2.5.1. Synthesis

The development of new polyester elastomers based on citric acid and diol groups has expanded the repertoire of soft biodegradable elastomers [5, 136]. Citric acid is a natural preservative and has been widely used in the food industry. Diols or glycols are chemical compounds containing two hydroxyl (-OH) groups. The synthesis of poly(diols citrate) (PDC) is similar to PGS. Firstly, a prepolymer is produced via thermal polycondensation of three acidic group monomers from citric acid and an aliphatic diol, which are typically 1,6-hexanediol, 1,8-octanediol, 1,10-decanediol, or 1, 12-dodecanediol. This is followed by post-polymerization at designed conditions (temperature / cure duration). Unlike other polycondensation reactions, PDC can be synthesized under relatively low temperature (as low as 37°C) and even without vacuum [5, 136].

2.5.2. Mechanical properties, degradation and compatibility of PDC

Four PDCs have been made separately with the four diols mentioned above, among which poly (1,8-octanediol) citrate (POC) is the most studied mainly because of its desirable mechanical properties: Young's modulus ranging from 0.92-16.4 MPa, UTS of 6.1 MPa and elongation at break of 117-265% [136]. By altering the post-polymerization temperature, time, and monomer molar ratio, one can optimise both the mechanical properties and the degradation rate simultaneously.

In vitro evaluation conducted with human aortic smooth muscle cells (HASMCs) and human aortic endothelial cells (HAECs) indicate that POC is as good as PLLA in terms of the growth and viability of the cells [107]. Subcutaneous implantation in Sprague-Dawley rats has demonstrated that the thickness of the fibrous capsule induced by POC was similar to that induced by PGS, but significantly smaller than that of PLGA [107]. Meanwhile, no chronic inflammatory response was observed. POC has been reported to have a life time of 6 months when incubated in PBS at

37°C *in vitro*, and to undergo both degradation and enzyme-catalysed hydrolysis *in vivo* [136], with implants remaining *in situ* for 2 months following subcutaneous implantation [136].

2.5.3. Applications of POCs in tissue engineering

One of the potential applications of POC is as a tubular scaffold used in blood vessel engineering. Biphasic tubular scaffolds are constructed of two layers: a nonporous, skin-like interior with 1,12-dodecanediol citrate (PDDC) and a porous exterior with POC. The developed PDC tubes are very well matched mechanically with native blood vessels [137], with an ability to undergo elastic recovery from deformation.

2.6. Other biodegradable soft elastomers

2.6.1. Polyester Amides

2.6.1.1. Synthesis

To overcome the deficiencies of rapid degradation of crosslinked aliphatic polyesters (such as PGS), Langer's research group developed poly(1,3-diamino-2-hydroxypropane-co-polyol-sebacate) (APS) [138], which is a biodegradable, elastomeric poly(ester amide) composed of hydrolytically stable amide bonds throughout the polyester matrix [138]. APS was made from three non-toxic monomers: 1,3-diamino-2-hydroxypropane (denoted as A), polyol (glycerol or D,L-threitol, denoted as P) and sebacic acid (denoted as S).

2.6.1.2. Mechanical properties, biocompatibility and degradability

APS elastomers have been characterised with Young's modulus of 1.45-4.34 MPa, UTS of 0.24-1.69 MPa and strain at break in the range of 21-92% [138]. The mechanical properties and degradation kinetics can both be influenced by adjusting the formulation of APS [32]. The widely tuneable mechanical properties, biodegradability and biocompatibility of APS indicates its great potential as a structural material for resorbable implantable devices [139], such as tissue engineering scaffolds, drug delivery systems and even temporary diagnostic systems [138].

In vitro assessments have revealed that APS had excellent biocompatibility, showing healthy cell morphology and maintained metabolic activity of primary human foreskin fibroblasts when cultured on APS. *In vivo* trials have demonstrated that APS produces less foreign body responses than

PLGA, with reduced fibrosis and fewer macrophages around APS implants compared to PLGA [138].

2.6.2. Cross-linked Poly (1,3-trimethylene carbonate)

Poly (1,3-trimethylene carbonate) (PTMC) was developed as a linear thermoplastic elastomer, displaying poor dimensional stability, tackiness and inadequate mechanical properties [140]. To improve its mechanical properties, amorphous PTMC of high molecular weight ($M_n \geq 100,000$) was explored [140], the new PTMC being flexible and durable, with much improved ultimate mechanical properties [140].

2.7. Fabricate of soft elastomeric scaffolds

In an organ, cells and their extracellular matrix (ECM) are usually organized into three-dimensional tissues. Therefore, in tissue engineering a highly porous 3D matrix (scaffold) is often necessary to accommodate cells and to guide their growth and tissue regeneration in three dimensions. Numerous techniques have been developed to process porous polymer scaffolds for use in tissue engineering. A number of reviews are available in the literature [18, 141-143]. Polymeric scaffold processing methods could be classified into four groups, as listed in Table 2.8: (i) melted-polymer based, (ii) solvent based, (iii) gas-foaming, and (iv) rapid prototyping (RP). The choice of the correct technique is critical because the fabrication can significantly alter the properties of the implant and its degradation characteristics.

As aforementioned, chemically crosslinked elastomers can be neither melted nor dissolved in any solvent. Hence, conventional reforming is normally difficult or impossible with chemically crosslinked elastomers [55]. This limitation, however, can be addressed with a prepolymer of elastomers, which can be dissolved in organic solvent and subsequently processed into various forms of tissue engineering substitutes, including porous scaffold [110], thin film or sheet [102] and even fibre.

2.7.1. Solvent casting and particle leaching

Solvent and particle leaching technology involves casting a dissolved prepolymer around packed leachable particles. After drying and crosslinking the prepolymer and leaching out the porogen, a

porous elastomeric scaffold with an interconnected pores forms. 3D PGS scaffolds with a random network of interconnected pores have been fabricated with this technology using a two-phase system of pores in which the large macroscopic pores (75-150 μm) are produced using sieved salt particles while the small microscopic pores (5-20 μm) are produced by vapour formation of glycerol [110]. Specifically, the PGS pre-polymer is dissolved in THF and cased to the fused template of sodium chloride particles. Then, the PGS prepolymer is thermally cured at an elevated temperature (e.g. 150 $^{\circ}\text{C}$) while being dispersed throughout the fused salt template. During the crosslinking treatment, volatile glycerol partially evaporates generating micropores. The dissolution of the salt and subsequent lyophilisation produced elastomer sponges with approximately 90% porosity, interconnected macropores and extensive micropores.

2.7.2. Melt-based replica moulding and lamination technique

Controlling the cellular microenvironment within the scaffolds is critical for eliciting desirable biological responses such as proliferation, migration and maturation. However, the micro- and nano-structure of the scaffold is difficult to achieve via the traditional fabrication techniques such as solvent casting and particle leaching, gas foaming and 3D printing. Polymer scaffold replica moulding on micro-machined silicon substrate can achieve a feature resolution of less than 10 μm [144], the same length-scale of mammalian cells. Melt-based replica moulding fabrication technologies have been employed to achieve well-defined feature geometries in polycrystalline or amorphous thermoplastic biomaterials.

Since high-temperature curing is required after melt-casting an PPS prepolymers, this processing requires the use of a sacrificial mould release layer consisting of a biologically benign material (e.g., sucrose) to prevent adhesion of these adhesive materials to the mould used during the final polymerisation [8]. Fig. 2.7 illustrates such a process of 3D microfluidic tissue engineering scaffolds. In this process, a negative silicon mould is fabricated using the standard photolithographic and plasma-etching techniques. Prior to replica moulding of PGS, a sacrificial sucrose release layer is spin-coated on the silicon master. For replica moulding of PGS, the melted PGS prepolymer is applied to the silicon substrate coated with sucrose. The PGS prepolymer sheet is then thermally crosslinked, forming the PGS sheet with the micro-pattern printed on it. The sheet is delaminated with the mould in water (Fig. 2.7). Finally, the PGS sheet is laminated by further curing (ester linkages from active hydroxyl and acid groups form between layers) to form a long-range ordered 3D microfluidic scaffold [8].

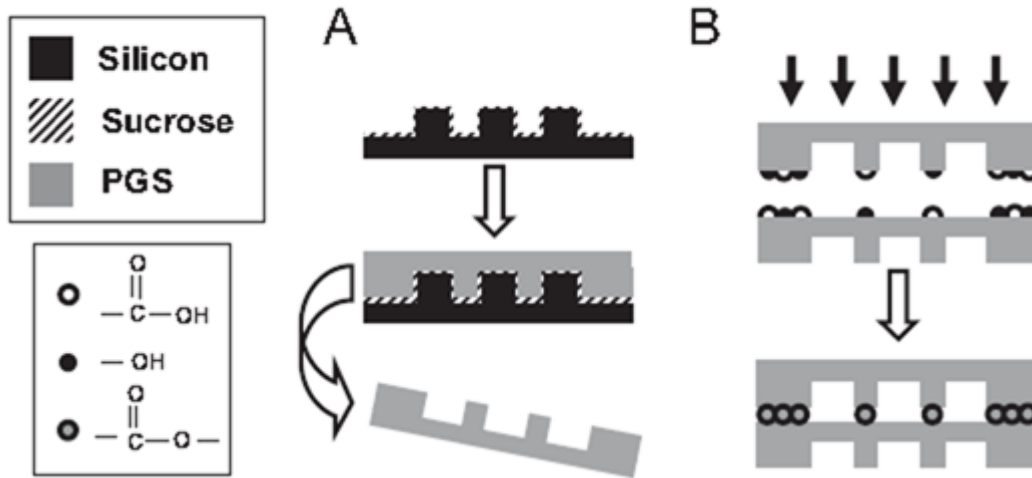


Fig. 2.7 Overview of fabrication strategy for PGS microfluidic devices: A) Replica moulding of PGS layers. PGS pre-polymer is cured into micro-patterned sheets and delaminated in water. B) Multiple layers are bonded by physically adhering individual sheets and curing the films together [8].

2.7.3. Electrospinning

Electrospinning is a convenient method of producing arrays of loose nano-scale fibrous networks. Aligned textures produced by this technique are favoured in some tissue engineering applications to guide cells (e.g., in myocardial tissue with an aligned texture). However, the major technical hurdle in electrospinning cross-linked elastomers is that these polymers cannot dissolve into any solvents for spinning once cross-linked, and any fibres spun from un-cross-linked pre-polymers would distort and flow in the subsequent cross-linking treatment.

To address this challenge, the core/shell electrospinning technique has been applied. In this technique, the core is fed with the pre-polymer of elastomer, and the shell is fed with a thermoplastic polymer that could remain solid and maintain the fibrous shape at an elevated temperature during the subsequent curing process. The core/shell electrospinning technique has been applied for fabricate PGS fibres. In this technique, the core is fed with the pre-polymer of PGS, and the shell is fed with PLLA that could remain solid and maintain the fibrous shape during the subsequent curing process of PGS [115]. Subsequently, PLLA was removed from the fibres to yield a PGS scaffold [115]. However, the organic solvents used to remove PLLA shell can infiltrate into PGS and damage the polymer network, eventually leaving an embrittled core fibre behind. Very recent work demonstrated that the PLLA plastic shell could be beneficial in improving

cytocompatibility, controlling the mechanical properties, as well as degradation rate of the final product when used as a cell delivery vehicle [63, 145]. The core/shell spun PGS/PLLA fibres have demonstrated soft-tissue like mechanical properties with J-shaped, elastic stress-strain curves [63, 145]. This scaffold is reported to support and foster the growth of enteric neural crest progenitor cells and provide the effective delivery of the progenitor cells to an embryonic and post-natal gut environment [63].

Electrospinning can be more appropriately applied to photo-cross-linkable biodegradable elastomers, which do not require a thermal curing process. PGSA macromers were used to produce a nanofibrous scaffold using electrospinning, with gelatine as a carrier polymer to facilitate fibre formation and cell adhesion. Post-UV light exposure was used to facilitate PGSA cross-linking. The properties of the bulk fibrous scaffold were tested: mechanics (tensile modulus varied from 60 kPa to 1 MPa) and degradation (mass losses between 45 and 70% by week 12) [146].

2.7.4. Rapid-prototyping

The rapid-prototyping or solid free-form (SFF) technique is a computer-aided fabrication process. Using the rapid-prototyping techniques of fused deposition modelling (FDM), selective laser sintering (SNL), 3D printing (3D-P), stereo lithography or extrusion free forming, 3D objects are constructed layer by layer. These methods have an advantage over conventional fabrication techniques due to their ability to create geometries with accurately designed complex architectures [147].

For cartilage tissue engineering, a 3D PGS scaffold was created [148] with designed pore shapes, pore sizes, porosities and architectures through a sacrificial mould produced using SFF techniques (Fig. 2.8) [148]. In this technique, SFF methods are used to create inverse wax moulds. Subsequently, the wax moulds are used to form sacrificial hydroxyapatite moulds, which are then used to mould the PGS pre-polymer. After curing, the hydroxyapatite phase is dissolved using a rapid decalcifying agent to achieve the final PGS scaffold [148]. The designed PGS 3D scaffold can be used in cartilage tissue engineering, and it has been demonstrated that the scaffold can support robust cartilage formation when seeded with porcine chondrocytes *in vitro* [148].

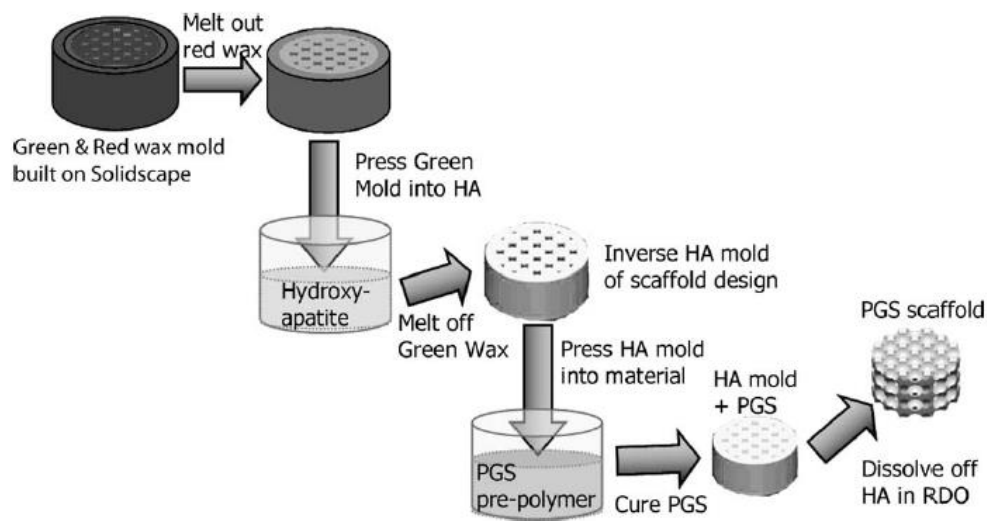


Fig.2.8 Fabrication of 3D designed PGS scaffolds involves creating wax moulds that are cast into hydroxyapatite to create an inverse mould and then cast into a PGS pre-polymer and cured, resulting in a PGS scaffold [148].

Recently, micro-fabrication technique has also been used to produce an accordion-like honeycomb microstructure 3D scaffolds for myocardial repair applications (Fig. 2.9) [112]. The 3D scaffold (highly porous and elastomeric with controllable stiffness and anisotropy) was fabricated by micro-ablating lateral array troughs in one PGS lamina, overlaying another PGS lamina, micro-ablating top-to-bottom pores through both lamina and then stabilizing the resultant scaffold by thermally crosslinking through autoclaving (121 °C for 30 min). The scaffold mechanically matches with the heart tissue in terms of stiffness and can guide the orientation of healthy cardiac cell. In addition under electric field stimulation, heart muscle cell were encouraged to grow and contract with directionally dependent electrical excitation threshold.

Stereo lithography is another popular method of fabrication by rapid-prototyping that uses light to polymerise, cross-link or harden a photosensitive material. A laser, which is guided by computer-assisted design software in the desired pattern, selectively polymerises material from a bath of photo-polymeric solution in a layer-by-layer process. The final product is washed to remove unreacted polymer and yield a 3D structure with specific micro architectures [143]. This method has yet been applied to soft biodegradable elastomers. There is a great deal of potential in applying stereo lithography to photo-cross-linkable PGSA elastomers with rapid photo-activation and robust mechanical properties, as mentioned above.

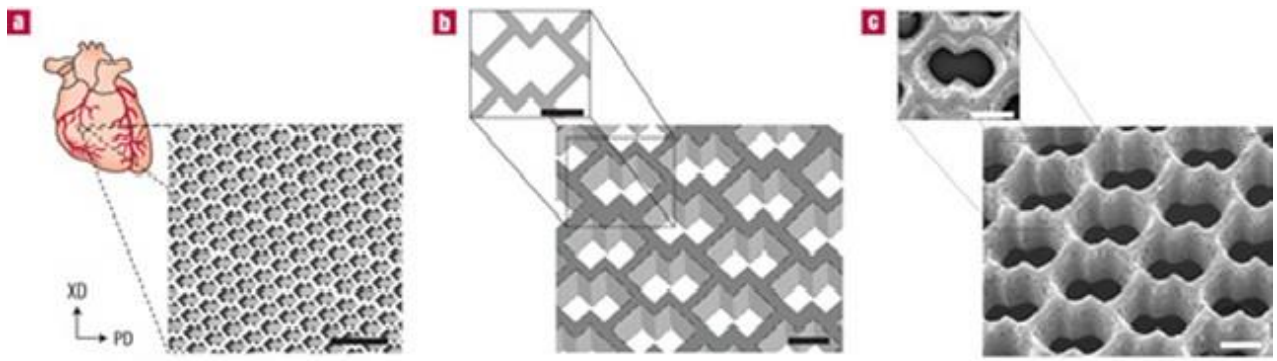


Fig. 2.9 Accordion-like honeycomb scaffolds for myocardium.(a, b). Computer-designed image of the scaffolds. Scale bars: 1mm (a) and 200 μm (b). (c) Scanning electron micrographs demonstrating the fidelity of excimer laser micro-ablation in rendering an accordion-like honeycomb design in PGS. Scale bar: 200 μm [112] .

Table 2.8 3D fabrication technologies of polymer scaffolds [18, 141-143, 147, 149, 150]

Fabrication technology	Required properties of materials	Available pore size (μm)	Porosity (%)	Porous structure
Melting -based				
Melt moulding	Thermoplastic	50-500	<80	Spherical pores/low interconnectivity
Extrusion/particle leaching	Thermoplastic	<100	<84	Spherical pores/low interconnectivity
Solvent-based				
Solvent casting/ particle leaching	Soluble	30-300	20-50	Irregular pores
Paraffin template	Soluble	100-70	>90	Spherical pores
Emulsion freeze drying	Soluble	<200	<97	High volume of interconnected micropores
Thermally induced phase separation/ freeze drying	Soluble	<200	<97	High volume of interconnected micropores
Electrospinning	Soluble	20-100	<95	Fibrous
Membrane lamination	Soluble	30-300	<85	Irregular pores
Gas-foaming				
Chemical reactant gas foaming	Amorphous	100-700	>90	High volume of non-interconnected micropores
Physical induced gas foaming/ particle leaching	Amorphous	Micropores <50 Macropores <400	<97	Low volume of non-interconnected micropores combined with high volume of interconnected macropores
Papad prototyping				
3D printing	Soluble	45-150	<70	100% interconnected macropores
Fused deposition modelling	Thermoplastic	160-700	48-77	Regular geometrical honeycomb pores
Selective laser sintering	Polymer/Ceramic and polymer composite	0.006-200	-	High volume of interconnectivity micropores

Table 2.9 Advantages and disadvantages of PPS fabrication techniques [18]

Techniques	Advantages	Disadvantages
Melt-based replicate moulding and lamination	Achievable high-feature resolution <math><10\mu\text{m}</math>	Laminated 3D scaffold may lack required mechanical strength for load-bearing tissue
Solvent casting and particle-leaching	Control over porosity, pore size and high porosity Simple, low cost	Poor quality control Uses organic chemicals and residual solvents
Electrospinning	Fabricate nanofibrous porous scaffolds Simple, low cost Aligned structure	Aligned texture may not always be desirable Post-processing curing required Low productivity
Rapid-prototyping	Controlled quality, pore size and porosity Advanced in fabricating scaffolds with precise and complex structures	Expensive

2.7.5. Summary of PPS scaffolding techniques

A number of fabrication techniques have been developed to produce PPS scaffolds for tissue engineering. In choosing a certain fabrication technique to produce scaffolds for different applications, it is necessary to weight the advantages and disadvantages of the techniques. Table 2.9 provides a comparison of the PPS fabrication techniques discussed in this review.

2.8. Objectives of this project

Biodegradable elastomers play a critical role in the field of soft tissue engineering, and the studies of these elastomers for many applications have been bloomed in the past two decades. This review focused on the synthesis, scaffold fabrication techniques and properties of elastomers and identified that PPSs are the most promising elastomeric biomaterials. PPSs and PPS-based elastomeric biomaterials are biocompatible, compliant and biodegradable. However, a number of issues associated with the PPS family remain to be addressed. First, very soft PGS materials can generate acidic degradation products, causing cytotoxicity, which hamper their application as a cell delivery vehicle. Second, the *in vivo* degradation rates of PPS materials are generally too fast to be applicable to tissue engineering of soft types. Last, the synthesis techniques of PPS materials need

to be improved to meet the highly demanded quality control in tissue engineering. To address the above issues of PPS form the aim of this project.

The objectives of this PhD research project are:

- (1) To characterise the PPS and explore the effect of the synthesis conditions on the PPS microstructure and properties in order to achieve high quality control and high reproducibility.
- (2) To expand the span of the chemical and mechanical properties of PPS aim to provide larger quantity of potential candidatures for various soft tissue engineering applications.
- (3) To further study the degradation mechanism of PPS and slow down the degradation rate of PPS to meet the scaffold requirement of specific tissue.
- (4) To design and fabricate porous scaffold from PPS elastomers by using electrospinning technique, aiming at achieve elastomeric scaffold to support growth of cells.

CHAPTER THREE

MATERIALS AND EXPERIMENTS

3.1. Materials

The raw materials of PGS and PXS, i.e. sugar alcohol: glycerol (purity 99%), xylitol (purity 99%) and the diacid, sebacic acid (purity 99%) from Sigma-Aldrich. Purasorb[®] PDL 20 is a poly (D,L-lactic acid) (PDLLA) purchased from PuraBiochem, Gorinchem, the Netherlands, with an inherent viscosity of 2.0 dl/g. Purasorb[®] PDLLA was completely amorphous and was used without further purification. It is a FDA approved biomaterial which was used as a control material in materials' biocompatibility test. To prepare the degradation experiment solutions the following raw material were chosen. The esterase of porcine liver was purchased from Fluka. The raw material of Fenton's reagent were prepared from the ferrous sulphate heptahydrate ($\text{FeSO}_4 \cdot 7\text{H}_2\text{O}$) which meets United States Pharmacopeia, USP, testing specification from Sigma-Aldrich and the hydrogen peroxide (H_2O_2) (30 wt. %) from Merk. The xanthine oxidase from bovine milk (Grade I, ammonium sulphate suspension, 0.4-1.0 unit/mg protein) and the xanthine (purity 99.5%) were purchased from Sigma-Aldrich. Dimethylformamide (DMF) was purchased from Merck (Kilsyth, VIC AU). To fabricate PXS/PVA spun fibres, PVA with various molecular weights 31,000–50,000 g/mol, 89,000–98,000 g/mol and 146,000–186,000 g/mol were purchased from Sigma-Aldrich. The melting point of PVA is approximately 200°C, which is well above the PXS cross-linking temperature, which ranges from 120 to 150°C [24, 151, 152]. Poly(L-lactic acid) (PLLA) was purchased from Castle Hill, NSW, AU.

3.2. Synthesis of PGS and PXS

According to previously published methods, PGS and PXS were synthesized in two steps [1, 7]. Initially, a pre-polymer of PGS or PXS was synthesized by polycondensation of a 1:1 molar ratio of either glycerol or xylitol mixed with sebacic acid. After, thorough mixing at room temperature, the monomers were reacted under a $\sim 130 \text{ cm}^3/\text{min}$ flow of nitrogen gas at either 130°C for 24 hours (PGS and PXS) or 150°C for 8 hours (PGS). These prepolymers were then dissolved in tetrahydrofuran (THF) at a concentration of 50 vol. % then the solution was cast onto glass slides, after which the THF evaporated at ambient conditions to produce thin sheets. Finally, the cast

sheets were cured at 130°C under vacuum for 1 to 12 days (24, 48, 72, 96, 144, 168 or 288 hours). After cooling to room temperature the vacuum was released and the 0.5-0.9 mm thick sheets of PGS-gel or PXS-gel were peeled off the glass slides.

3.3. Fabricate PVA/PXS electrospun fibres

3.3.1. Preparation of core and shell solutions

A PXS prepolymer was synthesised by polycondensation using a 2:5 mole ratio of xylitol mixed with sebacic acid. The monomer was reacted in a Kugelrohr apparatus under nitrogen gas atmosphere at 130°C for 12h. The prepolymer was then dissolved in DMF 50% v/v to prepare the core solution. Various amounts PVA was dissolved in 4ml of filtered water at room temperature for 12h and heated in a water bath at 90°C for 3h. Then 1ml of DMF was added to produce a total concentration of 5 ml of solution, which was heated for 3h. Table 3.1 lists three final concentrations that produced satisfactory core/shell fibres. The shell solutions were electrospun at room temperature.

3.3.2. Core/shell electrospinning

A Y-Flow 2.2D-350 electrospinner was set up with a two-fluid coaxial spinneret. The inner tube had inner and outer diameters of 0.6 and 0.9 mm respectively, while the outer tube had an inner diameter of 1.4 mm. A voltage range from 15 to 17 kV was applied at the tip of the spinneret. The distance between the tip and the drum collector was 18 cm. The feed flow rates to the core and the shell were set at 0.1:1 ml/h, 0.1:0.8 ml/h or 0.2:0.8 ml/h. When the core flow rate was higher than 0.2 ml/h, or the shell flow rate was higher than 1 ml/h, droplets were formed on the collector, which means the flow rate is too fast and electrostatic force can't match the combination of flow rate and viscosity thus the droplet at the tip of spinneret grew in size and dripped. The spun fibre mats were then heated at 130 °C in a vacuum oven for three days to cure the PXS. Some of the heated PXS/PVA fibre mats were washed in deionised water at room temperature for 24 h, followed with hot water at 90 °C for 4h. The water was changed every six hours during the washing process. Finally the materials were taken out and dried in a vacuum oven for three days. For the purpose of comparative study, thin sheets of PXS were also fabricated by casting the PXS core solution on glass slides, which were then heated at the same curing conditions. The processing steps of the above samples are summarised in Table 3.2.

Table 3.1 PVA polymers used in the work, optimal concentrations of solutions that produce satisfactory electrospun fibres

M_w (g/mol) of PVA	Percentage of hydrolyzation of PVA as purchased	Concentration of PVA (shell) solution (g/100ml solvent**)	Feeding rates of core:shell (mL/h)	Voltage (Positive/negative)
31,000-50,000	98–99 %	25	0.1:0.8	+13/-2 kV
89,000-98,000	> 99 %	13	0.2:0.8	+13/-2 kV
146,000-186,000	98–99 %	8	0.1:1	+15/-2 kV

* The concentration of PXS solution was 50% (v/v).

** The solvent was the mixture of water and DMF in the 4:1 volume ratio.

Table 3.2 Process of samples. All samples were heat treated at 130°C for 3 days in vacuum after fabrication

Samples	Fabrication process	PVA washed out	Mechanical test conditions
PXS sheet	Cast	No	dry
PVA	Electrospinning	No	
PXS/PVA	Core/shell electrospinning	No	
PXS/PVA-washed	Core/shell electrospinning	Yes	
PVA-wet	Electrospinning	No	wet
PXS/PVA-wet	Core/shell electrospinning	No	
PXS/PVA-ww	Core/shell electrospinning	Yes	

3.4. Characterisation

3.4.1. Determination of the degree of esterification in PGS and PXS

The esterification degree was determined by acid group titration of the remaining carboxyl groups in the PGS or PXS and by weight loss of the water condensation by-product. In the acid group titration method [153], 1 g of sample was dissolved (prepolymer) or swelled (crosslinked polymer) in an ethanol (25 wt. %)/toluene (75 wt. %) mixture in a flask sealed with Parafilm™ film. The crosslinked polymers were ground into a powder and soaked in the solvent mixture for 24 hours to achieve high degrees of swelling. The carboxyl groups were then titrated with a standardized 0.1 M solution of potassium hydroxide in ethanol, keeping the flask sealed from atmospheric CO₂ when standing. Bromothymol blue solution (10 drops) was used as a pH indicator and the end-point of the titration was taken when the solution changed from yellow to bluish green [153]. For the crosslinked samples, the end point was taken to have been reached when the colour of the indicator colour remained bluish green for one hour. The percentage of the reaction was calculated by Eq. 3.1:

$$\begin{aligned} \text{Percentage reaction (\%)} &= \left(1 - \frac{\text{mole unreacted carboxylic acid groups}}{\text{mole original carboxylic acid groups}}\right) \times 100 \\ &= 1 - \frac{(V_1 - V_0) \times C / m_0}{2 / (M_{SA} + M_{polyol} \times \frac{n_{polyol}}{n_{SA}})} \times 100 \end{aligned} \quad \text{Eq. 3.1}$$

where V_1 is the volume in litres of 0.1 M KOH used for the sample titration, V_0 is the volume for the blank test (without sample), C is the concentration of KOH (0.1M), m_0 is the mass of the sample, M_{SA} , M_{polyol} are the molecular weights of sebacic acid, glycerol or xylitol and n_{SA} and n_{polyol} are the number of moles of sebacic acid and glycerol or xylitol respectively in the sample.

For the second method, the reactants were weighed before and during reaction, and the weight loss during the polycondensation synthesis was assumed to be the amount of the water by-product. The percentage of carboxylic acid converted to sebacate ester was then calculated by Eq.3.2:

$$\text{Percentage reaction (\%)} = \frac{\text{mole of reacted carboxylic group}}{\text{mole of original carboxylic group}} (\%) = \frac{m_{H_2O} / M_{H_2O}}{2 \times m_{SA} / M_{SA}} \times 100 \quad \text{Eq. 3.2}$$

where m_{SA} is the weight of the sebacic acid used in the synthesis, m_{H_2O} is the weight of water evolved and M_{H_2O} is the molecular weight of water.

3.4.2. Gel point determination

The gel points of the PGS or PXS prepolymers which had been synthesized at 130°C/24h (PGS and PXS) or 150°C/8h (PGS) were determined by post curing them at 130°C for 16h and then removing duplicate samples from the oven every hour for solubility studies in THF (PGS) or DMF (PXS) - the gel point conversion was taken as that when the samples no longer dissolved in the solvent.

3.4.3. NMR analysis

The proton and ^{13}C NMR spectra were obtained for the PGS prepolymer samples in acetone- d_6 solutions. The PGS gel sample (prepolymerised at 150°C/8h then cured at 130°C/48h) was prepared for NMR by powdering in a liquid nitrogen-cooled 6870 large freezer/mill (SPEX SamplePrep LLC) and swelling in acetone- d_6 . The NMR-spectra were run with a Bruker DPX300 (7.05 Tesla magnet) with a 5mm quad $^1\text{H}/^{13}\text{C}$ switchable probe, ^1H at 300 MHz and ^{13}C at 75 MHz with Z-gradients at 30°C. The residual H-acetone peaks at 2.09 ppm were used as a reference in proton spectra and the ^{13}C resonance of acetone at 205.87 ppm was used in carbon spectra.

The heteronuclear shift correlation (also known as COSY) NMR spectrum of the prepolymer and gel were obtained with a Bruker Avance III 600 (14.1 Tesla magnet) with a 5mm CPTCI $^1\text{H}-^{13}\text{C}$ autotunable cryoprobe with Z-gradients and BACS 60 tube autosampler, ^1H at 600.27 MHz and ^{13}C at 150.95 MHz. This is a very useful technique because it correlates the chemical shift of each carbon to the chemical shifts of the protons which are attached to it [154].

The DEPT (distortionless enhancement by polarisation transfer) ^{13}C NMR technique was also employed. This method alters the amplitude and sign of the carbon resonances according to the number of attached protons, so that the methylene carbon signals have opposite phase to those of the methine carbon resonances which allows them to be readily distinguished [154].

3.4.4. Water and THF swelling of PGS and PXS

The aim of this experiment was to compare the diffusion rates of water molecules in the two PPS networks, which have the same degree of crosslink densities. The water (or THF)-vapour-swollen specimens were prepared by placing them in a sealed container above distilled water (or THF) at 37 °C, in which a 100% relative humidity was established. The swollen specimens were removed from the above sealed container at various intervals and surface water was removed with filter paper. After the mass of the swollen samples (m_{eq}) was measured in a sealed vial, the specimens were dried in a vacuum oven at room temperature for one week and weighed again to determine the mass in the dry condition (m_d). The weight swelling percentage was calculated as:

$$\frac{m_{eq} - m_d}{m_d} \times 100 \quad \text{Eq 3.3}$$

3.5. Mechanical properties

Dog-bone shaped specimens of $12.5 \times 3.25 \times t$ mm (length \times width \times thickness, $t = 0.5-0.9$ mm), with a gauge length of 12.5 mm, were cut from the cast PGS/PXS sheets or spun fibre mat for mechanical testing. The tensile and cyclic testing were performed at room temperature with a mechanical tester (Instron series 5860) equipped with a 100 N load cell and using a cross-head speed of 10 mm/min for tensile tests and 25mm/min for cyclic tests as employed previously [119, 155]. The cyclic test specimens were stretched to a maximum strain of 15%, typical of the dynamic loading strain of soft tissues, such as cardiac muscle, under normal physiological conditions, with strains of less than 15% being relevant for most clinical applications [156]. The mechanical tests of PVA, PVA/PXS fibres and washed PVA-PXS fibre mats were carried out under both wet and dry conditions corresponding to the *in vivo* conditions for scaffold applications. For the hydration state, the spun mat materials were immersed in distilled water before the test. Because the samples of PGS and PXS are in the rubbery state, their stress-strain behaviour can be described by the equation of elasticity (Eq. 3.4) [157].

$$\sigma = \nu RT \left(\lambda - \frac{1}{\lambda^2} \right) \approx 3\nu RT \varepsilon \quad \text{Eq. 3.4}$$

where σ is the engineering stress, $\lambda = 1 + \varepsilon$ is the extension ratio, ε is the tensile strain, ν is the strand density, R is the universal gas constant and T is the absolute temperature. At low strains (i.e. at $\varepsilon = 10\%$) Equation 3.4 can be linearized with an error about 5%. Hence, the Young's modulus of

each specimen was determined by σ/ϵ at a strain of 10%. The ultimate tensile stress (UST) and the elongation at breaking value (ϵ_{\max}) were read directly at the breaking point of the tensile test. Resilience, a parameter used to describe the ability of a material to deform reversibly without a loss of energy, was calculated from the stress-strain data of the cyclic tests. For a strain of 15 %, the resilience of the material was expressed using the formula below:

$$\text{Resilience} = \frac{\text{Area under unloading curve}}{\text{Area under loading curve}}. \quad \text{Eq. 3.5}$$

3.6. Cytocompatibility *in vitro* (ISO 10993)

The biocompatibility of materials *in vitro* were tested by exposure of proliferating cell cultures to the extra media conditioned by material samples as they degrade (Chapters 4-6) or directly placed test material contact with cell monolayer (Chapter 7), according to the standard cytotoxicity assessment study set by the International Standardization Organization (ISO 10993). In this method, extracts were obtained by soaking the test and control materials in separate cell culture media (DMEM supplemented with 10% fetal calf serum (FCS), 1% L-glutamine and 0.5% penicillin/streptomycin) under conditions of 0.2g/mL of culture medium for 24h at 37°C/5% CO₂ in an incubator. The PDLLA (Chapters 4-6) or PLLA spun mesh fabricated as previous paper [145] (Chapter 7), was used as the material control. All test and control materials were used after sterilization by 70% alcohol/de-ionized water solution and dried at ambient conditions. A sample of cell culture medium alone was the negative control. Mouse fibroblasts, SNL (STO-Neo-LIF, purchased from the University of California Davis, USA), were seeded in standard media at a density of approximately 2000 cells/well in 96 well tissue 0.1% w/v gelatine coated plates; when 70% confluence of cells was established (in approx. 2 days), the medium in each well was entirely replaced with 0.2 ml of extra medium samples (medium pre-exposed to materials) (Chapters 4-6) or replaced with 0.2 ml standard media and directly placed test samples and control sample in contact with the cell monolayers covered with cell culture medium in each well (Chapter 7). All cultures were then cultured for two days.

At the end of the incubation period, the quantitation of cytotoxicity was carried out using a commercial kit, Tox-7 (Sigma-Aldrich). Spent culture media were collected and the degree of cell death was determined by measurement of lactate dehydrogenase (LDH) levels, as released into the culture media ('DEAD LDH'), using TOX-7 as described previously [119]. Finally, each well containing living cells was filled with 0.2 ml fresh cell culture medium, and cells were treated with lysis solution of Tox-7. These lysates were then used to determine the cellular LDH content, which equates to the number of living cells per well ('LIVE LDH'). The overall LDH level was determined by measuring the absorbance of the supernatant from the centrifuged medium at 490 nm (after subtraction for background absorbance at 690 nm) using a multiwell plate format UV-vis spectrophotometer (Thermo Scientific). The absorbance results of LDH were converted to the number of cells according to a linear standard curve.

Hence, cytotoxicity can be expressed as follows:

$$\text{Percentage of dead cells (\%)} = \frac{\text{DEAD LDH}}{\text{DEAD LDH} + \text{LIVE LDH}} \times 100 \quad \text{Eq. 3.6}$$

3.7. Proliferation in vitro: MTS

Cell proliferation was also assessed using a commercial AlamarBlue™ assay kit (Life Technologies). AlamarBlue™ is non-toxic to cells and does not interrupt cell culture growth, which allows for a continuous measurement of the cell proliferation kinetics. Hence, the Alamarblue™ assay is appropriate for evaluating the long-term cytotoxicity of biomaterials that undergo biodegradation under physiological conditions [158]. For this assay, culture media wells were seeded with SNL fibroblasts (2500 cells per ml) into each well of a 48-well plate and cultured as above, in the presence of sterilised PGS and PXS (test material) or sterilised PDLA (material control). Material-free media with cells (positive controls) and the cell culture medium alone (negative control) were also included in independent wells on the same plate.

After culturing for 48 h, 0.1 ml of the AlamarBlue™ indicator was added to each well (except for the background controls) and incubated under standard culture conditions for a further 5 h. The medium was then transferred to a new plate, followed by the measurement of the UV-vis absorbance of the medium at wavelengths of 570 and 600 nm. This procedure was repeated every

48 h until confluence was reached, which was typically after 6 days. Cell proliferation was quantified by the percentage reduction of AlamarBlue™ using the following equation [124]:

$$\text{Reduced\%} = \frac{\varepsilon_{\text{OX}}(\lambda_2)A(\lambda_1) - \varepsilon_{\text{OX}}(\lambda_1)A(\lambda_2)}{\varepsilon_{\text{RED}}(\lambda_1)A'(\lambda_2) - \varepsilon_{\text{RED}}(\lambda_2)A'(\lambda_1)} \times 100 \quad \text{Eq. 3.7}$$

where $A(\lambda_1)$ and $A(\lambda_2)$ are the absorbance values of test wells measured at wavelengths $\lambda_1=570$ nm and $\lambda_2=600$ nm, respectively, and $A'(\lambda_1)$ and $A'(\lambda_2)$ are the values of absorbance at the same wavelengths for negative control wells containing only culture medium and AlamarBlue™. All absorbance values were corrected for baseline variations by subtracting the corresponding readings of the background controls. The other parameters are as follows: $\varepsilon_{\text{OX}}(\lambda_1)=80.586$, $\varepsilon_{\text{OX}}(\lambda_2)=117.216$, $\varepsilon_{\text{RED}}(\lambda_1)=155.677$ and $\varepsilon_{\text{RED}}(\lambda_2)=14.652$.

3.8. Degradation test

3.8.1. PPS degradation test *in vitro* with esterase

The experimental procedures were published previously [159]. Briefly, the experiment was conducted using 48-well tissue culture plates. Discs (diameter of 11 mm) of the PPS polymers were weighed (giving a mass m_{od}), sterilised in 70 % alcohol, and dried in a tissue culture hood. Each specimen was then soaked in 0.5 ml culture medium in a well, with the addition of esterase at the concentration of ~ 1.5 units of esterase per mm^2 . These culture plates were placed in an incubator at 37 °C, with the esterase being added every day. At the intervals of 1, 2, 3, 4, and 3 weeks, the specimens were removed and weighted (giving a mass m_{td}) after they were washed with water and dried under vacuum at room temperature. The weight change percentage was calculated by using Eq. 3.8:

$$\text{Weight loss (\%)} = \frac{m_{\text{td}} - m_{\text{od}}}{m_{\text{od}}} \times 100 \quad \text{Eq. 3.8}$$

where m_{od} is the initial dried mass, and m_{td} is the vacuum dried weight measured after incubation.

3.8.2. Enzymatic and oxidation degradation of PGS and PXS materials

The $\text{FeSO}_4/\text{H}_2\text{O}_2$ medium was prepared based on Fenton's reagent, which contains 1% (v/v) of hydrogen peroxide with the $\text{Fe}^{2+}/\text{H}_2\text{O}_2$ molar ratio being 0.11 [160, 161]. Xanthine oxidase was dissolved at a concentration of 0.025U/ml in culture medium (see below). 1U was defined as the conversion of 1 $\mu\text{mol}\cdot\text{min}^{-1}$ of xanthine to uric acid at pH 7.5 and 25°C. Xanthine (1 μM) was

added to the incubation mixture in order to generate hydrogen peroxide and superoxide through xanthine oxidase activity which could then oxidize the polymer [162].

Samples of ~ 50mg (~75mm² of surface area) PPS samples were weighed and sterilised with 70% alcohol for 15 min followed by drying in a tissue culture hood for overnight. PPS samples were placed in a 48-well tissue culture plate filled with 0.3ml of Dulbecco's Modified Eagles Medium (DMEM). The PPS samples were divided into six groups and soaked in: (1) culture medium (DMEM) alone (control), or test groups containing either, (2) esterase (from porcine liver; Fluka), 0.3 unit esterase per mg polymer which was defined in pervious experiment [163]; (3) FeSO₄/H₂O₂ Fenton's reagent; (4) XO₂ of a concentration defined previously [164]; (5) FeSO₄/H₂O₂ and esterase; or (6) XO₂ and esterase.

The above culture plates were then placed in a 37°C culture incubator. The culture medium with solutions of enzymes were changed every second day while the esterase was supplemented daily, a procedure used in previous work [165, 166]. After incubation for 7, 14, 21, 28 and 35 days, specimens were removed from the culture plated, wiped and washed with water and dried in vacuum oven at room temperature until no further change in weighed was detected (giving a mass m_d). Five specimens from each experiment were measured. The percentages of weight loss were given by Eq. 3.8. The thickness of each specimen was also measured.

3.9. pH measurements of culture medium after incubation with PPS samples

Samples from the solution of each group (containing enzyme and degradation products from the specimens) were collected after 2 days of incubation for pH measurement to provide an indication of the degree of acidification of degradation environments. The pH of each solution was measured at 20°C by insertion of a glass pH electrode into the solution and recording of the reading after the electrode stabilised. This data was recorded as the difference in pH value of the solution in which the PGS or PXS samples were immersed and incubated for 2 days comparing with the culture medium, which has a pH = 7.4.

3.10. SEM characterisation

The surface morphology of sheet polymers (PGS cured at 130°C for 7 days and PXS cured at 130°C for 12 days) after incubation in six groups of media (blank media, media added with esterase, FeSO₄/H₂O₂ reagent, XOX, esterase plus FeSO₄/H₂O₂ reagent, and esterase plus XOX) for 35 days were characterised in a field emission gun (FEG) scanning electron microscope (SEM) (JEOL JSM 7001F) in Monash Centre for Electron Microscopy. The dried samples were platinum-coated and observed at an accelerating voltage of 5 kV.

The surfaces of the fibre meshes of the PVA fibres, the PXS/PVA fibres, the PXS/PVA fibres after the heat treatment and the PXS/PVA fibres after the heat treatment and washing with water were sputter coated with platinum to a thickness of 1nm and characterised using a SEM (FEI Nova Nano SEM 430) in Melbourne centre for nanofabrication, operated in second electron imaging mode with an accelerating voltage of 5 kV.

3.11. Statistical analysis

All experiments were run with three to five samples per experimental group, and the uncertainty in the data is shown as the standard error of the mean. One-way analysis of variance with Tukey's post-hoc test (using Prism 4, GraphPad Software, 2003) was performed to analyse the statistical difference, and a *p*-value of less than 0.05 was considered significant.

CHAPTER FOUR

SYNTHESIS, CHARACTERISATION AND PROPERTIES OF PGS PRE-POLYMER AND GEL

4.1. Introduction

As discussed in Section 2.4.1 Chapter 2. Poly(glycerol sebacate) (PGS) is a polyester elastomer which is biocompatible, biodegradable, inexpensive and generally has soft and flexible mechanical properties that make them suitable for working with soft tissue and organs in a mechanically dynamic environment, such as the beating heart or breathing lung [167].

PGS is synthesized through the polycondensation/esterification of trifunctional glycerol, HOCH₂CH(OH)CH₂OH, and difunctional sebacic acid, (HOOC)(CH₂)₈(COOH), normally with an excess of the stoichiometric alcohol groups. This synthetic procedure is typically [1] conducted in two steps: namely the polymerisation of the monomers to form a solvent-soluble pre-polymer followed by the gelling and crosslinking reaction step. The prepolymer is formed by heating a mixture of glycerol and sebacic acid in an inert gas atmosphere, which is purged through the reacting chamber to prevent reactant oxidation and evaporation of the volatile glycerol monomers. The pre-polymerisation conditions can vary (see Table 4.1) from temperatures between 110°C to 160°C and for 1 to 48 h [7, 102, 112]. Based on the known difference in reactivity of primary (–CH₂–OH) and secondary alcohol groups (>CH–OH) [168] [169], it is expected that the primary alcohol groups of glycerol will react faster with the carboxylic acids, forming unbranched polymer chains in the early stages of polymerisation. This factor, in combination with the stoichiometric imbalance of alcohol to acid groups, the reaction temperature and the time of pre-polymerisation, is expected to result mainly in esterification of the primary hydroxyl groups to form linear polymer chains, with few reacted secondary –OH groups involved in the esterification process. The resulting non-crosslinked pre-polymer mixtures are soft, flow at about 50°C and can be dissolved into solvents, such as methanol, acetone and tetrahydrofuran (THF) for the fabrication of various forms (e.g. thin sheet [7], porous scaffold [170] and fibrous mesh [115]). This shaped pre-polymer is then further cured for several days at the same temperature as in the first step but under vacuum to remove the water by-product. During this second-step, it is assumed that the depletion of the primary alcohol groups in the reacting system would lead to reaction of the secondary hydroxy groups to form ester branches and crosslinks between the polymer chains [114].

Table 4.1 Thermal synthesis conditions of PGS in previous studies

Group	Pre-polymerisation conditions	Polymerisation conditions	Mechanical properties	Application	Ref
Langer (MIT)	120 °C-24h argon gas, then 120 °C-5h, 5.3 Pa	120 °C - 48h, 5.3Pa	Elongation 270±60% E=0.28±0.03MPa		[1, 111]
		Film with the capillary network pattern: 150 °C for 13h, 0.7 Pa Flat film: 120 °C - 28h, 0.7Pa Bond further cure 120 °C - 24h		Endothelialized microvasculature	[171]
	120 °C-24h nitrogen gas, then 120 °C-24h, 5.3 Pa	150 °C-48h, 13.3 Pa		PGS scaffold	[110]
	120 °C-24h nitrogen gas, then 120 °C-48h, 5.3 Pa	120 °C - 24h, 5.3 Pa		Nerve guide material	[125]
	120 °C-24h nitrogen gas 70-80% of the theoretical water by-product was collected	120 °C - 42, 66, 90 or 114h, 1.4 Pa	E, strain to failure and UTS varied with curing times (E=0.3-1.5MPa)		[120]
	120 °C-24h nitrogen gas, then 28h vacuum	Membrane: 150 °C-15h, 6.7 Pa Microfluidic device: 135-140 °C-18h and further bond layers at 120 °C - 15h, 150 °C-7.5h		Microfluidic scaffolds	[8, 102]
Chen (Monash University)	110 °C-24h argon gas	110 °C - 48h	E=0.056±0.011MPa	Elastomer for myocardial tissue	[7, 124]
	120 °C-24h argon gas	120 °C - 48h	E=0.22±0.03 MPa		
	130 °C-24h argon gas	130 °C - 48h	E=1.20±0.08 MPa		

PGS has been investigated by a number of research groups [7, 102, 112, 172] and synthesised under differing temperatures and durations, giving different mechanical properties, as listed in Table 4.1. However, the copolymerisation of glycerol and sebacic acid reported by various studies using similar conditions has not produced consistent materials [112, 113]. For example, in our previous studies on surgical sealants, a non-crosslinked pre-polymer of PGS synthesized at 110°C for 96 hours, was soluble in THF and flowed at 40-50°C [114], whereas a permanently crosslinked PGS solid was formed under the apparently identical synthesis conditions in another study [113]. Similar discrepancies in properties were also found in studies carried out by other research groups. For example, the synthesis of PGS at 120°C for 96 hours by Wang and co-workers [42] produced a crosslinked PGS elastomer, while in the work of Yi and Lavan[115] and of Ravichandran and co-workers [173], a PGS pre-polymer was synthesised under the same conditions but it was soluble in THF. Presumably, the above discrepancies result from differences in the extent of esterification, or in the ratio of esterified secondary to primary alcohols, or in the monomer composition of the final polymer. For example, the synthesis conditions can vary significantly from one research laboratory or group to another, and the temperature uniformity of a vacuum oven is $\pm 1^\circ\text{C}$ at best, and typically 2.5°C which can significantly change the crosslinking kinetics of PGS. Secondly, glycerol is volatile at the typical PGS synthetic temperatures (at 130 °C the vapour pressure is 173.3 Pa) [174] and forms an azeotrope with water [175] and so its loss during evaporation of the water by-product is inevitable, and both the flow rate of the inert gas purge and the capacity of the vacuum pump can

greatly affect the loss of glycerol during synthesis. Consequently, different research groups have reported different crosslink kinetics for the supposedly 'same' PGS polymers under the 'same' conditions. This work aims to determine the causes for these inconsistencies.

There have been several papers published on the characterisation of PGS and related polymers. Nagata and co-workers [176, 177] used infrared spectroscopy to estimate the extent of esterification in copolymers of glycerol with a series of aliphatic dicarboxylic acids and related this to their physical and mechanical properties and the rate of alkaline and enzymatic hydrolysis. Qui and co-workers [172] presented the proton NMR spectrum of a low molecular weight PGS prepolymers and characterized the swelling, thermal behaviour, mechanical properties of its crosslinked gel. The proton NMR spectrum of acrylate modified PGS was used by Nijst and co-workers [25] to verify the success of the acrylation reaction. Uyama and co-workers [178, 179] enzymatically synthesized linear polyesters from divinyl sebacate and triols (including glycerol) at 60°C and used ^{13}C NMR to investigate the glyceride units in the uncrosslinked PGS polymer. Very recently You and co-workers [180] synthesized novel linear PGS polymers by ring opening of diglycidyl sebacate and characterized the polymer by proton and carbon NMR. However, there do not appear to be any NMR studies of the crosslinked PGS gel which are needed to fully understand the properties of these materials.

Thus it appears that optimization of the properties of crosslinked PGS requires their structural characterisation and so the primary objective of this study is to explore the effect of synthesis conditions on the structure and properties. The extent of esterification reaction during the pre-polymerisation and curing process was estimated by titration of the unreacted carboxylic groups and by the mass loss during polymer synthesis associated with water evaporation. The extent of glycerol evaporation of monomers was determined by comparison of these two methods. We have also quantitatively analysed the molecular structure of the PGS pre-polymers and the cross-linked PGS polymer network by ^1H , ^{13}C and carbon-proton-2D-nuclear magnetic resonance (NMR). This structural information was then related to the mechanical properties and cytocompatibility of PGS gel.

4.2. Results and discussion

4.2.1. Esterification degree

As described above, the extent of reaction in the PGS prepolymers and gels was determined with two methods, i.e. titration of acid groups and measurement of mass loss. The data are given in Table 4.2 and illustrated in Fig. 4.1. The reaction percentages measured by the two methods were reasonably consistent for the PGS prepolymers, with the value estimated by the mass loss method being slightly higher than that measured by titration. However, in the crosslinked polymers, those estimated by mass loss were not only significantly higher than those measured by titration, but also unreasonably higher than 100%, which can be attributed to the loss of glycerol due to its volatile nature. Loss of reactants was confirmed by NMR spectra of the water condensed during the PGS synthesis - during the post-curing stage, the aqueous solution had considerable quantities of glycerol but only minimal levels of sebacic acid. In the case where equimolar amounts of glycerol and sebacic acid are used, the loss of glycerol by evaporation during the polymerization can be estimated from the percentage reaction measured by titration (P_1) and mass loss (P_2) methods:

$$P_2 - P_1 (\%) = \left[\frac{(m_{\text{H}_2\text{O}} + m_{\text{Gly lost}}) / M_{\text{H}_2\text{O}}}{2 \times m / (M_{\text{Gly}} + M_{\text{SA}})} - \frac{m_{\text{H}_2\text{O}} / M_{\text{H}_2\text{O}}}{2 \times m / (M_{\text{Gly}} + M_{\text{SA}})} \right] \times 100 = \frac{m_{\text{Gly lost}} / M_{\text{H}_2\text{O}}}{2 \times m / (M_{\text{Gly}} + M_{\text{SA}})} \times 100$$

$$\text{Glycerol loss (\%)} = \frac{m_{\text{Gly lost}} / M_{\text{Gly}}}{m / (M_{\text{SA}} + M_{\text{Gly}})} \times 100 = \frac{2 \times M_{\text{H}_2\text{O}} (P_2 - P_1)}{M_{\text{Gly}}} \quad \text{Eq. 4.1}$$

where $m_{\text{Gly lost}}$ is the mass loss of glycerol. In the prepolymerization stage only 1.5 wt% of glycerol was lost. Hence, the inert gas purging designed to prevent oxidation of the reactants can also avoid the loss of volatile glycerol. However in the postcuring stage of the cast sheets, large and increasing amounts of glycerol were lost, probably due to the vacuum conditions during the crosslinking treatment and the high surface area of the thin sheets. Hence, further modification of the crosslinking methodology is necessary to reduce glycerol evaporation.

Table 4.2 also shows that due to the differing reaction times at 130 °C and 150 °C, the percentage esterification is slightly higher at 130 °C but is between 67 and 74%. During the postcuring stage, the conversion of carboxylic acid groups increased relatively rapidly to > 90% during the first 48 hours of crosslinking treatment at 130°C, and then increased slowly to about 95-97%.

The 1:1 molar glycerol-sebacic acid system was found to gel at $84.02 \pm 0.03\%$ (for PGS prepolymerised at $130^\circ\text{C}/24\text{h}$ then cured at $130^\circ\text{C}/20\text{h}$) or $85.04 \pm 0.02\%$ (for PGS prepolymerised at $150^\circ\text{C}/8\text{h}$ and then cured at $130^\circ\text{C}/20\text{h}$) conversion of carboxylic acid groups. If one assumes that all the hydroxyl groups are equally reactive, then the theoretical value [181] for the gel point conversion of carboxylic acid groups has a similar value of 87% which suggests that, at least in the later stages of reaction, transesterification reactions tend to reduce the effect of differences in reactivity of the primary and secondary hydroxyl groups. It should be noted that the corresponding theoretical conversion of hydroxyl groups at the gel point for this equimolar system would be 58% implying that considerable amounts of free glycerol are available for evaporative loss in agreement with the calculated losses of glycerol listed in Table 4.2.

Table 4.2 Conversion estimated by weight loss of the water by-product and by acid group titration.

PGS Pre-polymerization condition	Post curing time at 130°C (hours)	Esterification percentage (%)		Fraction of glycerol loss (%)*
		Mass loss	Titration for $-\text{COOH}$ groups	
$130^\circ\text{C}/24\text{h}$	0	77.8 ± 0.2	74.3 ± 0.9	1.4
	19		82.92 ± 0.02	
	20		84.02 ± 0.03	
	48	143 ± 12	90.7 ± 0.2	20
	72	154 ± 8		
	96	166 ± 6	94.27 ± 0.07	23
	168	172 ± 4	95.51 ± 0.03	28
$150^\circ\text{C}/8\text{h}$	0	70.8 ± 0.4	67.0 ± 0.6	1.5
	19		83.41 ± 0.01	
	20		85.04 ± 0.02	
	48	159 ± 1.1	91.09 ± 0.03	26
	72		93.05 ± 0.10	
	96		93.62 ± 0.05	
	168	173 ± 1.2	97.5 ± 0.07	30

* estimated from the difference in conversion by mass loss and carboxylic acid consumption (see Equation 4.1)

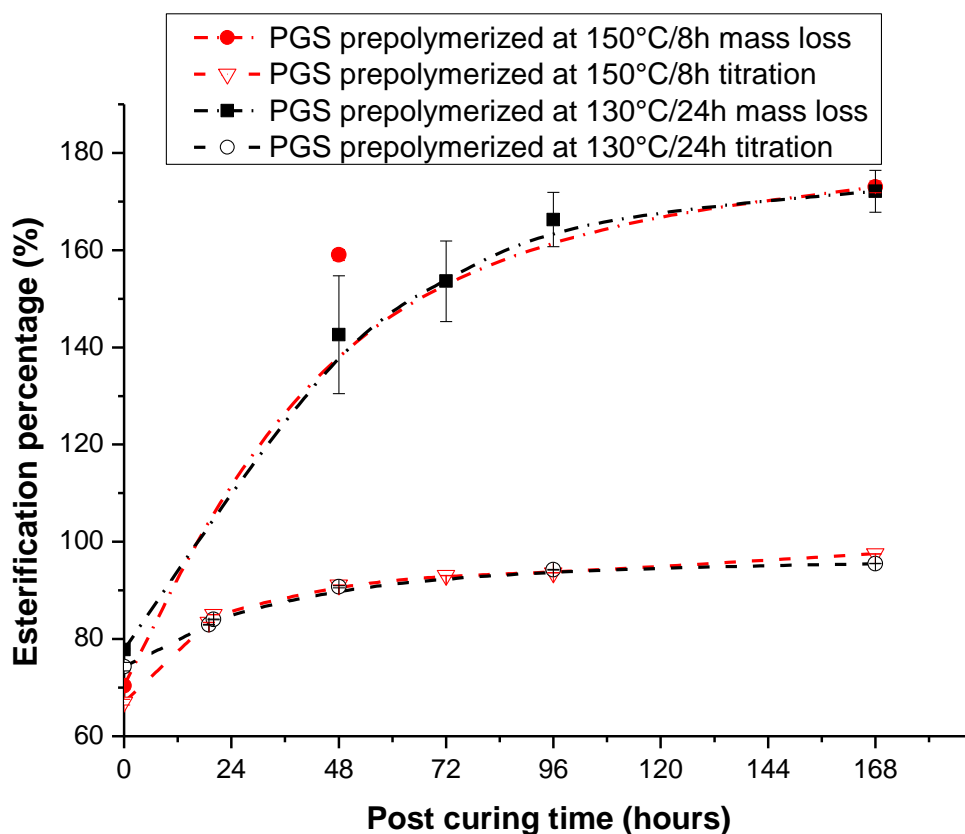


Fig. 4.1 The apparent percentage of esterification, calculated from mass loss and acid-group titration, in PGS samples prepared by different pre-polymerisation conditions: PGS treated for different pre-conditioning at 130 °C/24 hours or 150 °C/8 hours followed by post curing at 130 °C for different times. Samples postcured less than 20 hours were fully soluble in THF. After postcuring for 20h or more the PGS sample were not soluble in THF and formed crosslinked gel.

4.2.2. Analysis of PGS structure by NMR

PGS pre-polymers synthesized at 130°C for 24 hours or at 150°C for 8 hours, and also the crosslinked PGS synthesized for 8h at 150°C plus 48 hours at 130°C were analysed by NMR using acetone- d_6 as the deuterated solvent. This choice of this solvent was important because NMR signals are solvent dependent [154] and acetone- d_6 was a much better solvent for the pre-polymers compared with $CDCl_3$. The full 1H -NMR for the PGS prepolymer is given in Fig. 4.2a. As expected, the spectrum exhibits the shielded methylene protons of sebacic units between 1.3 and 2.5 ppm while the deshielded methylene protons of the glycerol unit occur between 3.5 and 4.4 ppm. The assignments given in Fig. 4.2a are based on their chemical shift and the integral ratios and are in agreement with the data of Liu and co-workers [172] on a PGS prepolymer in $CDCl_3$. Some of the methine protons of the glycerides are seen between 4.9 to 5.3 ppm as expected and in fact three of the five glycerides are observed in Fig. 4.2b [154].

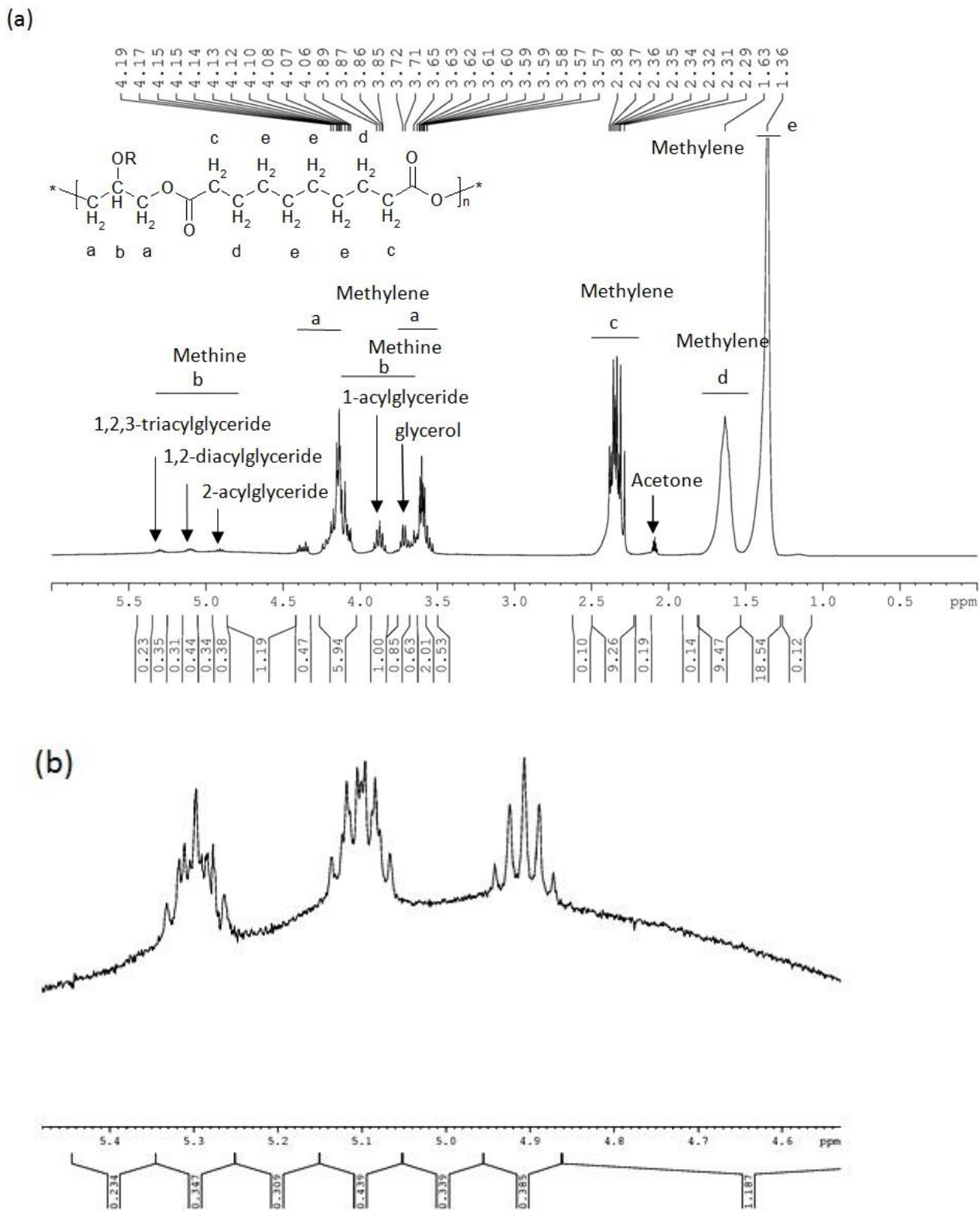


Fig. 4.2 a) Full ^1H -NMR spectrum, in acetone- d_6 , of the pre-polymer synthesized at 150°C for 8h. The resonance assignments of the polyester are given in the structure. The peak at 2.1 ppm is due to ^1H acetone impurities. b) Close up of the methine hydrogens of glycerol due to the 1-, 1,2- and 1,2,3-glycerides.

Fig. 4.3a shows the full ^{13}C NMR spectrum of PGS. The sebacate methylene carbons are located at 25-34ppm (the methylene next to the carboxylic acid at 33ppm, the methylenes adjacent to the $-\text{CH}_2-\text{COO}-$ near 29ppm and central methylenes at 24.5ppm), the methylene and methine carbons of the glycerol and glyceride units are between 60-75ppm, the carboxylic acid and ester carbon at 172.6 and 174ppm, respectively. These assignments are consistent with the ^{13}C NMR study of monocarboxylic esters of glycerol by Gunstone [87, 182, 183] and Vlahov [184]. The NMR spectrum of the PGS gel given in Fig. 4.3b and Fig. 4.4b shows considerable line broadening as expected of a crosslinked polymer [154, 185] but the peak positions correspond to those in the prepolymer.

For the pre-polymer synthesized at 150°C for 8h, twelve ^{13}C -NMR glyceride signals are visible in Fig. 4.4a and most of the corresponding peaks are also found in the PGS gel (Fig. 4.4b) except for the 2-acylglyceride. The corresponding DEPT NMR experiment identified eight CH_2 (up) and six CH - (down) signals in the glyceride region of the pre-polymer and glycerol monomer synthesized at 150°C for 8h, as shown in Fig. 4.5a, and these peaks also occur in the gel DEPT spectrum (Fig.4.5b) except for the 2-acylglyceride.

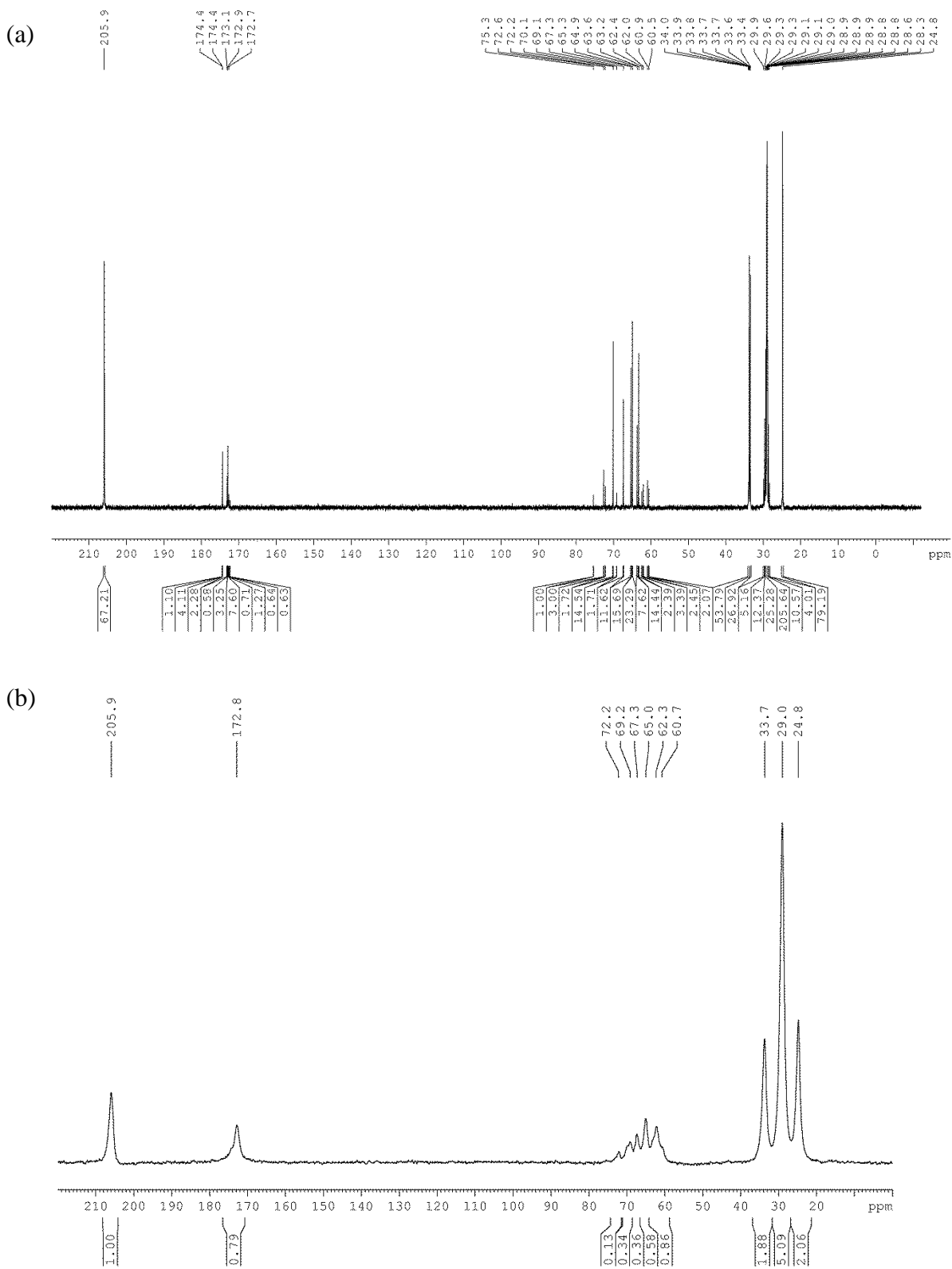


Fig. 4.3 ^{13}C -NMR spectra. a) Full spectrum of the PGS pre-polymer polymerized at 150°C for 8h. b) Full spectrum of cross-linked polymer gel of poly(glycerol sebacate) prepared at 150°C for 8h, then 130°C for 48 hours. The peak at 205.9 ppm is due to deuterated acetone solvent.

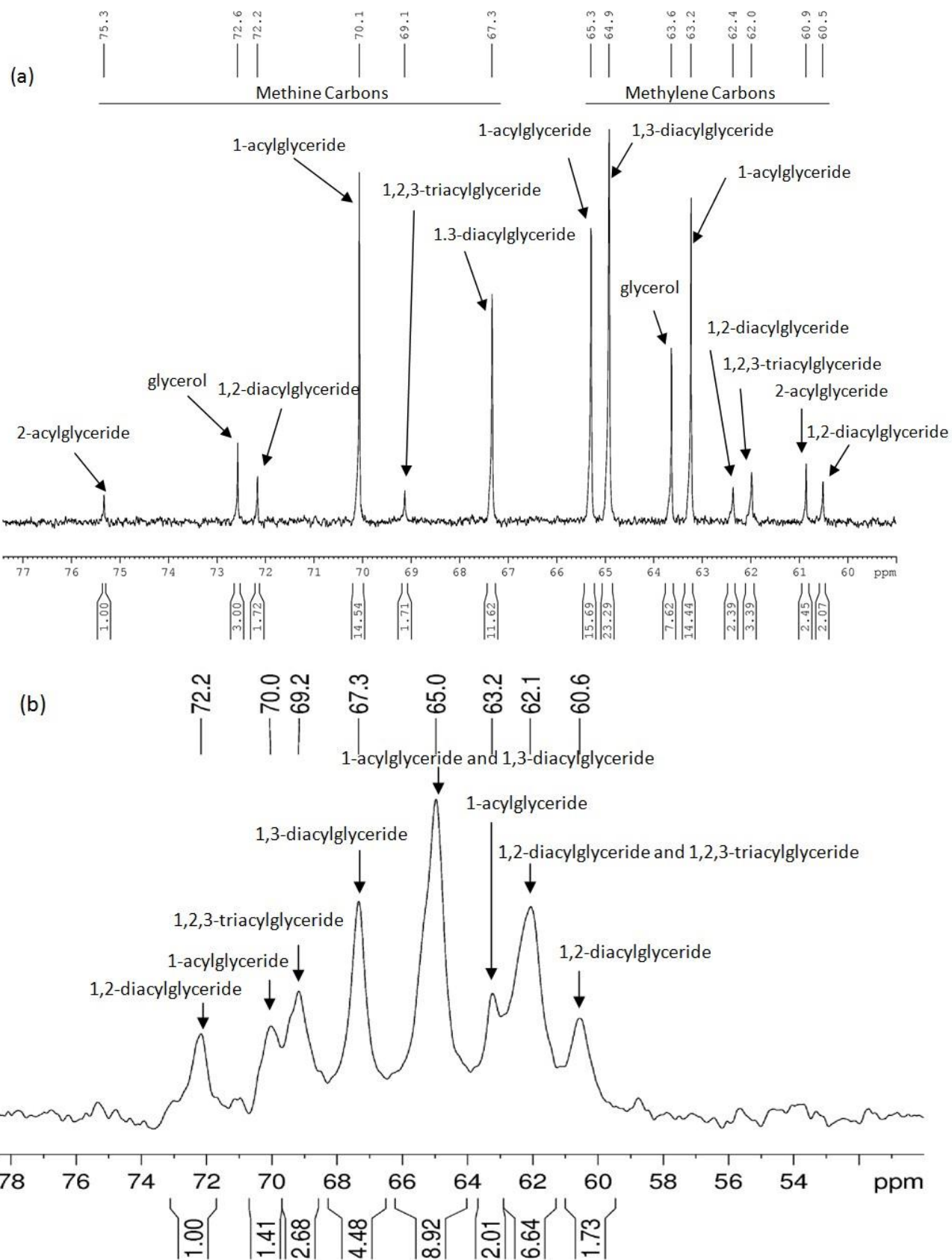


Fig. 4. ^{13}C NMR spectra in the of glyceride region. a) PGS pre-polymer polymerized at 150°C for 8h. b) Gel prepared at 150°C for 8h, then 130°C for 48 hours.

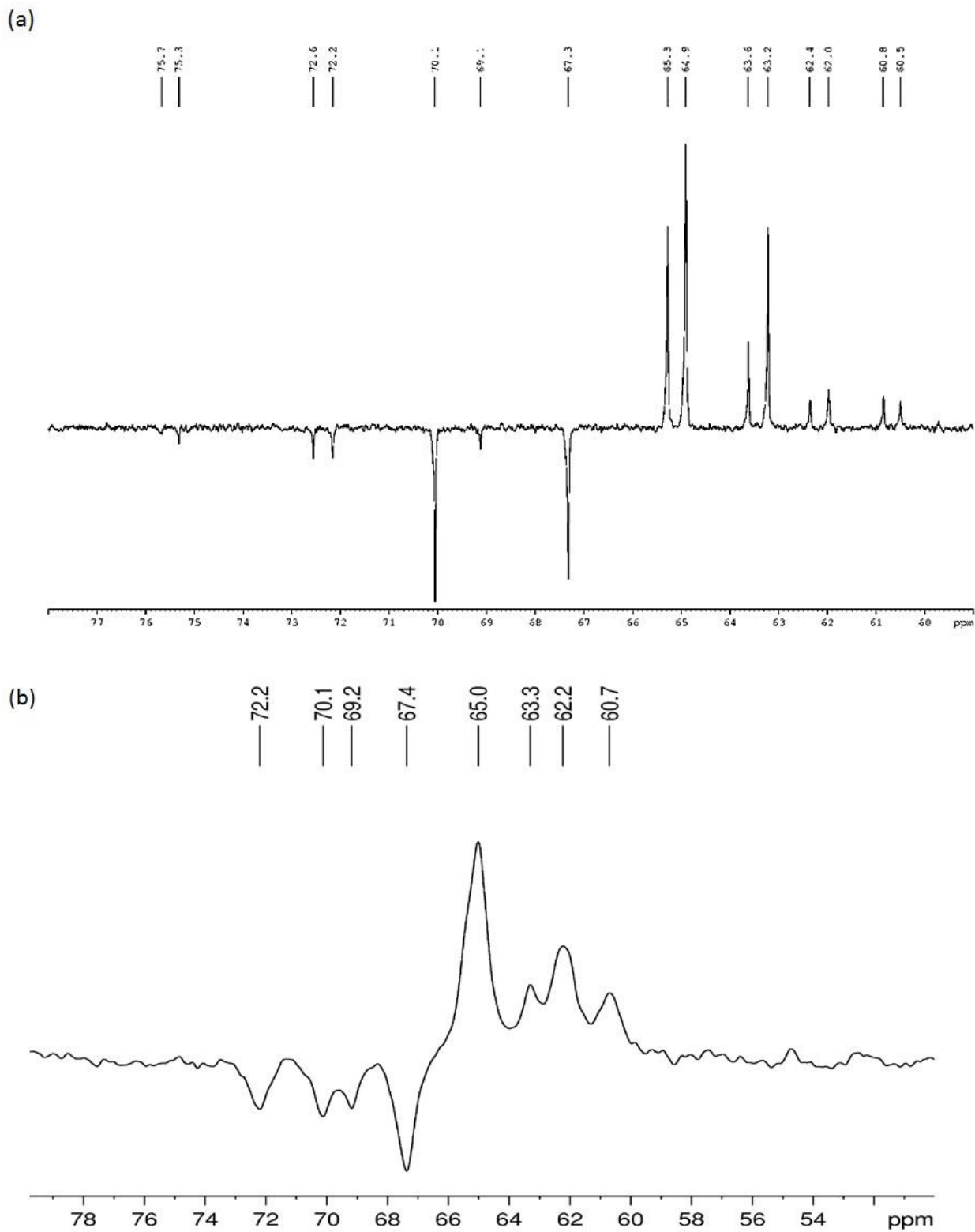


Fig. 4.5 DEPT ^{13}C NMR spectra differentiating the methine (downward pointing peaks) and methylene carbons (upward pointing peaks). a) Spectrum of PGS pre-polymer polymerized at 150°C for 8h. b) Spectrum of the polymer gel cross-linked 150°C for 8h, then 130°C for 48 hours.

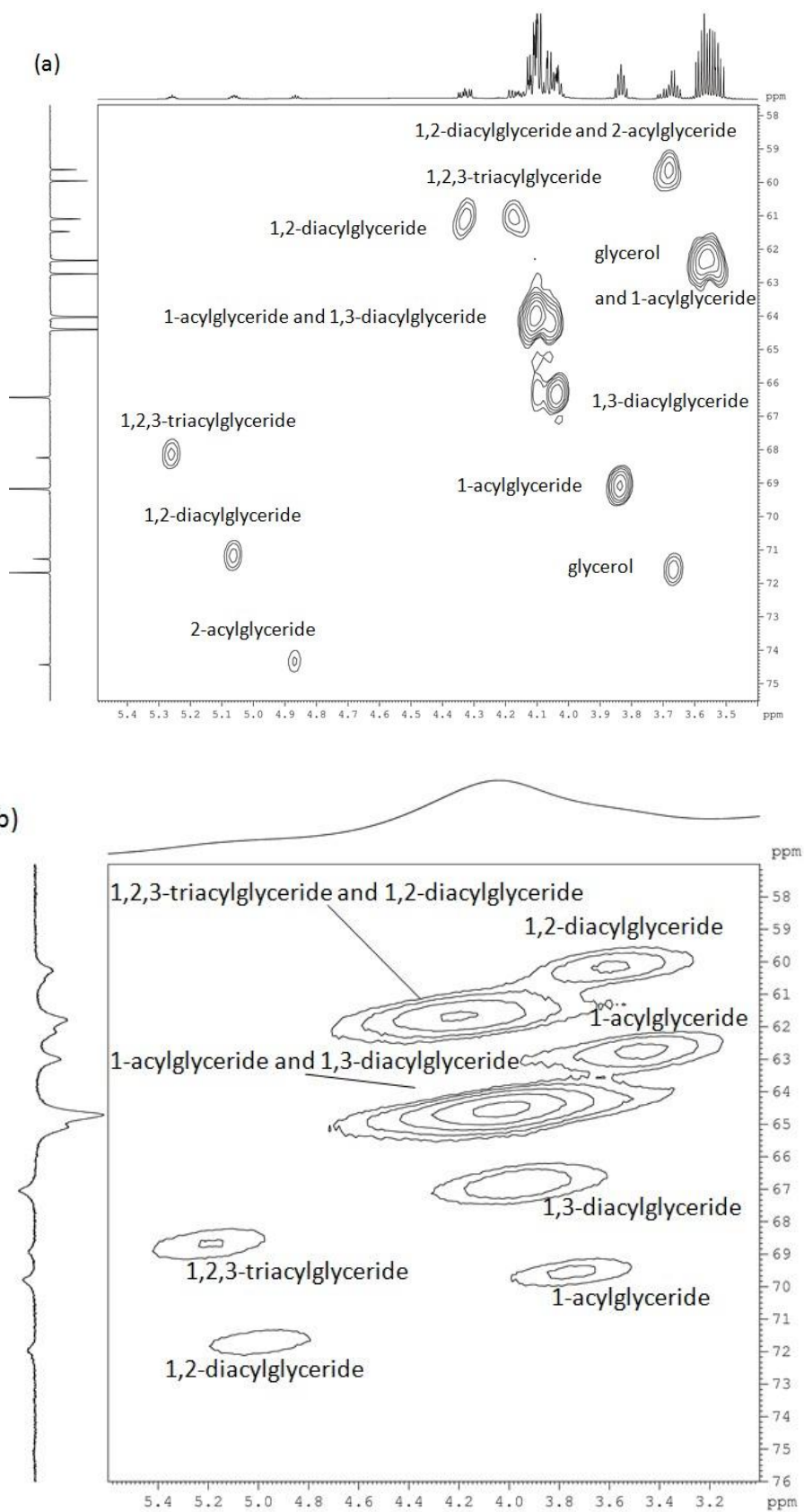


Fig. 4.6 Proton-carbon correlation spectrum of (a) PGS pre-polymerized at 150 °C for 8 hours and (b) PGS gel at 150 °C for 8 hours and cured 48 hours at 130 °C.

The proton-carbon correlation spectrum of the PGS prepolymer synthesized at 150 °C for 8 h accurately relate the carbons to their protons as shown in Fig. 4.6a. Thus the 2-acylglyceride (carbon at $\delta=75.3$ ppm is connected to the proton, with a pentet at $\delta=4.86$ ppm); the 1,2-diacylglyceride (carbon at $\delta=72.2$ ppm is connected to a proton with a deformed pentet at $\delta=5.06$ ppm); and the 1,2,3-triacylglyceride (carbon at $\delta=69.1$ ppm is connected to a proton with a symmetrical multiplet at $\delta=5.25$ ppm). Through space, these latter methine-protons are more deshielded as a result of the proximity of one or more polar carboxylic ester groups. The methine-carbons of the 1-acylglyceride and 1,3-diacylglycerides can also be mapped easily on the 2D NMR plot but only in the case of the 1-acylglyceride can this be directly related to a proton pentet at $\delta=3.87$ ppm. The unreacted glycerol methine proton is also visible at 3.7 ppm, however it is partly overlapped by the glyceride methylene protons. Although the proton axis of the proton-carbon correlation spectrum of the polymer gel in Fig. 4.6b shows only broad curves, this 2-D plot can be directly related to the proton-carbon correlation spectrum of the pre-polymer shown in Fig. 4.6a, and thus in conjunction with the ^{13}C -NMR spectrum (Fig. 4.4b) it is still a very useful indicator of the polymers structure and shows that the 2-acylglyceride fragment is not present. Thus by integration of the methine carbon signals, the distribution of the differing glycerides could be measured for both the pre-polymer and gel and these are given in Table 4.3.

For the pre-polymer synthesized at 150 °C for 8h, twelve ^{13}C -NMR signals in the spectrum corresponding to all twelve predictable ^{13}C -NMR signals for the 1-monoacylglyceride (three peaks), 2-monoacylglyceride (two peaks), 1,2-diacylglyceride (three peaks), 1,3- diacylglyceride (two peaks) and 1,2,3-triacylglyceride (two peaks) are visible in Fig. 4.4a, and two additional small peaks are present due to glycerol monomer. The assignments are consistent with the ^{13}C -NMR signals obtained by Gunstone on small molecule glycerides in CDCl_3 [87, 182, 183]. The pre-polymer synthesized at 130°C for 24h showed peaks with almost identical chemical shifts, but the 2-monoacylglyceride signal was very small and all of the peaks give slightly different integrations due to differences in the degree of polymerization and glyceride content.

Uyama[178, 179] used ^{13}C NMR to investigate the glyceride units in the PGS. Unfortunately, the solvent used in their NMR experiment was not given and so there is an unknown solvent effect on their chemical shifts [154]. Also unfortunately these workers did not focus on the proton NMR region between 4.85 to 5.3 ppm which shows the methine protons of the 2-acylglyceride (4.9 ppm, methine proton deshielded by one carboxylate group), 1,2-diacylglyceride (5.1 ppm, methine proton deshielded by two carboxylate groups) and the 1,2,3-triacylglyceride (5.3ppm, methine proton

deshielded by three carboxylate groups) (see Fig 4.2b). The ^1H NMR of their 2D-figure shows that the 2-acylglyceride is absent in their polymer. Since accurate assignment of the methine protons of the 2-acylglyceride, 1,2-diacylglyceride and 1,2,3-triacylglyceride is essential to show the relationship in the proton-carbon correlation experiment, it is difficult to understand how their assignment of the 1,2-diacylglyceride and 1,2,3-triacylglyceride methine carbons were made. In fact, the assignment of the 1-acyl and 1,2-diacyl substituted glycerides are reversed and six of their ten ^{13}C assignments are incorrect.

The percentage of glyceride esters units of poly(glycerol sebacate) measured from the integrated areas of the methine carbon peaks of the ^{13}C NMR spectra are listed in Table 4.3 and this can be related to the extent of reaction which increases in the order: PGS prepolymer (150 °C/8h) < PGS prepolymer (130 °C/24h) < PGS gel. Thus the percentages of glycerol and the two monoacylglycerides decrease (see Table 4.3) as the extent of reaction proceeds whereas the concentrations of diacylglycerides and the triacylglyceride increase, as is expected. In addition, in all cases the 2-monoacylglyceride concentration is less than for the 1-monoacylglyceride, as expected from the reactivity differences in the secondary and primary glycerol alcohols [168, 169], and in the case of the prepolymers this is even less than the concentration of free glycerol. Unexpectedly, for all polymers the 2-monoacylglyceride is in lower concentration than the 1,2-diacylglyceride and the reason for this is unclear. For the two most highly reacted polymers (PGS prepolymer reacted at 130 °C/24h and PGS gel), the 1,3-diacylglyceride has the highest concentration whereas the main glyceride for the PGS prepolymer (150 °C/8h) is the 1-substituted species. Because the 1,2,3-triacylglyceride is the branching point in the polymer and thus leads to crosslinking, it is not surprising that the gel has by far the greatest concentration of this species.

As a comparison of the number fraction of each glyceride structures measured by the integrated areas of the methine carbon peaks of the ^{13}C NMR spectra of the polymer (see Table 4.3), we have also estimated these fractions from simple probability theory, based on an assumption that each hydroxy group had equal reactivity. For example, if q is the fraction of hydroxyl groups, the fraction of 1,2,3-trisubstituted glyceride is $(q)^3$ and the fraction of 1,2-disubstituted triglyceride is $2(1-q)(q)^2$. The values in Table 4.3 were calculated from the conversion of the COOH (p) groups determined by and the stoichiometry of the system:

$$q = \frac{[\text{COOH}]_0}{[\text{OH}]_0} \times p \quad \text{Eq. 4.2}$$

If there is no glycerol loss in the synthesised polymer then $q = 3p/2$, but in Table 4.3 corrections were made when significant levels of glycerol were lost. The predicted acyl-glyceride fractions in the PGS samples are significantly different from those calculated from the integrated areas of the methine carbon peaks of the ^{13}C NMR spectra of the polymers. When one allows for glycerol loss during synthesis, the amount of triglyceride was overestimated by the statistical calculation because the secondary alcohol was assumed to be as reactive as the primary alcohols - of course if the secondary alcohol was non-reactive then no triglyceride would be formed. The 1,2-diglyceride was overestimated and the 1,3-diglyceride was underestimated because the secondary alcohol is less reactive than the primary alcohols. Similarly the 2-monoglyceride was overestimated and, when one allows for glycerol loss during synthesis, the 1-monoglyceride was underestimated by the theoretical calculations. Finally, for the same reasons the amount of glycerol remaining in the reaction mixture was overestimated by theory. Thus, the NMR data suggests that primary hydroxy groups have higher reactivity than the secondary hydroxy groups as demonstrated by Rowland and co-workers [169] from studies of the reaction rate and the equilibrium constant for the primary and secondary hydroxyl groups.

Table 4.3 The percentage of glyceride esters units in PGS samples measured from the integrated areas of the methine carbon peaks of the ^{13}C NMR spectra of the polymers in acetone- d_6 at 30°C , with the reference peak of acetone, $\text{C}=\text{O}$, at 205.87 ppm. The chemical shifts beneath the structures refer to the carbon atoms above them. These are compared with those calculated from the statistical distribution of species assuming the fractional conversion of hydroxyl groups (q) is the same for primary and secondary alcohols.

	Glycerol		1-monoacylglyceride		2-monoacylglyceride		1,2-diacylglyceride		1,3-diacylglyceride		1,2,3-triacylglyceride	
Structure and chemical shift (ppm) of glycerides	$\text{HO}-\text{CH}_2-\overset{\text{OH}}{\text{CH}}-\text{CH}_2-\text{OH}$ 64.0 72.9 64.0		$\text{RO}-\text{CH}_2-\overset{\text{OH}}{\text{CH}}-\text{CH}_2-\text{OH}$ 63.2 70.1 65.3		$\text{HO}-\text{CH}_2-\overset{\text{OR}}{\text{CH}}-\text{CH}_2-\text{OH}$ 60.9 75.3 60.9		$\text{RO}-\text{CH}_2-\overset{\text{OR}}{\text{CH}}-\text{CH}_2-\text{OH}$ 60.5 72.2 62.4		$\text{RO}-\text{CH}_2-\overset{\text{OH}}{\text{CH}}-\text{CH}_2-\text{OR}$ 64.9 67.3 64.9		$\text{RO}-\text{CH}_2-\overset{\text{OR}}{\text{CH}}-\text{CH}_2-\text{OR}$ 62.0 69.1 62.0	
Percentage of glyceride ester units (%)	NMR*	$(1-q)^3$	NMR*	$2(1-q)^2q$	NMR*	$(1-q)^2q$	NMR*	$2(1-q)q^2$	NMR*	$(1-q)q^2$	NMR*	q^3
PGS: 150°C -8 h	9	17 ^a	43 ^a	27 ^a	3	14 ^a	5	22 ^a	35	11 ^a	5	9 ^a
PGS: 130°C -24 h	3	13 ^a	32 ^a	25 ^a	~0	13 ^a	7	25 ^a	48	12 ^a	10	12 ^a
PGS: 150°C -8 h + 130°C -48 h (crosslinked)	~0	6 ^a	15	19 ^a	~0	10 ^a	10	29 ^a	47	14 ^a	28	22 ^a
		1 ^b		6 ^b		3 ^b		24 ^b		12 ^b		55 ^b
		3 ^c		12 ^c		6 ^c		29 ^c		15 ^c		35 ^c

*: Percentage of glyceride esters in PGS samples measured from the integrated areas of the methine carbon peaks of the ^{13}C NMR spectra of the polymers

^{a,b,c} These values are calculated based on the titration results of $-\text{COOH}$ groups given in Table 4.2:

^a Assuming glycerol loss is 0%;

^b Assuming glycerol loss is 26% (the value calculated from mass loss in Table 4.2);

^c Assuming glycerol loss is 14%, which is calculated from the integrated areas of the glyceride region (59-79 ppm) and methylene carbon peaks of the sebacic region (20-40 ppm) in ^{13}C NMR spectra of the polymer. The latter area also contains the peaks for methyl acetone- d_6 peak (~30 ppm) and this was subtracted from the integral on the basis that it is equal to twice the integrated area of the carbonyl acetone- d_6 peak (~205.87 ppm).

4.2.3. Mechanical properties of PGS

When the PGS polymers were synthesised under different conditions, they showed similarly shaped stress-strain curves (Fig. 4.7a) with no stress whitening or plastic deformation artefacts which is consistent with their elastomeric state. The average ultimate tensile stress (UTS) and Young's modulus (E) of the PGS polymers monotonically increased with curing duration, ($p > 0.05$) while the strain at break (ϵ_{\max}) decreased, as shown in Fig. 4.7b. After a long curing time (> 96 hours), a high conversion percentage of the materials was achieved and the UTS, E and ϵ_{\max} approached a plateau.

The UTS and ϵ_{\max} of PGS samples synthesised under different reaction conditions are plotted in Fig. 4.8 against the strand density calculated from the rubbery modulus using Equation 3.4. The tensile strength rises and the elongation to break decreases monotonically as the strand density increases. Taylor and Darin[186] have derived a theory for the dependence of the extension ratio at break ($\lambda_{\max} = 1 + \epsilon_{\max}$) and UTS on the strand density:

$$\lambda_{\max} = k_1 \nu^{-0.5} \quad \text{Eq. 4.3}$$

$$\text{UTS} = k_2 \nu \left\{ 1 - \frac{1}{(1 + k_3 \lambda_{\max}^3)^{0.5}} \right\} \approx k_2 \nu \quad \text{when } \lambda_{\max} \text{ is high (i.e. UTS is low)} \quad \text{Eq. 4.4}$$

where ν is the strand density (calculated by Eq. 3.4), k_1 , k_2 and k_3 are constants and the exponent n has a theoretical value of 0.5. This theory is based on the concept that the UTS is determined by the extent of strand orientation during deformation, and that λ_{\max} is determined from the average Gaussian end-to-end distance of the network strands (proportional to the square root of the number of chain bonds) and the extended strand length (proportional to the number of chain bonds). The values of ϵ_{\max} for the PGS samples are plotted versus the strand density in Fig. 4.8a. The data fits to a power law with exponents of 0.541 and 0.498 which is very close to the theory. In Fig. 4.8b the UTS data is found to be approximately linear with strand density in agreement with the prediction of Taylor and Darin[186].

Fig. 4.8 also shows that PGS samples prepolymerized at the lower temperature (130 °C) but with the same strand density as those prepolymerized at 150°C have higher UTS and a marginally higher ϵ_{\max} . This observation of lower UTS and ϵ_{\max} of PGS prepolymerised at 150°C compared

to 130°C (Fig. 4.7 and Fig 4.8) may be due to a greater fraction of longer and more orientable network strands caused by a greater loss of excess glycerol at the higher temperature which according to the theory of Taylor and Darin [186] should raise the strength. From the conversion estimates in Table 4.2, PGS pre-polymerised at higher temperature 150°C loses slightly more glycerol (1.5%) than same prepolymer synthesized at the lower temperature (1.4%). In addition the NMR results show that the higher temperature decreases the orientable chain length by encouraging the secondary hydroxyl with low level 2-monoacylglyceride formation (3%) compared to none formed at 130°C (Table 4.3).

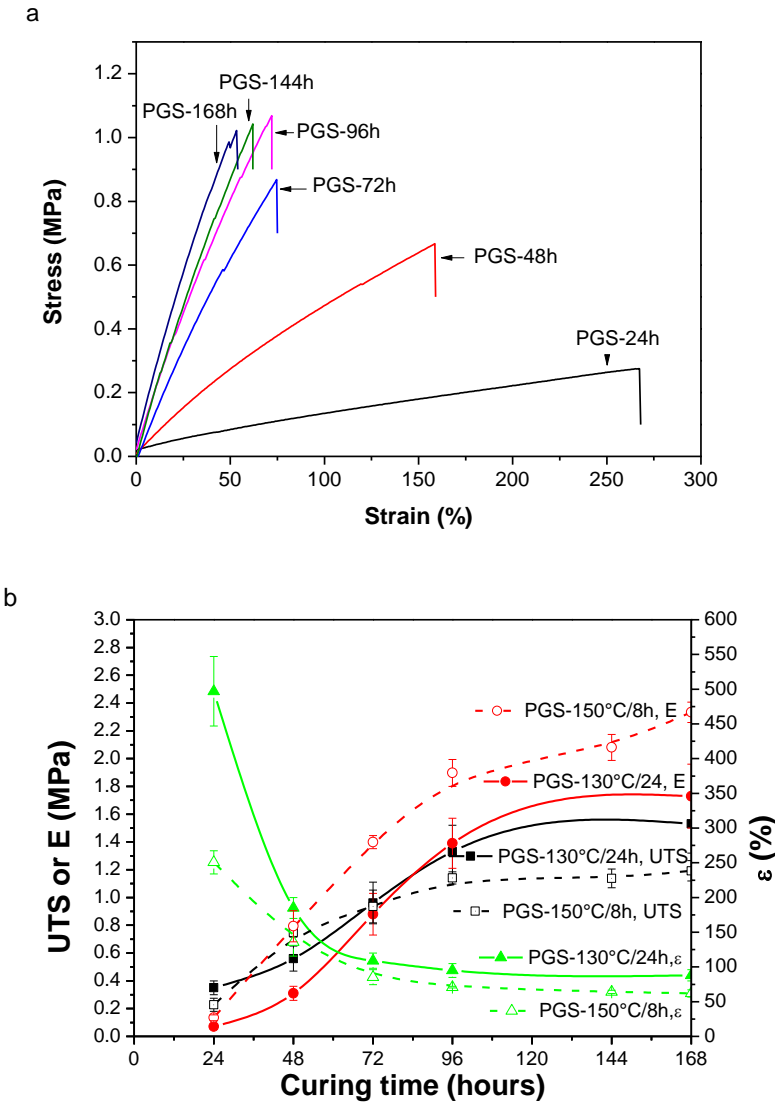


Fig. 4.7 (a) Typical tensile stress-strain curves of PGS treated at 150 °C/8 hours but crosslinked at 130 °C for different times; (b) Mechanical properties of PGS treated at 150 °C/8 hours or 130 °C/24h, but crosslinked at 130 °C for different times: Ultimate tensile strength (UTS), Young's modulus (E) and strain at break (ϵ) of materials versus crosslinking time. The error bars represent one standard error.

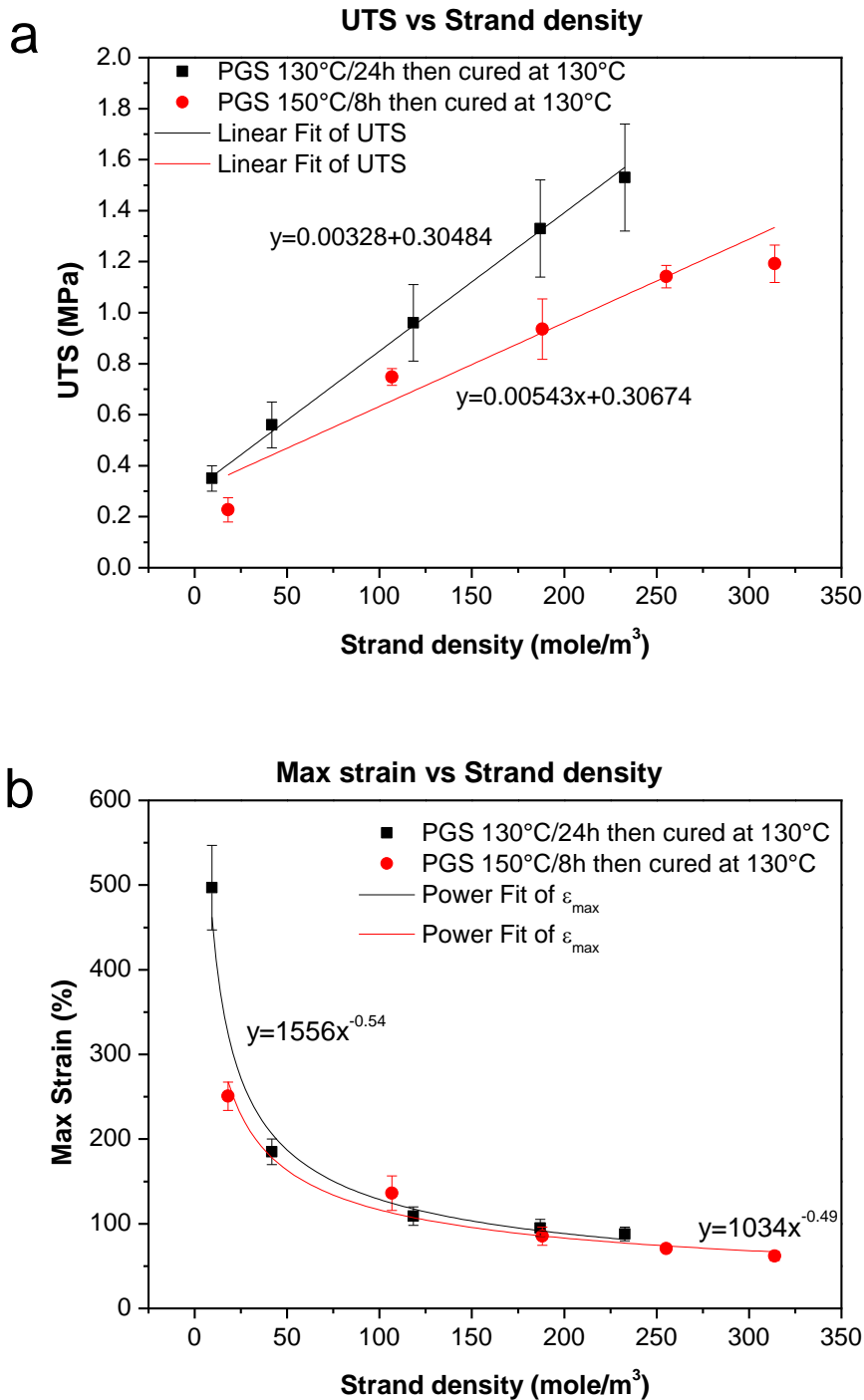


Fig 4.8 (a) Ultimate tensile strength (UTS), and (b) maximum strain (ϵ_{max}) at break of PGS samples versus the strand density calculated from Equation 3.4. The data was fitted to theoretical curves of Eq. 4.3 and Eq. 4.4 (the latter by use of the non-linear Solver method in Microsoft Excel 2007).

4.2.4. Biocompatibility of PGS

SNL mouse fibroblasts were used to conduct the in vitro cytotoxicity assessment of crosslinked PGS cured for a short (48 hours) or long period (96 hours) at 130°C. The cell morphology remained normal after two days culture in the extract media of the free culture medium, of the PDLLA and of the PGS which had been crosslinked for 96 hours. However, the cells showed abnormally round morphology and low proliferation levels (Fig. 4.9) in the extract media of the PGS crosslinked for 48 hours.

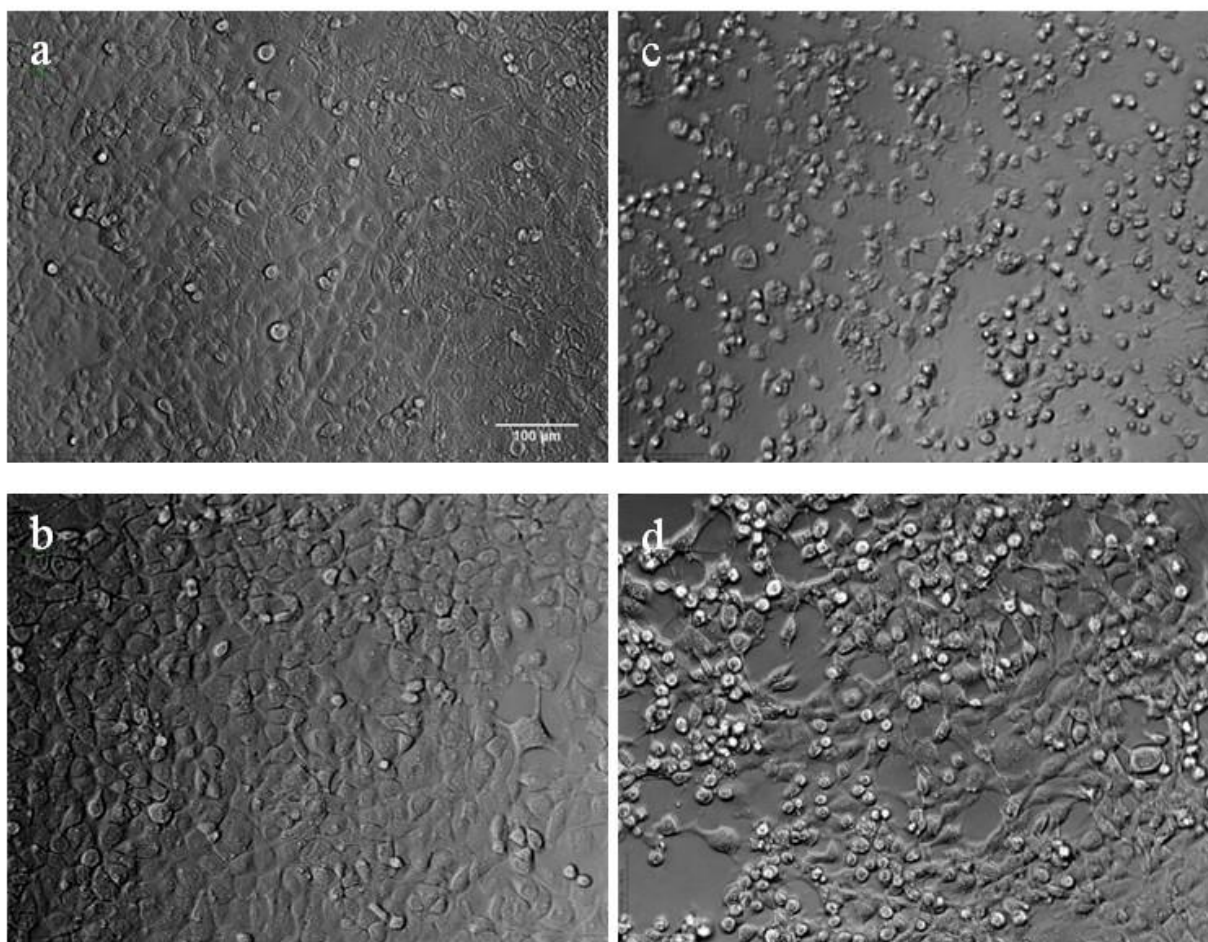


Fig. 4.9 Images of SNL cells cultured in extracts prepared with different samples after 24h (a-d): (a) free culture medium; (b) PDLLA; (c) PGS treated at 150 °C for 8 h, but crosslinked at 130 °C for 48 h; (d) PGS treated at 150 °C for 8 h, but crosslinked at 130 °C for 96 h.

Quantitative LDH assessment (Fig. 4.10) confirmed that the proportions of dead cells were significantly lower in the SNL cells exposed to the extracts of PGS crosslinked for a longer period than those crosslinked for a short period ($p < 0.001$). The cytotoxicity differences between PDLLA and long-period cured PGS were not significant ($p > 0.05$), according to LDH release (Fig. 4.10). Quantitative measurements using the AlamarBlue™ reagent demonstrated (Fig. 4.11) that almost no cell proliferation occurred in the extract media of the PGS sample which had been cured at 130 °C for 48 hours, but that SNL cells proliferated exponentially in the extract media of the PGS cured at 130 °C for 96 hours, as well as in the two control groups, as shown in Fig. 4.11. Fig. 4.10 and Fig. 4.11 demonstrate that the cytocompatibility of the PGS cured at the long periods was as good as the two control groups, with no significant differences in either cell death or proliferation between cultures containing the tested materials and material-free control cultures.

The cytotoxicity of the PGS crosslinked at 130°C/48h appear to be caused by unreacted carboxylic acid groups in the gel or the free sebacic acid produced by aqueous hydrolysis of PGS ester groups. However, PGS cured for a longer period showed low cytotoxicity which is comparable to the PDLLA control material due to the higher degree of esterification which means that more carboxylic groups are converted to ester groups (above 94% converted), and which reduces the hydrolysis kinetics of ester group by retarding diffusion into and out of the polymer network. Therefore, lower PGS cytotoxicity can be achieved by increased curing duration.

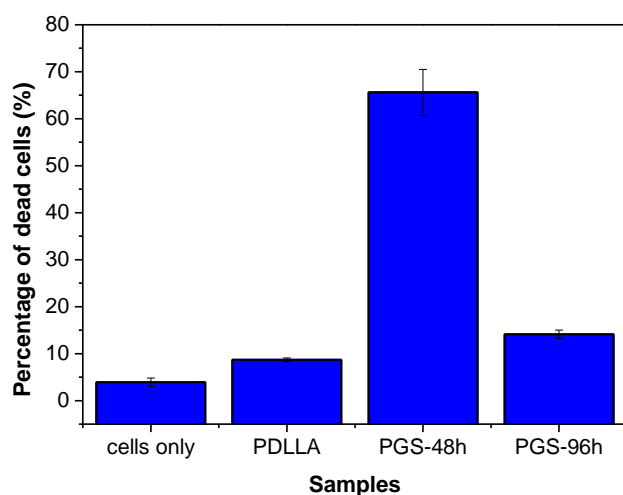


Fig. 4.10 Effect on lactic dehydrogenase (LDH) evolution of extract-free medium (the negative control), PDLLA, PGS cured for 48 h or 96 h, indicating the viability of SNL mouse fibroblasts. After 48h culture, the percentage of dead cells was significantly higher in the cultures containing the extracts of PGS cured for 48 h than in the other three cultures ($p < 0.001$), while PGS cured for 96 h did not show significant differences from the negative control and PDLLA ($p > 0.05$).

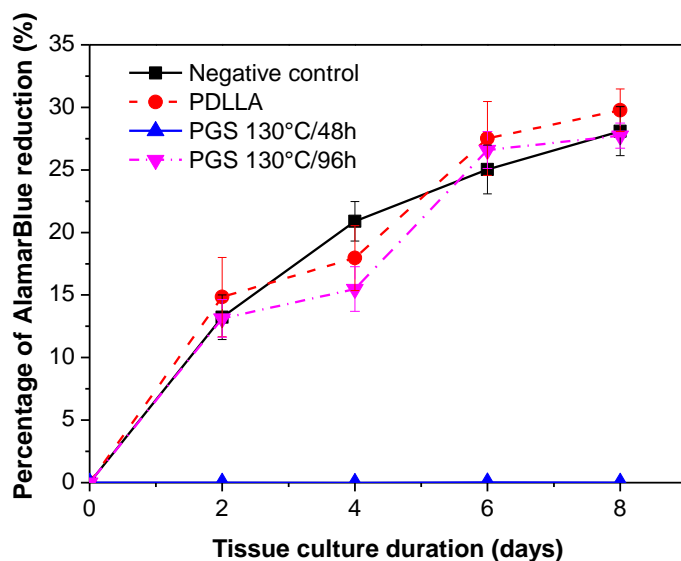


Fig. 4.11 SNL cell proliferation kinetics measured by the AlamarBlue™ technique. The initial plating density was 5000 cells per well in a 48-well plate ($n=5$). The difference between negative control PDLLA and PGS cured at 130°C/96h material were not significant ($p > 0.05$). The cells proliferated significantly more slowly on PGS cured at 130°C/48h, compared with those on negative control, PDLLA and PGS cured at 130°C/96h ($p < 0.01$).

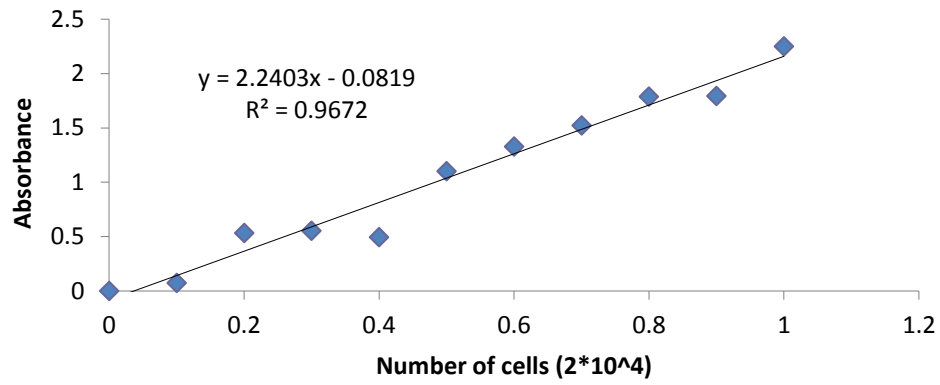
4.3. Conclusions

In this study, we have investigated the polymerisation of PGS synthesised under different conditions by monitoring the mass loss of volatile products and the conversion of carboxylic acid groups into ester groups. Although high temperatures accelerated the reaction kinetics and shortened the polymerization time, they also increased the evaporation of glycerol which resulted in lower reproducibility of the polymer. The use of ^1H and ^{13}C NMR have shown that the secondary alcohol groups, which are responsible for crosslinking forms, are esterified more slowly and are present in only small quantities in the pre-polymers but have higher levels in the gel, and these techniques provide qualitative and semi-quantitative structural information on the synthesised PGS.

This work has also examined the influence of synthesis conditions (temperature and curing time) on the mechanical properties and cytocompatibility of PGS. It was found that the UTS and Young's modulus of PGS increased with curing duration, while the maximum strain at break decreased. The cytocompatibility of PGS was improved by a longer curing time, as demonstrated by *in vitro* cytotoxicity studies.

Appendix 4.1. Standard Curve of MTS testing

Standard curve of MTS testing



Appendix: standard curve of MTS testing

CHAPTER FIVE

A COMPARATIVE STUDY ON PGS AND PXS: MECHANICAL PROPERTIES, BIODEGRADATION AND CYTOCOMPATIBILITY

5.1. Introduction

As discussed in Section 2.4 Chapter 2, PPS is a new family of crosslinked elastomers and PGS is the most widely studied PPS member [2, 42, 117, 118, 187, 188]. The Young's modulus of PGS is in the range of 0.05-1.5MPa [7]. In general, flexible PGS of a low Young's modulus (< 0.5 MPa) has good stretchability (i.e. rupture strains of over 100%), but degrades rapidly (4-6weeks) [116] and exhibits cytotoxicity *in vitro* due to acidic by-products of its degradation [7]. The rapid degradation kinetics of soft PGS has impeded any applications as scaffolding materials for tissues that have healing rates of several months or years (e.g., muscle) [116, 159]. Although a slower degradation rate and thus satisfactory cytocompatibility can be achieved in PGS by increasing the crosslink density of the network, such PGS loses its elasticity as shown in Chapter 4 [189]. Thus it is difficult to achieve a slow degradation rate in pure PGS without compromising the flexibility and stretchability of the network. Indeed, an elastomer, which is as soft as muscle, which degrades slowly and has satisfactory cytocompatibility, has yet to be developed.

For an ideal balance between controlled degradation and suitable flexibility required in medical applications, as mentioned above, a potential approach to enhance the stretchability of the highly crosslinked PPS-based elastomers is the usage of relatively longer polyol monomers (such as xylitol), which can space out crosslinks and thus enhance the flexibility of the polymer network, compared with the PGS counterpart. However, long polyol monomers have more than 3 hydroxyl groups, and the effect of the extra $-OH$ groups on the hydrolysis of the PPS network is an open question. On the one hand, the hydroxyl groups are hydrophilic and thus may enhance water absorption of the network. On the other hand, the large sized $-OH$ groups can have a steric hindrance effect on the hydrolysis of the ester bonds of the network [190]. Hence, it is necessary to carry out an investigation on the effect of long polyol monomers on the elastic mechanical properties and hydrolysis of PPS network. The aim of this work, therefore, was to investigate

whether extra –OH groups of polyol monomers could simultaneously enhance the flexibility and reduced the hydrolytic rate (as well as cytotoxicity) of PPS-based elastomers. To this end, we carefully conducted a comparative study on the PPS networks of two polyols, glycerol and xylitol, in terms of their mechanical properties, enzymatic degradation rates and biocompatibility.

5.2. Results and Discussion

5.2.1. Degree of Esterification

The mechanical properties of a polyester network are directly determined by the level of polymerisation and crosslinking, i.e. the degree of esterification. Table 5.1 provides the degrees of reaction in the PGS and PXS pre-polymers and the crosslinked PGS and PXS determined by two methods: measurement of mass loss and titration of carboxylic acid groups. It was found that the percentages of the esterified carboxylic group in the PPS prepolymers (i.e., cured for zero days) determined with the two methods were consistent for both PGS and PXS, being ~75% and ~ 65 %, respectively (Table 5.1). However, for the crosslinked PPS polymer, the percentages of reaction determined with the two methods were significantly different. The nominal reaction percentage of over 100 % measured by the ‘water’ loss indicated the evaporation of volatile polyol. During the crosslinking treatment of PGS and PXS, the melted polymer sheets exposed a large surface area under vacuum, which escalated the evaporation of xylitol, a volatile component. Thus, the mass loss measured actually contained both the water by-product and evaporated glycerol or xylitol monomers, and resulted in an over-estimated percentage from Eq. 3.2, which was formulated under the assumption that the weight loss during the crosslinking treatment was the amount of the by-product water.

The loss of polyol during polymerisation can be calculated from the nominal percentage of reaction (P_1) determined from mass loss and ‘actual’ percentage of reaction (P_2) determined by the titration technique, as discussed as follows. The difference between P_1 and P_2 is given by Eq. 5.1:

$$\begin{aligned}
P_1 - P_2 (\%) &= \left[\frac{(m_{\text{H}_2\text{O}} + m_{\text{xylitol}}) / M_{\text{H}_2\text{O}}}{2 \times m / (M_{\text{sebacic}} + M_{\text{polyol}})} - \frac{m_{\text{H}_2\text{O}} / M_{\text{H}_2\text{O}}}{2 \times m / (M_{\text{sebacic}} + M_{\text{polyol}})} \right] \times 100 \\
&= \frac{m_{\text{xylitol}} / M_{\text{H}_2\text{O}}}{2 \times m / (M_{\text{sebacic}} + M_{\text{polyol}})} \times 100
\end{aligned} \tag{Eq. 5.1}$$

Then the molar percentage of lost xylitol is given by Eq. 5.2:

$$\text{Loss of polyol (\%)} = \frac{m_{\text{polyol}} / M_{\text{polyol}}}{m / (M_{\text{sebacic}} + M_{\text{polyol}})} \times 100 = \frac{2 \times M_{\text{H}_2\text{O}} (P_1 - P_2)}{M_{\text{polyol}}} \tag{Eq. 5.2}$$

The results (Table 5.1) revealed that the loss of polyol during the synthesis of pre-polymer was ignorable. However, the evaporation of the polyol was severe during the crosslinking treatment of the cast thin sheets, and the loss of glycerol (small molecules) was higher than xylitol (relatively large molecule), with the maximum loss percentage being 28 and 16 %, respectively. The above results were attributable to the processing conditions, as described as follows. During the pre-polymerisation process, a relatively large amount (~50 g) of melted precursor mixture exposed a very limited (~ 30 cm²) surface area to the vacuum environment in the reaction container, whereas a thin sheet (~ 1 g) exposed a relatively large surface area (~ 20 cm²) during the curing process. This issue remains to be addressed.

The titration method produced reasonable results (Table 5.1). The PGS system was found to gel at 84.02±0.03% (for PGS prepolymerised at 130°C/24h then cured at 130°C/20h) while the PXS formed gel at 85.04 ±0.02% (for PXS prepolymerised at 130°C/24h then cured at 130°C/21h). The results also showed that the percentage of esterified carboxylic groups in PGS increased steadily during the first 3 days of crosslink treatment and reached a saturation plateau of 95 % by the end of 4-days curing, after which there was no considerable increment in the reaction percentage. With the PXS system, a saturation plateau of 97 % was reached by the end of 7-days curing, after which there was no considerable increment in the reaction percentage.

Table 5.1 Degrees of esterification estimated by mass loss of the water by-product and the titration of acid groups. PPS materials were pre-polymerised at 130 °C for 1 day and cured at 130 °C for up to 12 days.

Polymers & Pre-polymerization conditions	Curing time at 130 °C (day)	Percentage of esterification (%)		Molar fraction of evaporated polyol (%)
		By mass loss (P_1)	By titration for – COOH (P_2)	
PGS 130 °C / 1 day	0	77.8 ± 0.2	74.3 ± 0.9	1.4
	2	143 ± 12	90.7 ± 0.2	20
	3	154 ± 8		22
	4	166 ± 6	94.3 ± 0.1	23
	7	172 ± 4	95.5 ± 0.0	28
PXS 130 °C / 1 day	0	65.2 ± 8	64.5 ± 10.8	0
	2	100 ± 9	86.8 ± 0.2	3
	3	127 ± 12	92.4 ± 0.1	8
	4	146 ± 14	93.0 ± 0.1	13
	7	162 ± 7	97.0 ± 0.1	15
	9	165 ± 6	98.0 ± 0.1	16
	12	165 ± 6	98.0 ± 0.1	16

5.2.2. Mechanical properties of PGS and PXS

5.2.2.1. Effects of curing time on mechanical properties

As a typical elastomer, no stress whitening or plastic deformation artefacts were visually observed during the tensile testing. The shifting profiles of the stress-strain curves of PGS and PXS with curing time are demonstrated in Fig. 5.1. Fig. 5.1 indicates that the PXS network collectively produced a wider range of mechanical properties than the PGS, including Young's modulus, UTS and elongation at break. The maximal UTS and elongation at rupture, for example, were ~2.5 MPa and >750% in the PXS group, whereas these properties were ~1.5 MPa and ~500% in the PGS group.

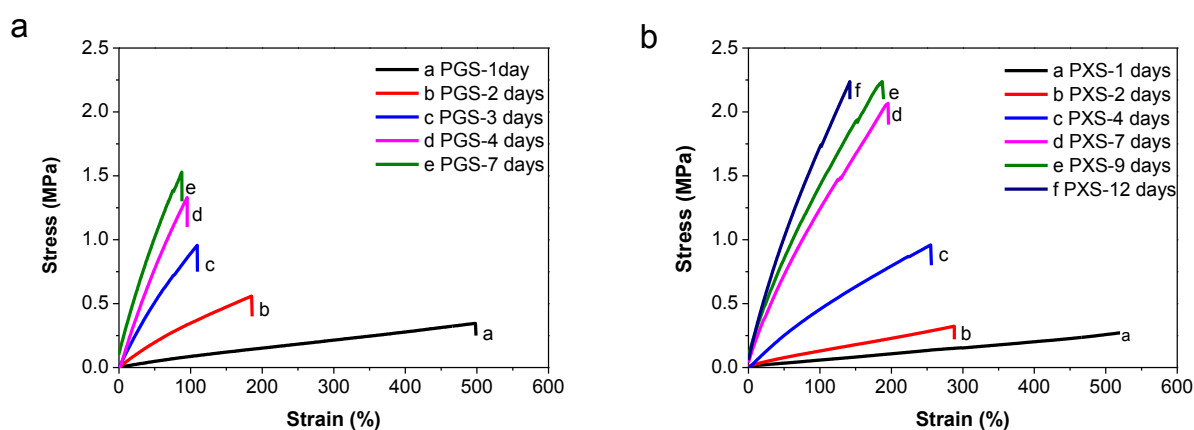


Fig.5.1 Typical stress-strain curves of the PGS and PXS polymer sheets. Both PGS and PXS were pre-polymerised at 130 °C for 1 day, but PGS and PXS were treated for crosslink at 130 °C for up to 7 and 12 days, respectively. The specimen of PXS cured at 130 °C for 1 day did not break due to the tension limit of the tensile tester used.

As expected, the average values of UTS and Young's moduli (E) of the PGS and PXS polymers increased with curing time ($p > 0.05$), whereas the strain at break (ϵ_{\max}) decreased, as shown in Fig. 5.2. The values of Young's modulus and UTS of PGS and PXS plateaued after curing for 4 and 7 days, respectively, which is consistent with the results of reaction degrees (Table 5.1). The Young's moduli of the PXS polymers (0.05 - 2.0 MPa) had a wider range than that of the PGS polymers (0.05 - 1.5 MPa) (Fig. 5.2a). However, the PXS polymers collectively exhibited significantly larger strains at break than the PGS polymers (Fig. 5.2b). After treatment for crosslinking at 130 °C for 4 (PGS) or 7 (PXS) days, for instance, the PGS and PXS polymers had

a similar Young's modulus (1.2-1.5 MPa). However, the PXS polymer showed a rupture strain of ~ 200 %, whereas the breaking strain value of the PGS counterpart was ~ 100 %. The enhanced stretchability of PXS is primarily attributed to the relatively longer and more orientable xylitol monomers, compared with glycerol molecules.

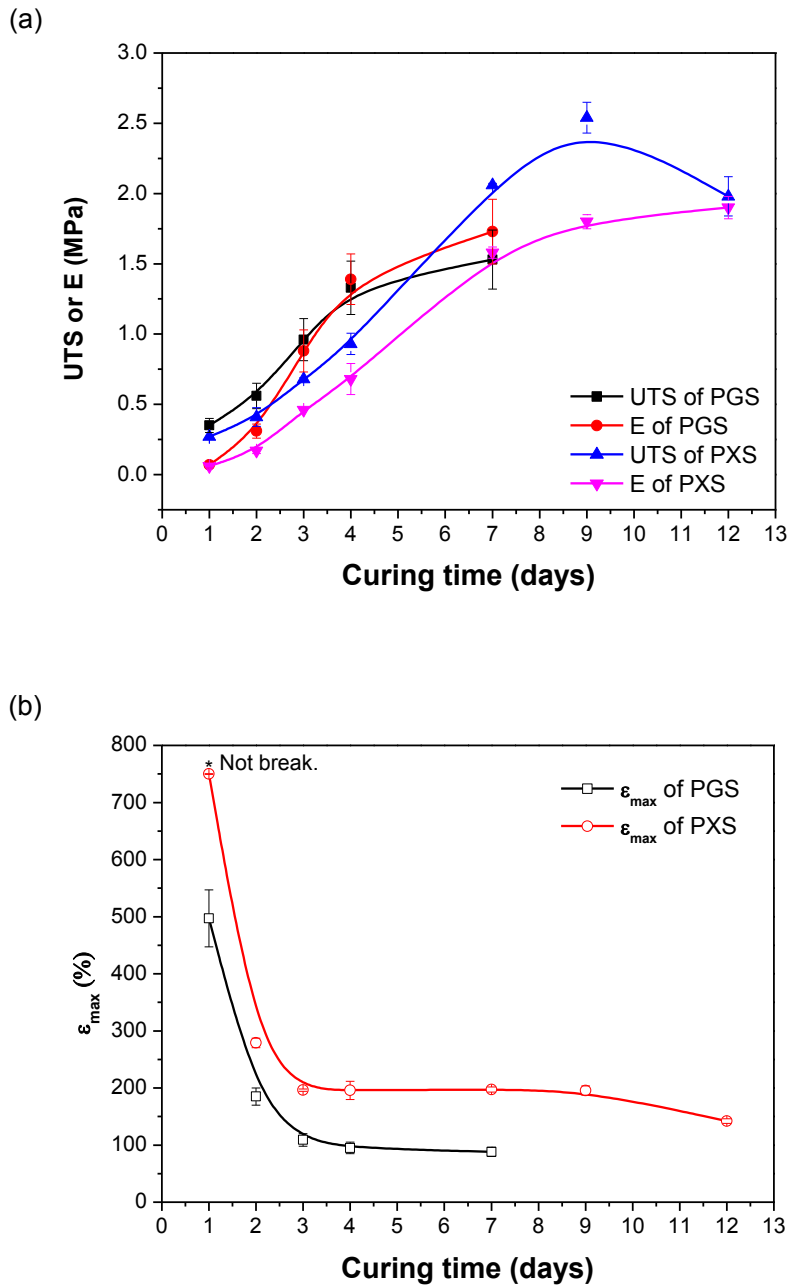


Fig.5.2 (a) Ultimate tensile strength (UTS), Young's modulus (E), and (b) strain at break (ϵ) of the PGS and PXS versus curing time

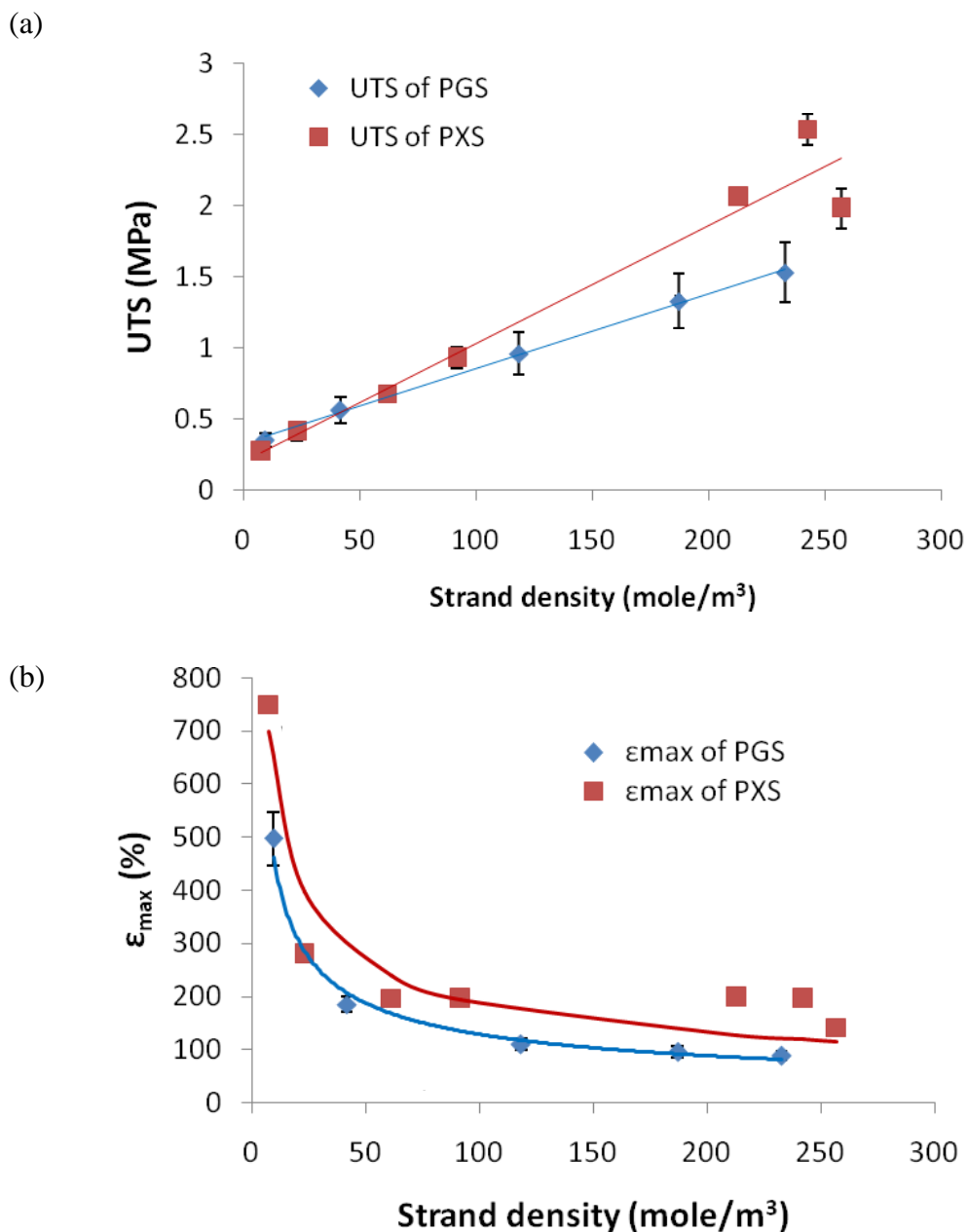


Fig. 5.3 Plots of (a) UTS and (b) elongation at break versus strand density (calculated from E) and linear fit analysis using the Origin software. The PGS and PXS materials were pre-polymerised at 130 °C for 1 day, and treated for crosslinking at 130 °C for up to 7 and 12 days, respectively.

The UTS and ϵ_{\max} of PGS and PXS samples synthesised under different reaction conditions are plotted in Fig. 5.3 against the strand density calculated from the rubbery modulus using Eq. 3.4. The tensile strength linearly rises as the strand density increases (Fig. 5.3a), while the elongation to break decreases monotonically following a power law (Fig. 5.3b). Taylor and Darin [186] have derived a theory for the dependence of the extension ratio at break ($\lambda_{\max} = 1 + \epsilon_{\max}$) and UTS on the strand density:

$$\lambda_{\max} = k_1 \nu^{-0.5} \quad \text{Eq.5.3}$$

$$\text{UTS} = k_2 \nu \left\{ 1 - \frac{1}{(1 + k_3 \lambda_{\max}^3)^{0.5}} \right\} \approx k_2 \nu \quad \text{when } \lambda_{\max} \text{ is high (i.e. UTS is low)} \quad \text{Eq. 5.4}$$

where ν is the strand density (calculated by Eq. 3.4), and the exponent n has a theoretical value of 0.5. k_1 , k_2 and k_3 are constants determined by the polymer network structure, i.e. molecular weight of the uncrosslinked polymer and molecular weight of the vulcanizate per crosslinked unit [186]. In general, k_1 indicates stretchability (elongation) and k_2 reflects the resistance of the network against deformation (strength). The PXS network has higher values in both k_1 and k_2 than PGS, indicating that PXS gains a better stretchability without compromise its deformation strength. This theory is based on the concept that the UTS is determined by the extent of strand orientation during deformation, and that λ_{\max} is determined from the average Gaussian end-to-end distance of the network strands (proportional to the square root of the number of chain bonds) and the extended strand length (proportional to the number of chain bonds). In Fig. 5.3a the UTS data is found to be approximately linear with strand density in agreement with the prediction of Taylor and Darin [186]. The values of ϵ_{\max} for the PGS and PXS samples versus the strand density in Fig. 5.3b fit to a power law with exponents of 0.541 and 0.515 respectively, with a 95% confidence interval being (0.48, 0.52) and (0.49, 0.51), respectively.

More importantly, Fig. 5.3b consistently shows that with the same crosslink density PXS is more stretchable than the PGS counterparts; with the rupture strain value of PXS being early double those of PGS, especially at the high end of strand density. The higher UTS (Fig. 5.3a) and greater rupture elongation (Fig. 5.3b) of PXS indicated that PXS can offer more reliable elastic performance than the PGS counterpart of a similar Young's modulus. Moreover, to achieve the same stretchability (e.g. 200% elongation at break), the PXS network can have a much higher crosslink density (i.e. 250 mole/cm³), whereas the strand density of the PGS network has to remain lower than 50

mole/cm³ (Fig. 5.3b). Slow degradation rates of elastomers are directly determined by the high crosslink density of the network. Hence, it is possible to achieve significantly reduced degradation kinetics without compromising elastic stretchability with PXS, compared with PGS, as described in Section 5.2.3.

5.2.3. Diffusion rates of water and THF molecules in PGS and PXS

The level of water and THF absorption in highly crosslinked PPS is very low such that the swelling measurement cannot detect any considerable difference of water and THF diffusion in the PGS and PXS networks. Hence, the PGS and PXS samples of a low crosslink density were selected for the studies described in this section. At the same level of crosslink density (~ 25 mole / m³ in the present study), the PGS network swollen slowly than that of PXS in THF (Fig. 5.4a). The above observation is attributable to the hydrophobic nature of THF molecules and the hydrophilic properties of the PXS and PGS networks, i.e. the PXS network are more hydrophilic than the PGS counterpart due to the increased number of –OH groups in the former. It is thus not surprising to observe that the level of water absorption was higher in the PXS than in the PGS networks (Fig. 5.4b). Apparently, the above observation was attributed to the two more extra –OH groups on each xylitol monomer.

Both PXS and PGS showed low water swelling of less than 8% in Fig. 5.4. This low water swelling behaviour of the materials will benefit some clinical applications, such as smaller delivery device for fine ophthalmic surgery, or neurosurgery which require low swell to avoid pressure on anatomical structure.

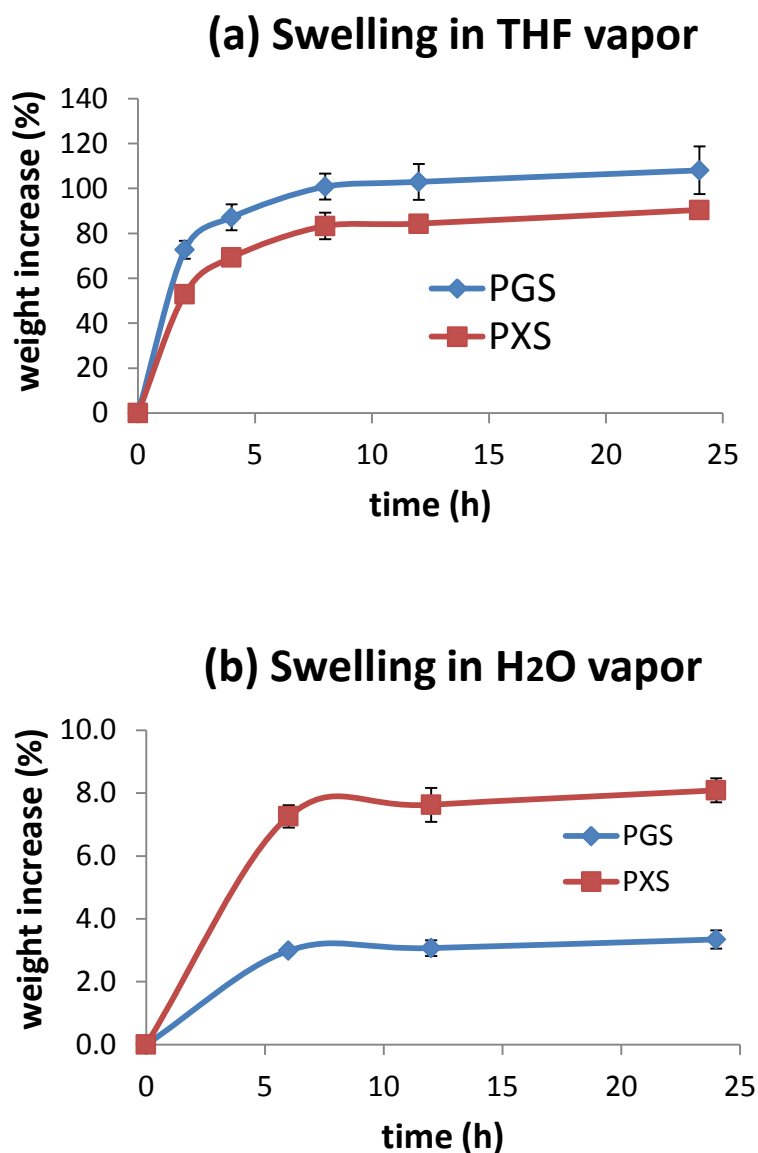


Fig. 5.4 Swelling ratios of PGS and PXS vs swelling time in (a) THF and (b) water vapours. The PGS and PXS materials were pre-polymerised at 130 °C for 1 day, and treated for crosslinking at 130 °C for up to 1.5 and 2 days, respectively. The strand densities in the two polymers were ~ 25 mole/ m³.

5.2.4. Enzymatic degradation of PGS and PXS

The aim of this study was to test whether extra –OH groups of xylitol have steric hindrance effect on the hydrolysis of ester bonds of PXS network. To this end, it is essential to select PGS and PXS polymers of very similar crosslink density, if exactly the same is impossible. Fig. 5.2a indicates that the Young’s moduli of PGS crosslinked for 7 days and PXS crosslinked for 9 days are both approximately 1.7 MPa, and the crosslink densities in these two elastomer networks are

approximately 240 mole / m³. Moreover, these two polymers are of interest because of their good cytocompatibility (Section 5.2.5). Hence, these two elastomers were selected for the enzymatic study of this work.

The weight loss of the PGS samples crosslinked at 130 °C for 7 days was on average 13 % after incubation for 35 days, whereas the PXS samples crosslinked at 130 °C for 9 days lost approximately 8 % of its original weight (Fig. 5.5). The enzyme-mediated degradation of polyesters is a hydrolysis process. In the PXS network, the extra –OH groups could influence hydrolysis in two ways. First, the –OH groups attract water molecules in the polymer network, and thus could potentially enhance the availability of water molecules around each ester bond (Fig. 5.6). However, the availability of water molecules does not necessarily increase their chance to attack ester bonds. Indeed, the large sized –OH groups could have a shield effect on an ester bond from water attack [190].

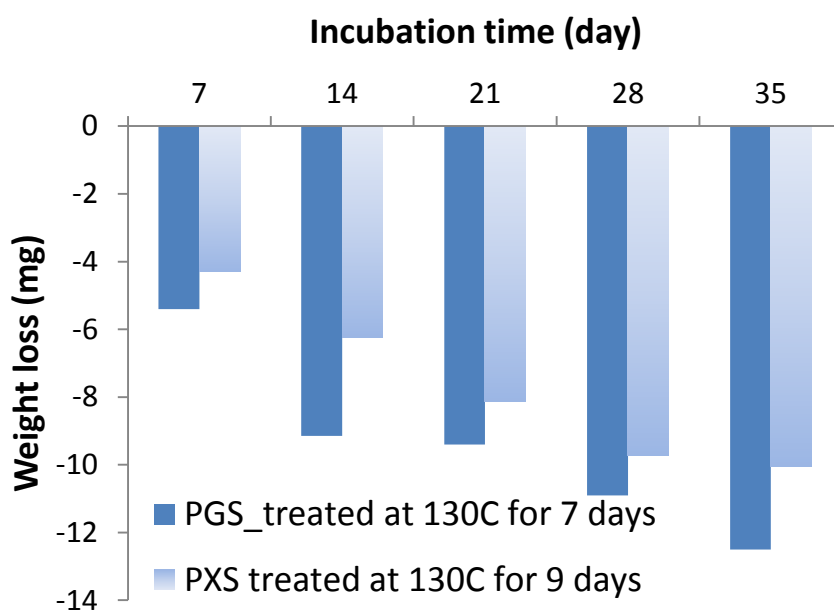


Fig. 5.5 The weight loss of the PGS and PXS polymers after incubation at 37 °C in the tissue culture medium with the addition of esterase (0.3 units of enzyme per mg of biomaterial) for up to 35 days. The PGS and PXS materials were pre-polymerised at 130 °C for 1 day and treated for crosslinking at 130 °C for 7 and 9 days, respectively.

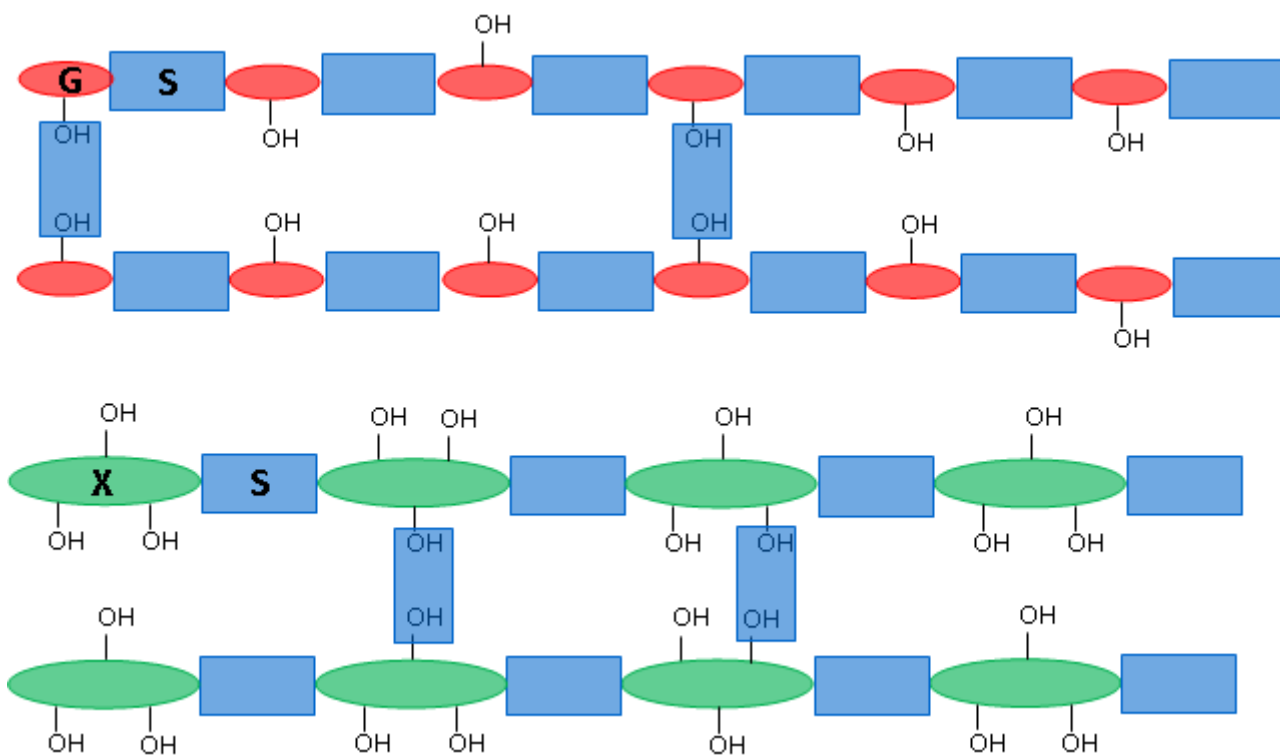


Fig 5.6 Schematic illustrations of (a) the PGS and (b) the PXS networks. G = Glycerol, S = Sebacic acid, X = Xylitol

It should be mentioned here that the copolymerisation of PPS with other polyesters, such as polylactide (PLA) or polyhydroxyalkanoates (P3HB, P3HV, etc) is another approach to further enhance stretchability while tuning down hydrolysis of elastomeric polyesters. These non-crosslinkable thermoplastic polyester chains can greatly space out crosslinks. At the same time, the side chains, $-(CH_2)_n-CH_3$, can sterically hinder ester-bond hydrolysis [191] and may effectively slow down the mediation of enzyme molecules.

5.2.5. Biocompatibility of PGS and PXS

SNL mouse fibroblasts were used to conduct the *in vitro* cytotoxicity assessment of the PGS and PXS polymers. PGS and PXS polymers cured 130 °C for a short (2 days) and longer (4 or 7 days respectively) periods were assessed. A visual examination showed that the cell morphology remained normal after two days culture in the negative control (i.e., extractant-free medium), positive control (i.e., containing the PDLLA extractant) and the testing medium of PGS and PXS cured for 4 or 7 days (Figs. 5.7a, b, d and f). However, the cytotoxicity was apparent in the extract media of the PGS and PXS cured 130 °C for 2 days (Fig. 5.7c and e). Quantitative LDH assessment confirmed that the proportions of dead cells was significantly lower in the SNL cells exposed to the

extracts of PGS and PXS cured for a longer period (4 or 7 days, respectively) than those treated for 2 days ($p < 0.001$). No significant differences were detected in the cytotoxicity between the (negative and positive) control groups and the PGS and PXS samples cured at 130 °C for 4 or 7 days ($p > 0.05$) (Fig. 5.8).

Quantitative measurements using the AlamarBlue™ reagent demonstrated that almost no cell proliferation in the extractant media of PGS and PXS cured at 130 °C for 2 days, and that SNL cells proliferated exponentially in the extractant media of the PGS and PXS cured for 4 or 7 days, as well as in the two control groups, as shown in Fig. 5.9. Figs 5.8 and 5.9 demonstrate that the cytocompatibility of the PGS and PXS cured at the long periods was as good as the two control groups, with no significant differences in either cell death or proliferation between cultures containing the tested materials and material-free control cultures.

The toxicity of the PGS and PXS crosslinked at 130°C for 2 days was most likely caused by either unreacted carboxylic acid groups and/or the carboxylic acids produced by aqueous hydrolysis of PPS ester groups, which resulted in severe acidity in the extracts. However, PPS cured for a sufficiently long period showed good compatibility, which is comparable with the both negative and positive (PDLLA) controls. The improved compatibility by a long curing time can be attributed to the high crosslink density of the materials, in which most carboxylic groups are converted into ester groups (> 94 %) shown in Fig. 5.8(b) and the hydrolytic kinetics of ester groups is slow due to the hindered diffusion rate of water in a highly crosslinked polymer network. The low cytotoxicity of PXS has been achieved while maintaining good elasticity (ϵ_{\max} is ~ 200 %, Fig. 5.2b).



Fig. 5.7 Images of SNL cells cultured in extracts prepared with different samples after 24 h, without any pre-conditioning treatments. (a) Negative control (free culture medium); (b) positive control with PDLLA; PGS were polymerised at 130 °C for one day and cured at 130 °C for (c) 2 or (d) 4 days; PXS polymerised at 130 °C for one day and cured at 130 °C for (e) 2 or (f) 7 days.

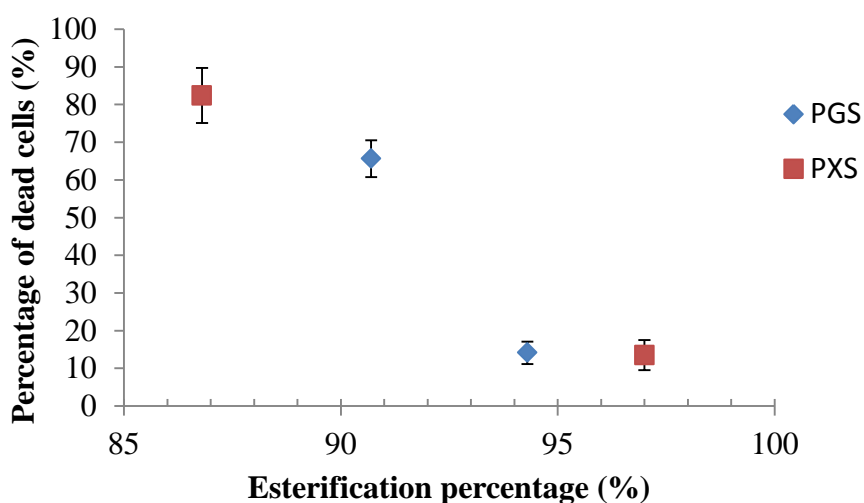
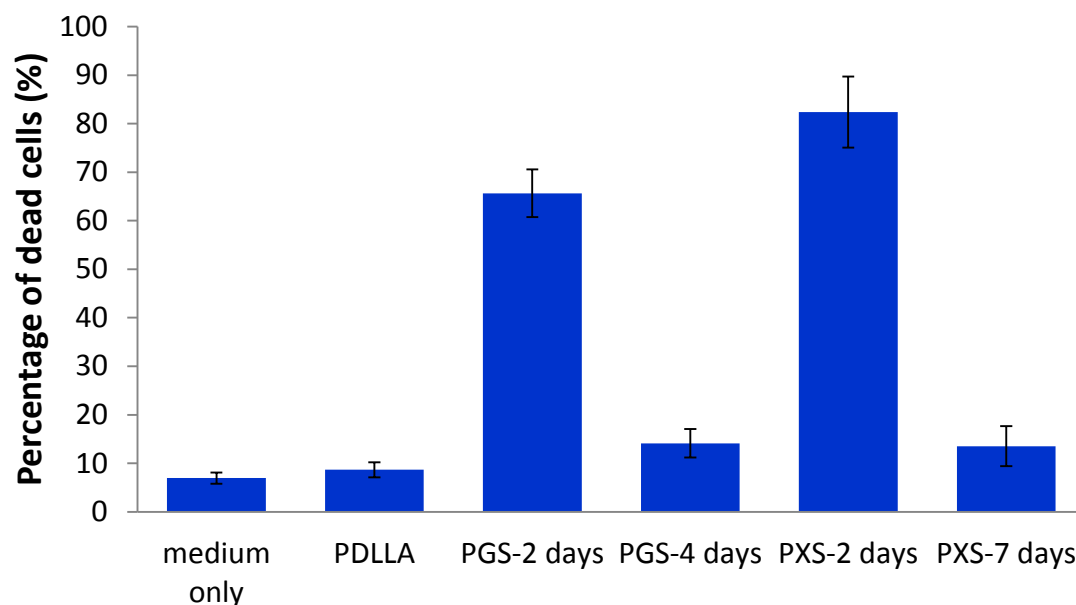


Fig. 5.8 (a) Cytotoxicity of the PGS and PXS, determined by measuring the release of lactate dehydrogenase (LDH) after 2 days culture. The positive control group was PDLLA. The percentages of dead cells were significantly higher in the cultures containing the extracts of PGS and PXS cured for 2 days than those of other five cultures ($p < 0.001$), whereas the PGS and PXS specimens cured for longer time (4 or 7 days respectively) did not show significant differences from the either negative or positive control (PDLLA) group ($p > 0.05$); (b) with the esterification percentage of PGS and PXS cured for 2 days or longer (4 or 7 days respectively).

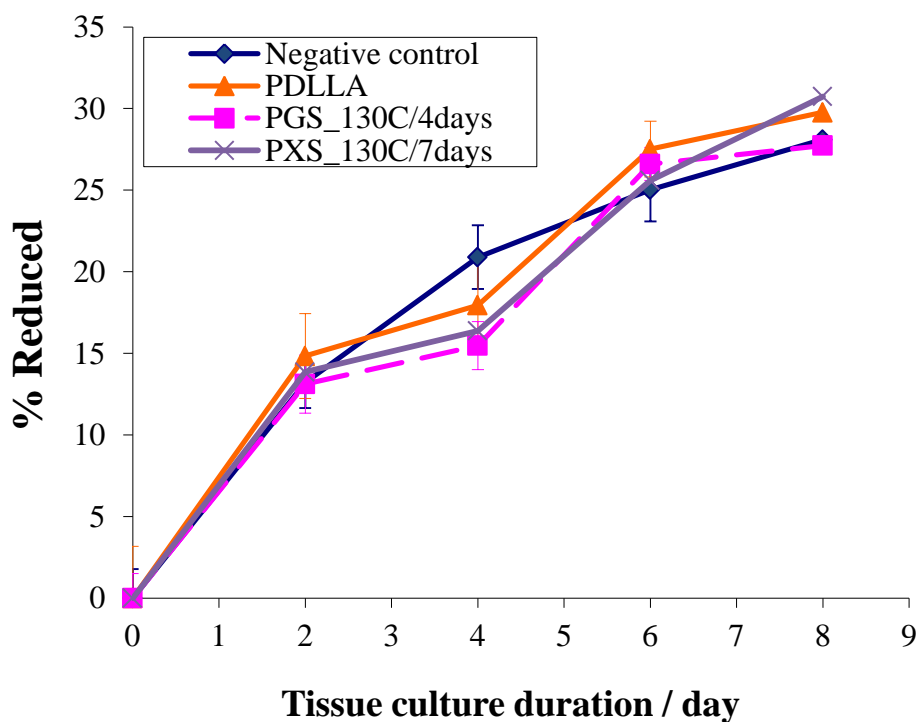


Fig. 5.9 SNL cell proliferation kinetics measured by the AlamarBlue™ technique. The initial plating density was 2500 cells per well in a 48-well plate ($n = 5$). Overall, there were no significant differences between any two of the four groups that were analysed ($p > 0.05$).

5.3. Conclusions

In order to develop flexible and slowly degradable polyester elastomers, PXS and PGS, two members of the PPS family but with 3 or 5 hydroxyl groups respectively, have been comparatively investigated in terms of mechanical properties, enzymatic degradation and biocompatibility. Under the condition of the same crosslinked density, the PXS elastomer networks have approximately twice higher stretchability (elongation at break) than the PGS counterparts. This observation is attributable to the relatively longer and more orientable xylitol monomers, compared with glycerol molecules. Although xylitol monomers have two more hydroxyl groups, these hydrophilic side chains do not necessarily accelerate water attack on the ester bonds of the network. Rather they have a hindrance effect on the hydrolysis of ester bonds. Hence, the PXS network degrades considerably slower than the PGS counterpart. In conclusion, the use of polyols of more than three –OH groups in the fabrication of PPS can enhance flexibility while tuning down degradation rate of polyester elastomers.

CHAPTER SIX

ENZYMATIC AND OXIDATIVE DEGRADATION OF PPS

6.1. Introduction

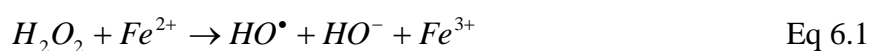
The degradation rates of PPS are generally faster than other polyesters, such as polylactide and polyglycolide [192]. In a previous *in vitro* study, Wang and co-workers [1] reported that PGS degraded 17 % by weight after incubation in enzyme-free phosphate-buffered saline (PBS) at 37 °C for 60 days. Similar results were reported by the present authors, showing that the weight loss of PGS and PGS/Bioglass[®] composite was around 10-25 % after 60 days of incubation in a standard tissue culture medium, without the addition of enzymes [159]. However, a significantly higher degradation rate of PGS *in vivo* was reported by Wang and co-workers [111], in which PGS implanted in rats was completely resorbed at 60 days post implantation. Stuckey and co-workers [95], who used PGS sheets as a pericardial heart patch, similarly reported that the PGS patch was completely resorbed in 6 weeks. These *in vivo* studies suggest that the accelerated biodegradation may result from more efficient hydrolysis of PPS polymer chains, likely catalysed by enzyme action during wound healing.

Enzyme-mediated degradation has been investigated for a number of polymeric biomaterials [160, 165, 193]. In general, two classes of enzymes are known to be primarily involved in the *in vivo* degradation of polyester implants [193-195]. The first group is hydrolases, including phosphatases, esterases and amino peptidases, named after the side groups they cleave. These enzymes are predominantly lysosomal in origin, secreted mainly by macrophages and lymphoblast giant cells, white blood cells that infiltrate healing tissues [159]. The second class of enzymes is represented by oxidoreductases, which cause further hydrolytic breakdown, mainly acting on hydroxyl groups [195]. While the enzymatic effect of esterase on the degradation of polyester polymers has been consistently reported *in vitro* and *in vivo*, the effects of these enzymes on polymeric biomaterials remain controversial [159, 195-197].

Polymeric biomaterials may also be attacked by free radical oxidation when exposed to the body fluids and tissues. It is well documented that during the inflammatory response of injured tissue to a foreign material, phagocytes (particularly leukocytes) and macrophages are able to produce highly reactive oxygen species such as superoxide(O_2^-), hydrogen peroxide (H_2O_2), nitric oxide(NO), and

hypochlorous acid (HClO) [193, 198-200]. These species play an essential role in the physiological function of phagocytes to eliminate invading microorganisms. These species are relatively harmless on their own, but in the presence of iron or other transition-metal catalysts, a secondary generation of highly toxic radicals are produced, such as hydroxyl radicals (HO^{\bullet}). The oxidative effect of these species, especially hydroxyl radical, may cause polymer chain scission and thus contribute to their degradation.

Several studies have been carried out to assess the effect of oxidative species in the degradation of polymeric biomaterials [193, 199, 201]. Hydroxyl radicals have been thought to be responsible for many biological phenomena, such as radiation damage, phagocytic activity, and inflammation [202]. Williams and co-workers [200, 203] investigated the biodegrading action of hydroxyl radicals on biomaterial polymers in an aqueous Fenton's reagent shown in Eq. 6.1, which is believed to more closely represent *in vivo* conditions. Their research showed that the hydroxyl radical is likely to be one of the main inducers of polymer degradation in implantable devices made from poly(D,L-lactide) (PDLLA) and polycaprolactone [200].



Lee and Chu [201] studied the reactivity of superoxide ions in aprotic solvents, on biodegradable biomaterials such as PDLLA, and found that these species could accelerate the degradation of aliphatic polyesters via nucleophilic attack and cleavage of ester bonds.

The biological roles of various oxidative enzymes have been documented. Xanthine oxidase, for example, plays an important role in myocardial ischemia. During reperfusion, molecular oxygen is reintroduced into the tissue, whereby it reacts with hypoxanthine and xanthine oxidase (catalyst) to synthesize xanthine. Xanthine oxidase then further catalyzes the oxidation of xanthine to uric acid, and a burst of superoxide anion and hydrogen peroxide are produced in these reactions [164]. The effects of oxidative enzymes, such as horseradish peroxidase, xanthine oxidase and catalase on the degradation of polyurethanes (PUs) have also been studied [162]. However, each of the oxidative enzymes could not elicit significant degradation of PUs [162, 204]. The effects of oxidative enzyme on aliphatic polyesters are still an open question.

Recently, our research group established an *in vitro* enzymatic degradation protocol to simulate and quantitatively capture the features of esterase-mediated degradation of PPS-based materials [159, 163]. However, *in vivo* degradation of PPSs is believed to be mediated not only by the hydrolysis

enzyme but also the oxidation species. Hence, the objective of this work was to investigate the synergetic effects of enzyme-based hydrolytic and oxidative species on the degradation of PPS biomaterials. The specific objectives were to investigate the specific effects of Fenton solution and xanthine oxidase/xanthine (XOX) on the degradation of PPS in the presence of esterase, which was found to be highly effective [159, 163].

6.2. Results and discussion

6.2.1. Mechanical properties and crosslink density

The mechanical properties of PGS and PXS materials cured for up to 12 days were determined, from which the crosslink (i.e. strand) densities were calculated via Eq. 3.4. The data are given in Table 6.1. For both PGS and PXS samples, the ultimate tensile stress σ and the Young's modulus E of longer curing time samples are larger compared to the shorter curing time (2 days) samples while the ε_{Max} decrease after extended the curing time. To compare the degradation behaviours, the crosslink density of polymer is a significant factor influence the degradation rate. Therefore, it is essential to conduct the degradation experiment based the 7 days cured PGS and 12 cured PXS with the similar crosslink densities. The crosslink density of PPS produced in this work increases in the following order: PXS-2 days < PGS-2 days < PGS-7days \approx PXS-12days.

The degradation kinetics of crosslinked polymers is directly controlled by the crosslink density of the network. To investigate the effects of any factors other than the crosslink density on the degradation rates, it is critical to select polymers having an approximately identical crosslink density, if exactly the same is impossible. In present work, the PGS cured for 7 days and PXS cured for 12 days were used, because the crosslink densities of these two polymers were almost the same ($\sim 300\text{mol/m}^3$), as shown in Table 6.1.

Table 6.1 The mechanical properties of PGS and PXS and strand density ν calculated from Eq. 3.4

	PGS-2days	PGS-7days	PXS-2days	PXS-12days
σ (MPa)	0.56 \pm 0.09	1.53 \pm 0.21	0.41 \pm 0.07	1.98 \pm 0.14
ε_{Max} (%)	135 \pm 15	64 \pm 8	268 \pm 9	116 \pm 4
E (MPa)	0.73 \pm 0.05	2.35 \pm 0.23	0.23 \pm 0.02	2.27 \pm 0.08
ν (mole/m ³)	99 \pm 7	320 \pm 31	31 \pm 3	310 \pm 1

6.2.2. Mediation of degradation by enzymatic and oxidative action

As a first step of understanding the synergetic effects of enzymes and oxidative on degradation, we studied the mediation role of each species when added individually.

6.2.2.1. Influence of polymer network structure

Fig. 6.1 demonstrates the degradation rates, in terms of mass loss, of PGS and PXS in standard tissue culture medium and medium supplemented with esterase, $\text{FeSO}_4/\text{H}_2\text{O}_2$, or oxidase (xanthine) individually. In the four groups of tested samples (Fig. 6.1a-d), the weight losses of both PGS and PXS materials were relatively faster during the first seven days, compared to the later degradation profile. This observation was attributable to the leaching out of unreacted monomers. The mass loss of each material then experienced a decline from the second week and presented an approximately linear relationship against the incubation time. The linear degradation kinetics is attributed to the PPS polymers predominantly undergoing surface layer erosion in the degradation process [159, 163].

After incubation for 35 days in medium added with esterase, the weight loss of PXS cured for 2 days, PGS cured for 2 days, PGS cured for 7 days, and PXS cured for 12 days were 36.4%, 15.6%, 10.7% and 8.0 %, respectively (Fig. 6.1b). i.e., the loss value in mass of the polymers primarily decreased with the increase of strand density (Table 6.1). For the PGS and PXS of similar strand densities (PGS cured for 7 days, and PXS cured for 12 days), PXS degraded slightly slower than PGS, which is consistent with our previous work [163]. The same trend was also observed with other three groups of samples (Fig. 6.1a, c, and d).

The reduction in thickness of specimens was also measured (Fig. 6.2). The data of thickness reduction were found to be in reasonable agreement with their weight loss for all PGS and PXS materials and in all media, showing the same trend, i.e. the reduction value in thickness of these polymers increased with the decrease of strand density. The percentages of reduction in thickness were found always slightly smaller than those of weight loss. After 35 days induction in medium added with esterase, for example, the percentage of reduction in weight or thickness of PXS-2day material was measured to be 36.5 or 27 %, respectively. The small difference of these two percentages was caused by the degradation process on the circumference surfaces of specimens. Therefore, it is concluded that the degradation rate of PGS and PXS polymers are primarily controlled by the crosslink density of the network, with a less cross-linked network degrading faster.

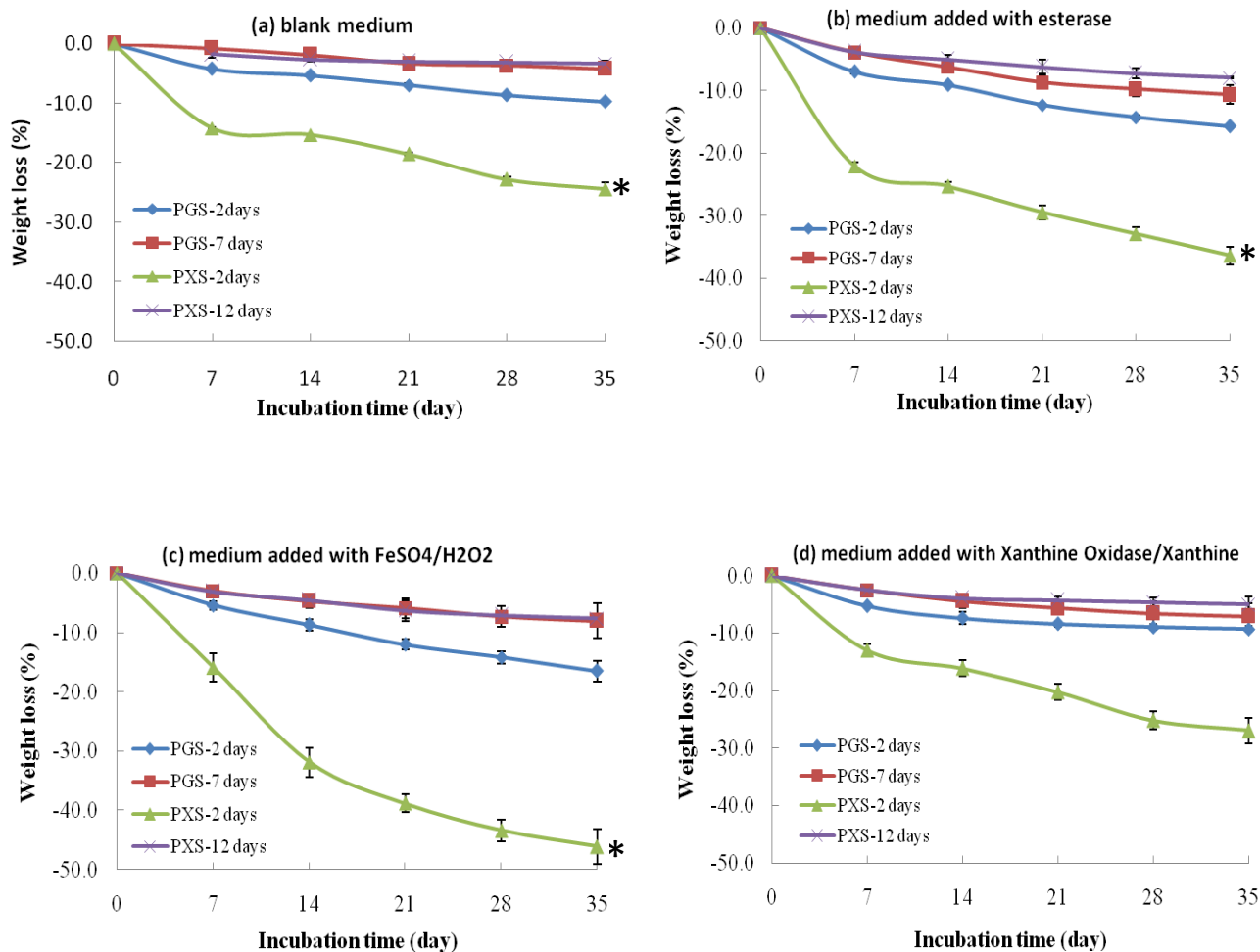


Fig. 6.1 Percentage weight changes of PGS and PXS during incubation at 37 °C in (a) blank medium, medium added with (b) esterase, (c) FeSO₄/H₂O₂, or (d) xanthine oxidase/xanthine (XOX), individually. The PGS material was treated for crosslinking at 130 °C for 2 or 7 days. The PXS material was treated for crosslinking at 130 °C for 2 or 12 days.* significant difference (p < 0.01).

6.2.2.2 Effects of esterase, oxidase or hydroxyl radical

Comparing between Fig. 6.1a, b, c and d, following results can be drawn.

- The degradation rates of these polymers were faster in the medium added with esterase (Fig. 6.1b) than in blank medium (Fig. 6.1a), which is consistent with previous work [196].
- Comparing with the esterase group (Fig. 6.1b), the PGX and PXS materials degraded faster in the medium added with FeSO₄/ H₂O₂ (Fig. 6.1c). However, the mass loss in the two media was only significantly different for the PXS-2days polymer ($p < 0.01$), being 36.5% and 46.1 % after 35 days incubation in medium added with esterase or FeSO₄/ H₂O₂,

respectively.

(c) The effect of XOX (Fig. 6.1d) is ignorable, similar degradation rates being observed in the both blank-medium (Fig. 6.1a) and XOX (Fig. 6.1d) groups.

In summary, the addition of esterase or hydroxyl radical accelerated the degradation rate of PGS and PXS polymers in the tissue culture medium compared with the blank group. The degradation rate of PGS and PXS polymers in the four media increases in the following order:

Blank medium group \approx XOX group $<$ Esterase group $<$ FeSO₄/ H₂O₂ group.

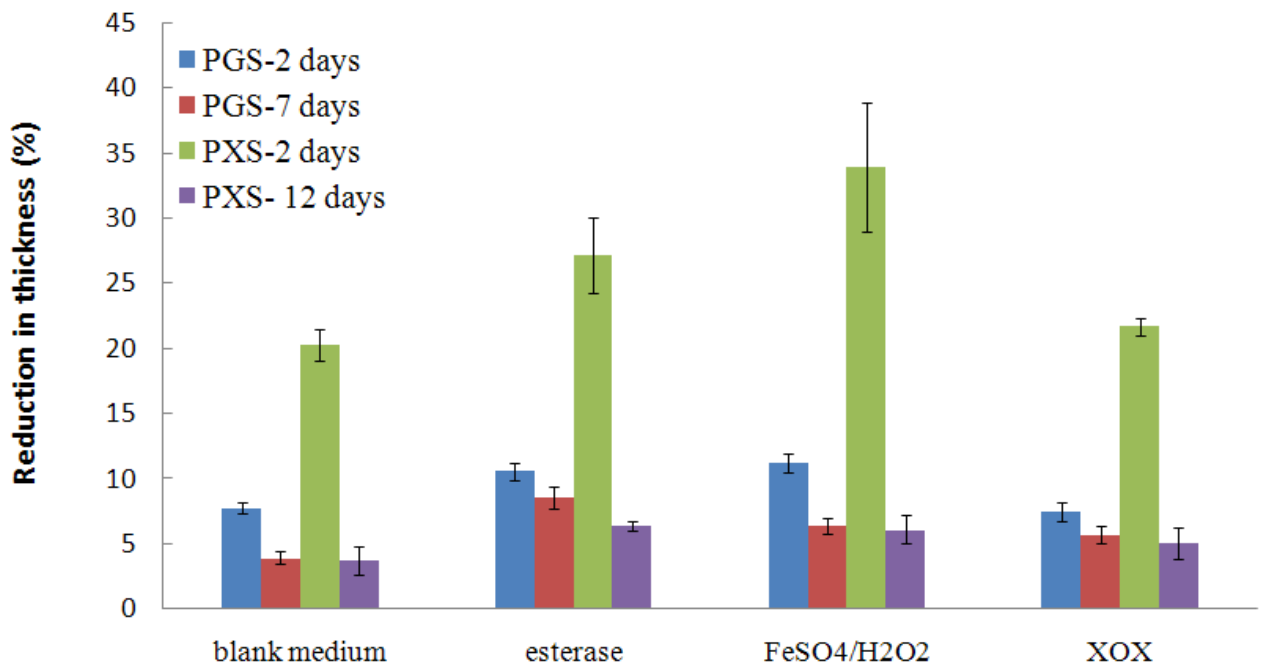


Fig. 6.2 Percentage thickness reductions of the present PGS and PXS materials after 35 days incubation in blank medium, or medium added with esterase, FeSO₄/H₂O₂, or XOX, separately. The PGS material was treated for crosslinking at 130 °C for 2 or 7 days. The PXS material was treated for crosslinking at 130 °C for 2 or 12 days.

6.2.3. Secondary effects of oxidative chemicals

Compared with the materials soaked in the medium added with esterase (Fig. 6.1b), the PGS and PXS materials degraded slightly faster in the Fenton's medium containing both esterase and $\text{FeSO}_4/\text{H}_2\text{O}_2$ (Fig. 6.3a), but no considerable difference was detected with the degradation of the polymers in the medium added with both esterase and XOX (Fig. 6.3b). After being soaked in the medium containing esterase and $\text{FeSO}_4/\text{H}_2\text{O}_2$ for 35 days (Fig. 6.3a), the samples of PGS-2days, PGS-7days, PXS-2days and PXS-12days lost 10%, 5.5%, 8.0% and 1.5 % more mass respectively, than the counterpart material incubated in esterase-containing but $\text{FeSO}_4/\text{H}_2\text{O}_2$ -free medium. Meanwhile, the degradation profiles of these materials in the medium with the addition of esterase plus XOX are more similar to those in the medium added with esterase only. The above observation on the added effects of $\text{FeSO}_4/\text{H}_2\text{O}_2$ and XOX was also confirmed by the thickness reduction of the samples soaked in the medium added with esterase and either $\text{FeSO}_4/\text{H}_2\text{O}_2$ or XOX (Fig. 6.4).

The accelerating effect of $\text{FeSO}_4/\text{H}_2\text{O}_2$ on the degradation process of PPS can be explained by the hydrolyzing action on ester bonds, often influenced by a process called the free radical degradation, an oxidative mechanism believed to accelerate the degradation process. As mentioned in the introduction, the Fenton's reagent ($\text{FeSO}_4/\text{H}_2\text{O}_2$) can generate hydroxyl radicals (HO^\bullet) via the reaction given in Eq. 6.1. In the free radical degradation process, the hydroxyl radicals primarily initiated the auto-oxidation on the surface of the polymers, but they can also diffuse into the bulk polymer network whereby causing the scission of the C-O bonds [193, 200]. The PXS network contains more C-O bonds than the PGS polymer, which could partially explain why the degradation of PXS materials was more subject to the influence of the Fenton's reagent than that of PGS polymers.

It has been reported that xanthine oxidase can metabolize hypoxanthine to xanthine and uric acid, generating superoxide anion and hydrogen peroxide around implants *in vivo* [164]. However, the above effect was not detected in the present *in vitro* experiments. The weight losses of each material in the esterase-containing media added with or without XOX were very similar (Fig. 6.1b and 6.3b). Our observation is in agreement with previous work which demonstrated that neither xanthine oxidase [197] nor XOX [162] has significant effects on the degradation of polymeric implants. Although it is unwise to conclude from the present *in vitro* experiment that the degradation of PPS polymers is not affected by the present of XOX, it is very likely that the influence of either xanthine oxidase or XOX, if any, is secondarily or very little.

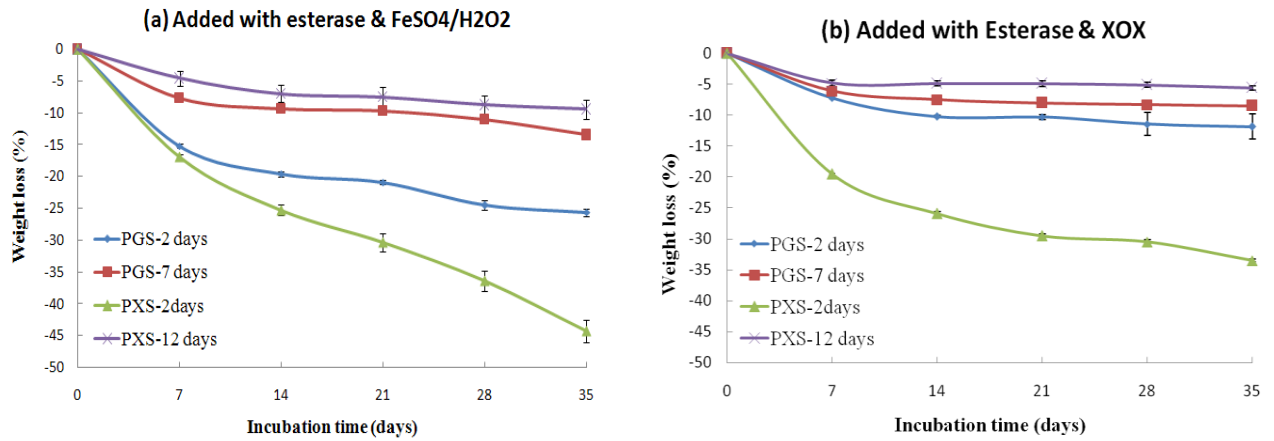


Fig. 6.3 The weight loss of the present PGS and PXS materials incubated in tissue culture medium added with (a) FeSO₄/H₂O₂ and esterase; (b) XOX and esterase. The PGS material was treated for crosslinking at 130 °C for 2 or 7 days. The PXS material was treated for crosslinking at 130 °C for 2 or 12 days.

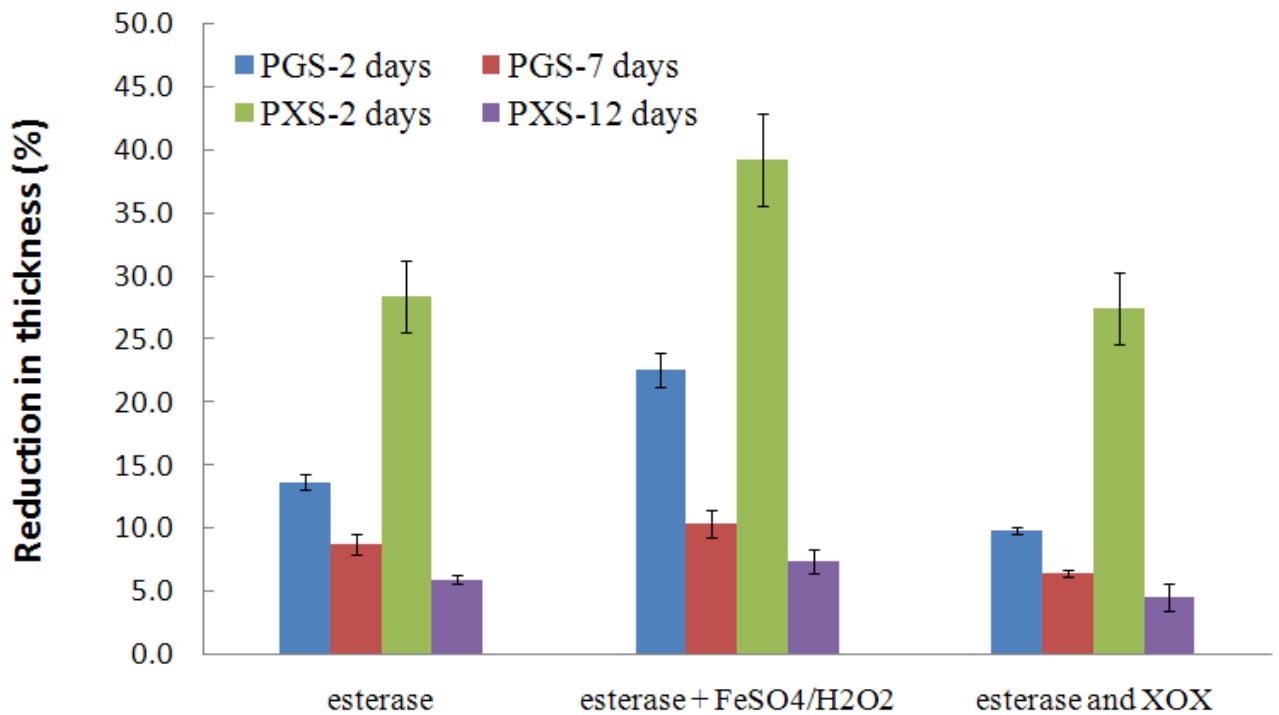


Fig. 6.4 The reduction in thickness after 35 days incubation in media added with esterases; esterases plus FeSO₄/H₂O₂; and esterases plus XOX. The PGS material was treated for crosslinking at 130 °C for 2 or 7 days. The PXS material was treated for crosslinking at 130 °C for 2 or 12 days.

6.2.4. Changes in pH value in media before and during the degradation test

As the pH value has a considerable influence on both the enzyme activity [205] and the hydrolytic degradation rate of polymers [206], it is important to monitor the pH value in the media before and during the polymer degradation. The pH value of the present DMEM was adjusted to be around 7.4 before the addition of enzymes and oxidation reagent. Before soaking polymers, a small drops (~ 0.5) were detected in pH values of medium after the addition of esterase (pH = 7.0) and XOX (pH = 7.0). However, the addition of $\text{FeSO}_4/\text{H}_2\text{O}_2$ immediately lowered the pH value of medium from 7.4 to 3.11, which was not a normal physiological condition. The total drops of pH value in media after 2 days incubation of PGS and PXS materials were illustrated in Fig. 6.5. The drastic drops of pH value in the culture medium added with $\text{FeSO}_4/\text{H}_2\text{O}_2$ alone or together with esterase were primarily due to the acidity of $\text{FeSO}_4/\text{H}_2\text{O}_2$. Besides the oxidation effect of $\text{FeSO}_4/\text{H}_2\text{O}_2$, the severe acidity of medium could enhance the degradation of polyester polymer as well, as it is well documented that the degradation of polyester is accelerated in an acidic environment [206].

After one-day incubation (Fig. 6.5a), the blank culture medium (no addition of any enzyme and oxidative chemicals) experienced the least drop (~ 0.5) of pH value. It is apparent that the soaking of PGX-7days and PXS-12days causes little further acidification, with the drop of ~ 0.5 (or 1) being primarily contributed by the addition of esterase (or the addition of both esterase and XOX). In contrast, PGX-2days and PXS-2days caused considerable further acidification in media, with the further drop of pH values being approximately 0.5 after one-day soaking of the polymers' specimens. The acidification of media was more prominent after two-day incubation (Fig. 6.5b). The above observation on pH values was in good agreement with the results of degradation rate, indicating the catalyzing effect of acidic environments. As described in Sections 6.2.2 and 6.2.3, the degradation rate of PGS and PXS polymers in the four media increased in the following order: blank medium group \approx XOX < Esterase group < $\text{FeSO}_4/\text{H}_2\text{O}_2$ group (Figs. 6.1-6.4), the addition of $\text{FeSO}_4/\text{H}_2\text{O}_2$ further accelerated the degradation of PPS materials in the esterase-containing medium (Fig. 6.3a), and that the addition of XOX did not have considerable influence on the degradation rates of the polymers (Fig. 6.3b).

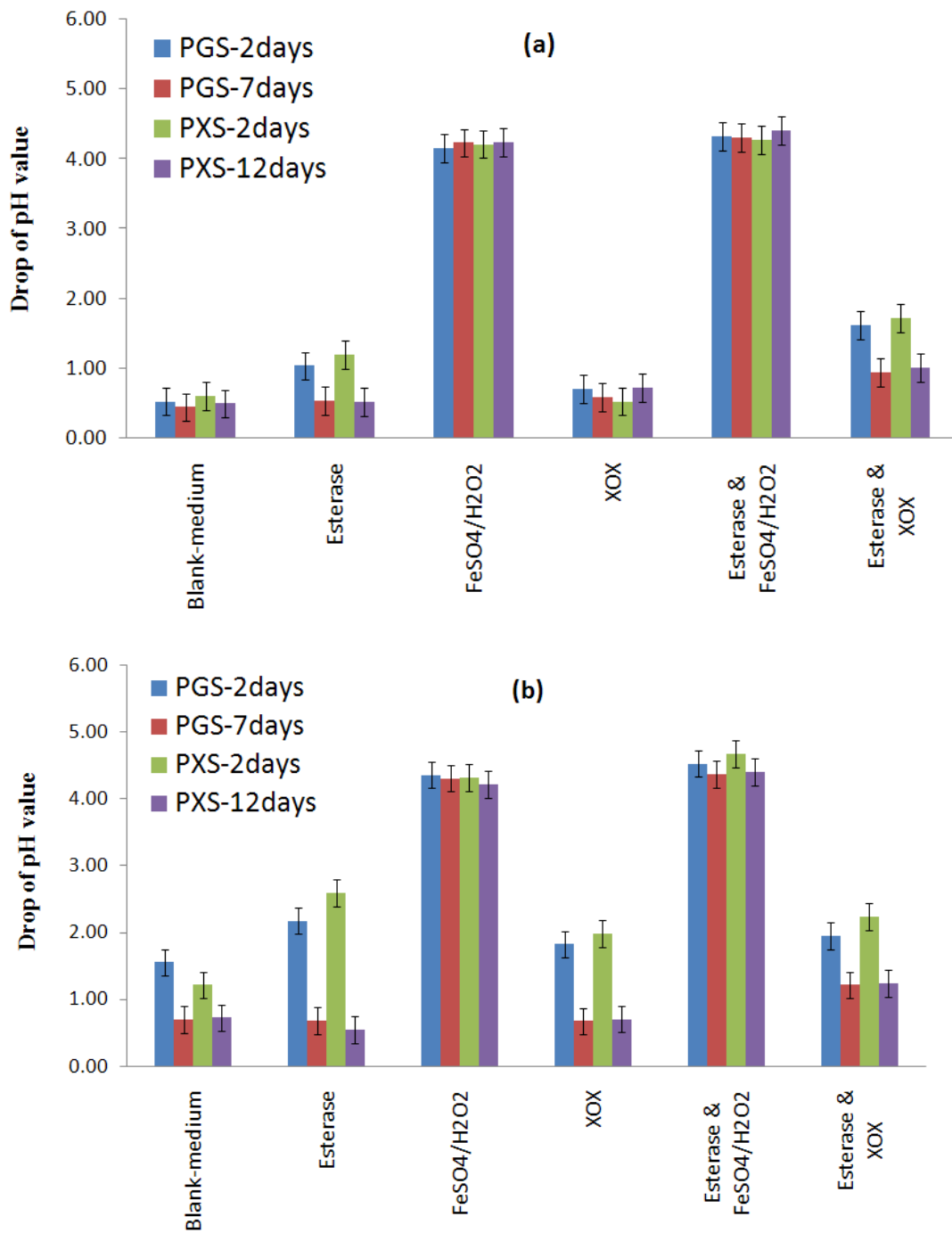


Fig. 6.5 Decrease in pH value in DEMEN tissue culture medium after soaking with PGS and PXS specimens for (a) one and (b) two days. The media were blank, or added with esterase, FeSO₄/H₂O₂, XOx, esterase plus FeSO₄/H₂O₂, or esterase plus XOx.

6.2.5. SEM examination

Fig. 6.6 shows the surface morphology of relatively highly cross-linked PGS and PXS samples after 35 days of degradations in tissue culture medium with different additives. PGS and PXS samples treated in the tissue culture medium alone or added with esterase surface layer degradation as indicated by the thin films of degradation by-products (Fig. 6.6b, the SEM image of PXS was not shown). Once the thin films were manually wiped off, smooth surfaces were revealed (Fig. 6.6a, the SEM image of PXS was not shown). Microcracks were observed on the surface of both PGS and PXS, which were tested in the medium added with $\text{FeSO}_4/\text{H}_2\text{O}_2$ (Fig. 6.6c, the SEM image of PGS was not shown) or esterase and $\text{FeSO}_4/\text{H}_2\text{O}_2$ (Fig. 6.6d, the SEM image of PGS was not shown). The microcracks were probably caused by the free-radical degradation. Similar microcracking phenomenon was also reported with the degradation of other polyesters, such as PDLLA in the $\text{FeSO}_4/\text{H}_2\text{O}_2$ solution [200]. The surface of PGS and PXS treated in the medium added with XOX was relatively smooth (Fig. 6.6e and f). Hence, $\text{FeSO}_4/\text{H}_2\text{O}_2$ accelerated the degradation rates of PGS and PXS, probably via the synergetic effect of hydrolysis (mediated by esterase), free radical mechanisms (mediated by $\text{FeSO}_4/\text{H}_2\text{O}_2$), and the acidic environments.

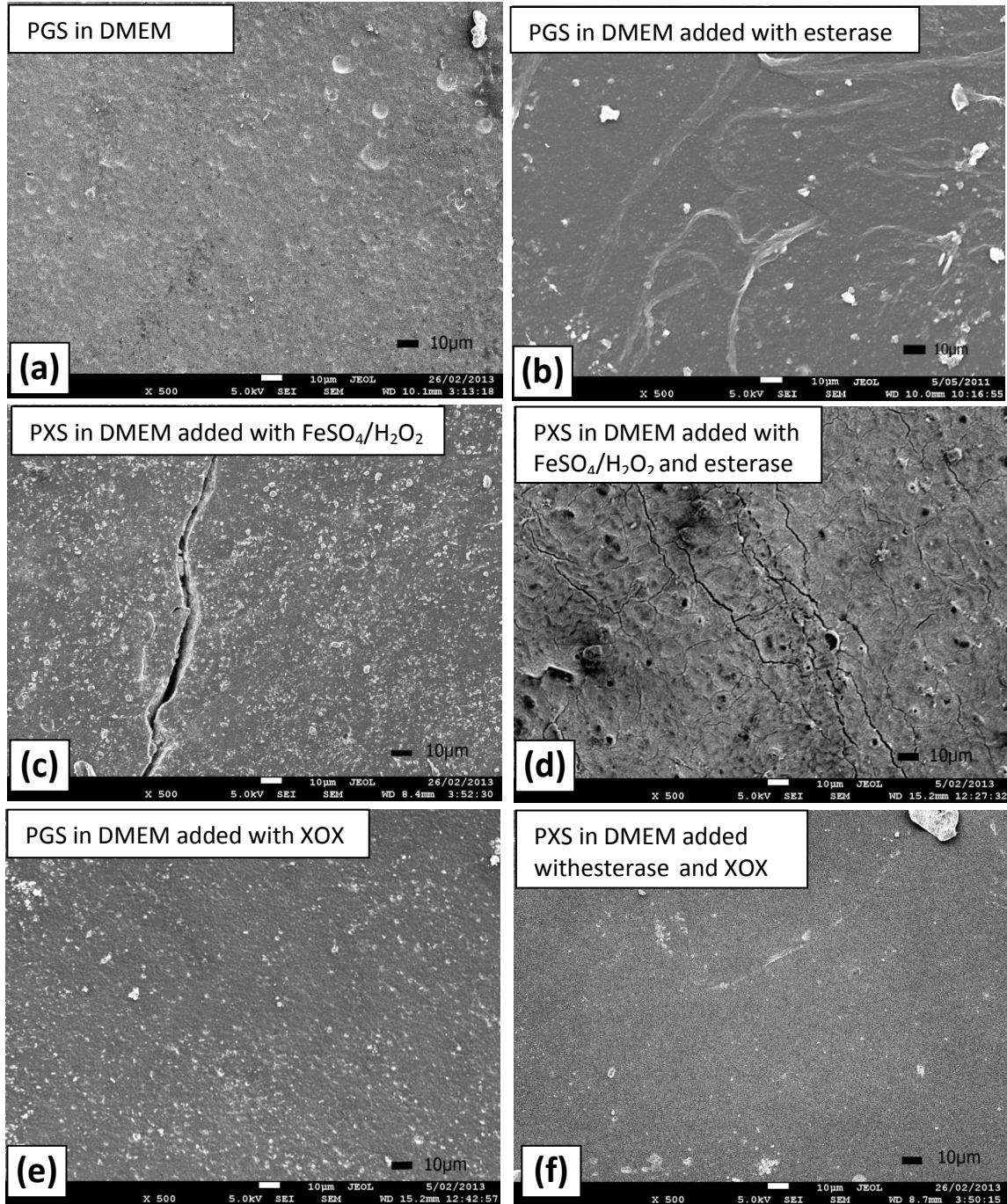


Fig. 6.6 SEM images of the surface morphologies of PGS and PXS samples after incubation for 35 days in (a) blank tissue culture medium, or media added with (b) esterase, (c) FeSO₄/H₂O₂, (d) esterase plus FeSO₄/H₂O₂, (e) XOX, and (d) esterase plus XOX. The PGS was cured at 130°C for 7 days, and PXS was cured at 130°C for 12 days.

6.2.6. Cytotoxicity of degradation product

To assess the cytotoxicity of degradation products, SNL cells were cultured in the media collected after 1 or 2 days incubation of the polymers. Visual examination showed that cells remained in a healthy phenotype in the $\text{FeSO}_4/\text{H}_2\text{O}_2$ -free media free collected after 1 day immersion of polymers (Fig. 6.7a-d). The death of cells in the $\text{FeSO}_4/\text{H}_2\text{O}_2$ -containing media (Fig. 6.7e-f) was directly correlated with the severe acidification of the media (non-physiological conditions), which was primarily caused by the acidic nature of $\text{FeSO}_4/\text{H}_2\text{O}_2$ rather than the degradation product. All the media collected after two-day incubation of polymers, except for the PGS-7days and PXS-12days materials in $\text{FeSO}_4/\text{H}_2\text{O}_2$ -free DMEM media, exhibited mild to severe toxicity (Fig. 6.8). The above observation on cell viability was further qualified by LDH measurements (Fig. 6.9).

Although cytotoxicity was widely detected in the media collected after two-day incubation of polymers, the toxic incidence does not necessarily occur *in vivo* because the concentration of degradation products will be significantly reduced in an open, constantly flowing environment *in vivo*. Hence, the health cellular phenotype in the $\text{FeSO}_4/\text{H}_2\text{O}_2$ -free media collected after one-day immersion of polymers (Fig. 6.7) is considered to better represent the environment *in vivo* than those collected after two-days immersion of polymers. Previously, *in vivo* study on a heart patch made of PGS has demonstrated that the degradation of PGS do not cause unexpected inflammation [95]. To summarise, the *in vivo* (i.e. esterase-mediated) degradation of the present PGS and PXS polymers would likely have little toxic impact on the host body.

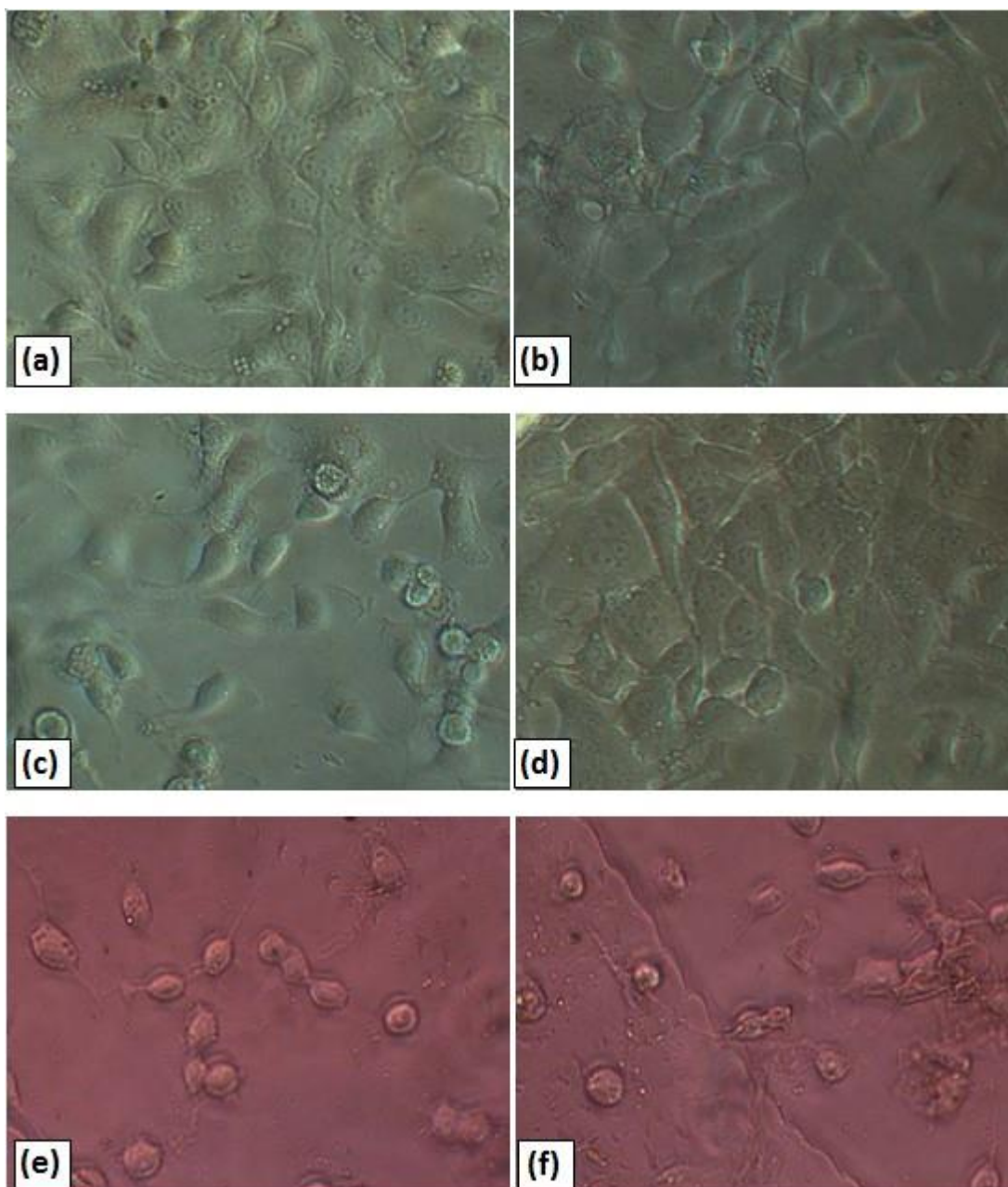


Fig. 6.7 Live imaging of SNL cells cultured in the DMEM media which were soaked with PPS samples for one day. (a) DMEM alone, DMEM added with, (b) esterase, (c) XOX, (d) esterase plus XOX, (e) $\text{FeSO}_4/\text{H}_2\text{O}_2$, or (f) esterase plus $\text{FeSO}_4/\text{H}_2\text{O}_2$. The PGS was cured at 130°C for 2 days. Other PPS showed similar phenotypes of SNL cells in the above media.

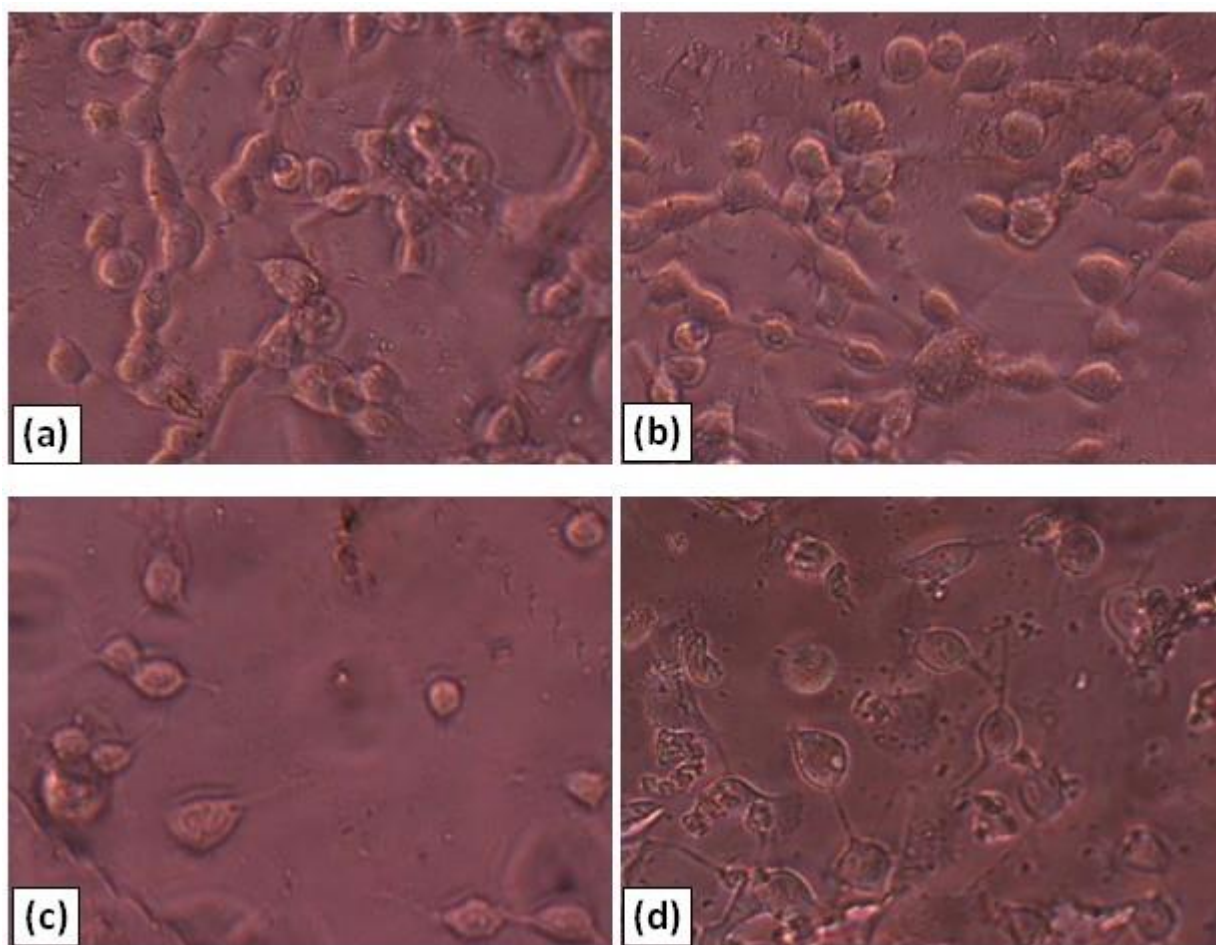


Fig. 6.8 Representative morphologies of SNL cells cultured in the DMEM media which were soaked with PPS samples for two days. (a) blank DMEM, DMEM added with (b) esterase, (c) XOX, or (d) esterase plus XOX. PXS was cured at 130°C for 2 days.

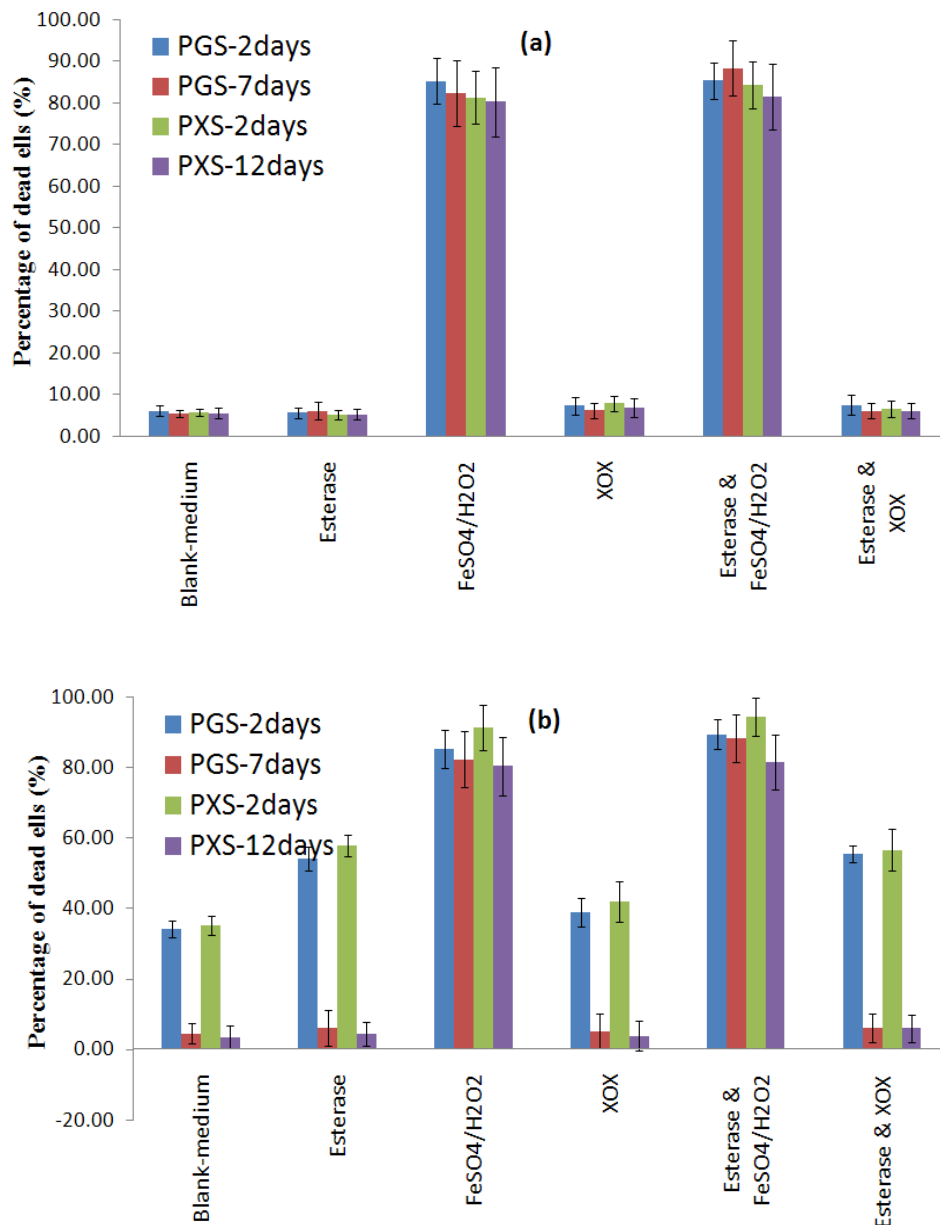


Fig. 6.9 Lactic dehydrogenase (LDH) based evaluation on the effect of extractant media soaked with PPS samples for (a) one or (b) two days, on the viability of SNL mouse fibroblasts, extract-free (blank) medium being the negative control. The PGS material was treated for crosslinking at 130 °C for 2 or 7 days. The PXS material was treated for crosslinking at 130 °C for 2 or 12 days. (a) the four materials within each group did not exhibit a significant difference ($p > 0.05$); the differences between the groups of blank medium, medium added with esterase, XOX or esterase plus XOX were not significant ($p > 0.05$). The cell death percentages in the media added with FeSO4/H2O2 with or without esterase were significantly higher than other groups ($p < 0.001$). (b) The degradation of PGS-7days and PXS-12days materials in blank medium, medium added with esterase, XOX, or esterase plus XOX, showed a significantly lower toxicity than other PPS polymers and than in other media ($p < 0.001$).

6.3. Conclusions

The mediation effects of esterase (hydrolytical enzyme), xanthine oxidase/xanthine (oxidative enzyme) and $\text{FeSO}_4/\text{H}_2\text{O}_2$ (biological oxidation chemical) on the degradation of PPS polymers have been investigated with the PGS and PXS of different crosslink densities. The study has revealed that (1) the degradation kinetics of PPS materials were primarily determined by the degree of crosslink density in the polymer network, with high crosslink density of the materials demonstrating a slow degradation rate; (2) the degradation rates of PGS and PPS were primarily accelerated by the presence of esterase and secondarily by $\text{FeSO}_4/\text{H}_2\text{O}_2$; (3) the influence of xanthine oxidase/xanthine on the degradation of PPS *in vitro* was not considerable; and (4) the cytotoxicity evaluation indicated that the esterase-mediated degradation of PGS and PXS polymers with low-level cross-linking have high toxicity due to degradation causing the pH drop of surrounding medium, while highly crosslinked PGS and PXS polymers would likely have little toxic impact on the host body. So basically, PGS and PXS with lower crosslink density may not possible to use (depending on the enzyme kinetics of wound sites), but PGS and PXS with higher crosslink density are probably to useful for medical applications.

CHAPTER SEVEN

ELASTOMERIC PXS/PVA FIBROUS SHEETS PRODUCED BY CORE/SHELL ELECTROSPINNING: FABRICATION, CHARACTERISATION AND PROPERTIES

7.1. Introduction

The electrospinning technique has been used to produce scaffolds for tissue engineering applications for the past decade, producing similar morphological and structural features to the fibrous extracellular matrix of natural tissue. Spun fibre scaffolds are characterised by a wide range of pore diameter distribution, high porosity and effective mechanical properties [207]. Studies have demonstrated that the electrospun nanofibrous scaffolds are very good at supporting attachment and cell proliferation [208]. Various synthetic biopolymers, such as PLA, PGA, PCL and their copolymers, have been electrospun for tissue engineering applications. However, thermoplastic materials are generally unsuitable for use in the repair of organs/tissues working under dynamic mechanical conditions, such as heart and lung, because they lack reshaping ability [62]. Elastomeric biomaterials, such as PPS, a relatively new family of cross-linked biodegradable elastomers, do not suffer from this problem, so they fill an important need for scaffolds in soft tissue engineering [1, 112, 209].

The production of nanofibres from chemically crosslinked elastomers is technically challenging. A major hurdle is that these polymers cannot dissolve into any solvents once cross-linked, and that fibres spun from uncrosslinked prepolymers would melt when they underwent crosslink treatment. This problem could be addressed by core/shell electrospinning, a recently developed technique [63, 115, 173]. In the core/shell electrospinning process, a non-crosslinked prepolymer, e.g. PGS, is sheathed by a thermoplastic, such as poly (L-lactic acid) (PLLA), when both materials are fed to the electrospinner simultaneously but via separate flows; in this case, PGS flows from inner tube, while and PLLA flows from outer tube. During the thermal crosslinking treatment, the solid thermoplastic PLLA shell maintains the tube shape and contains the core PGS material which melts and undergoes a cross-link reaction. PGS/PLA core/shell fibres have been fabricated using the above procedures [63, 115, 173]. A shortcoming associated with shells made from PLA is that the organic solvent used to dissolve and remove it can infiltrate into PGS and damage the polymer network,

eventually leaving a brittle core fibre behind. In practice, it is a difficult task to avoid any contact between the solvent and the PGS core.

To eliminate the above drawback, the PLA shell can be replaced with polyvinyl alcohol (PVA). Unlike PLA, which must be dissolved in an organic solvent [115], PVA is water soluble. PVA has been electrospun by a number of research groups [210-212] because it is inexpensive and biocompatible. PVA gel is not degradable in most physiological situations. Therefore, it is useful for long-term or permanent scaffolds in tissue engineering. PVA hydrogels have been utilised in regenerating artificial articular cartilage [213] and adhesion shields in tendon regeneration [214]. In this work, PXS rather than PGS was used as the core material because the PXS elastomer networks have a more suitable combination of elasticity and degradability compared with their PGS counterparts [152].

In Chapter 5, the PXS synthesized from a monomer mole ratio of 1:1 and cured for a short time showed higher cytotoxicity, while longer curing times improved the cytocompatibility due to its higher crosslink density. To shorten the curing time without affecting crosslink density, and therefore cytocompatibility, we hypothesized that synthesis of PXS with 2:5 mole ratio (xylitol :sebacic acid) and curing for a shorter time could achieve equally high crosslink density. Thus, in this chapter the core PXS material was synthesized with 2:5 mole ratio (xylitol : sebacic acid) and cured for 3 days at 130°C.

Therefore, this chapter work was aimed at establishing a reliable and reproducible fabrication procedure for PXS/PVA core/shell electrospinning, to produce mechanically effective and safe scaffolds. The mechanical properties and biocompatibility of fibrous PXS scaffolds were assessed in under aqueous conditions, to simulate the *in vivo* physiological environment.

7.2. Results and discussion

7.2.1. Optimisation of PXS/PVA core/shell electrospinning conditions

It was found that the concentration of PVA solution allowing production of an optimal fibrous structure decreased at higher PVA molecular weights shown in Table 7.1. This result was in agreement with previous work [215], and can be interpreted by the influence of ηC on the formation of fibres [211, 215], where η is the intrinsic viscosity of the polymer and C is the concentration of the polymer solution in wt %. To produce fibres in the electrospinning process, the ηC of the polymer solution must be at a certain value. This value is typically in the range of 5-12, depending on the chemistry of thermoplastic solute [75, 76, 215]. The Mark–Houwink relationship for PVA in water has been given by Tacx and co-workers[216]:

$$\eta = 6.51 \times 10^{-4} M_w^{0.628}. \quad \text{Eq. 7.1}$$

Using Eq. 7.1, the ηC value of the PVA solutions that produced stable PVA fibres (Fig.7.1) and PXS/PVA core/shell fibres (Fig. 7.2) were calculated to be 9-12 (PVA 31,000–50,000 g/mol, $C = 20$ wt %), 10 (PVA 89,000–98,000 g/mol, $C = 11.5$ wt %), and 8-10 (PVA 146,000–186,000 g/mol, $C = 7.4$ wt %), respectively. Hence, we concluded that the ηC value of the optimised PVA solutions were around 10. These results were slightly higher than those of Koski and co-worker[215], who found that PVA fibres with a circular-shaped cross-section could be stabilised when ηC is in between 5 to 9 [215]. When $\eta C > 9$, flat fibres were produced.

In addition, the diameters of the both PVA and PXS/PVA electrospun fibres in the present work were increased with the increment of the molecular weight of PVA, as listed in Table 7.1. This is because the fibre diameters are reduced via the relaxation of polymer chains during spinning, and the relaxation of large polymer chains is difficult [215].

The molecular weight of PVA also influenced the quality of the PXS/PVA core/shell fibres (Fig. 7. 2). The PVA of a low molecular weight (e.g. 31,000–50,000 g/mol) generally produced well-defined, small-diameter fibres at the condition of 0.1 ml/h core feeding rate (Fig. 7.2a and a'). The PVA of high-molecular weight (i.e. 146,000–186,000 g/mol) always produce webbed PXS/PVA core/shell fibre as, shown in Fig. 7.2c, due to the low concentration of the PVA solution. As discussed above, the concentration of high-molecular weight PVA solution had to be as low as to 8 % (wt/v) in order to produce stable PVA fibres. This concentration, which worked fine with single-

tube electrospinning, however, produced a very thin PVA shell such that it could not fully cover the PXS core in the core/shell spinning process. In the subsequent curing treatment, the PXS melted and flowed out of the shell. However, an overly thick shell of PVA would result in a very fragile PXS network after PVA was washed off (see the next section). Among the three PVA polymers used in this study work, PVA of a molecular weight of 89,000–98,000 g/mol was considered to be optimal for the fabrication of stable PXS/PVA fibres and PXS fibres. It must be noted that both PVA and PXS/PVA fibres were fused at their contacting point, as observed at high magnification (Fig. 7.1 a'-c' and Fig. 7.2a'-c').

Table 7.1 PVA polymers used in this work, optimal concentrations of solutions that produced satisfactory electrospun fibres, and subsequent diameters of PVA and PXS/PVA fibres*

M_w (g/mol) of PVA	Percentage of hydrolyzation of PVA as purchased	Concentration of PVA (shell) solution (g /100 mL solution**)	Fibre diameter (μm)		Feeding rates of core:shell (mL/h)	Voltage (Positive/negative)
			PVA	PVA /PXS		
31,000-50,000	98–99 %	25	0.22 \pm 0.01	0.38 \pm 0.03	0.1:0.8	+13/-2 kV
89,000-98,000	> 99 %	13	0.36 \pm 0.03	0.51 \pm 0.04	0.2:0.8	+13/-2 kV
146,000-186,000	98–99 %	8	0.39 \pm 0.04	0.79 \pm 0.05	0.1:1	+15/-2 kV

* The concentration of PXS solution was 50% (v/v).

** The solvent was the mixture of water and DMF in the 4:1 volume ratio.

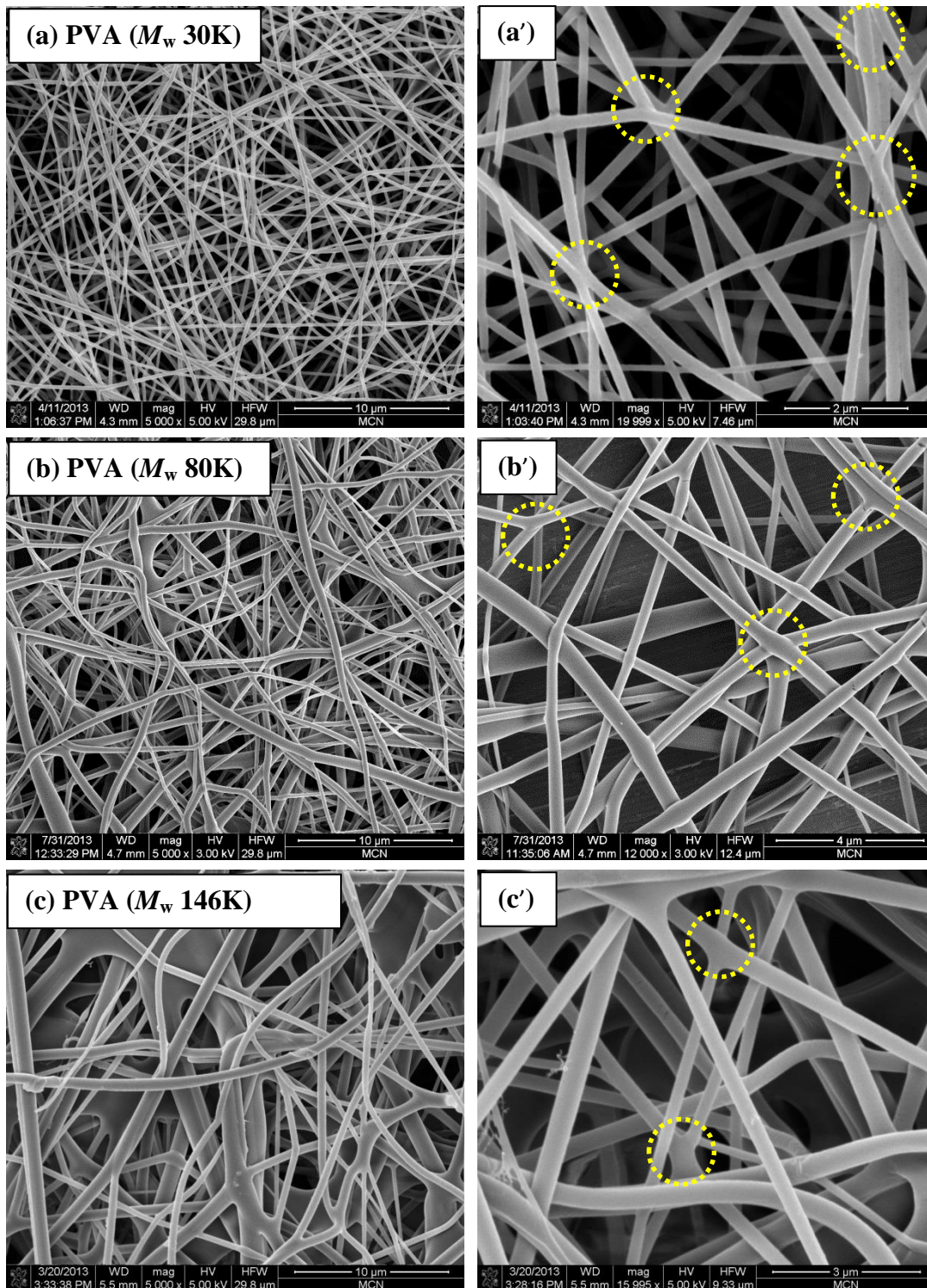


Fig. 7.1 SEM images of PVA fibre mats after heating at 130°C for 3 days. (a) PVA 31,000-50,000 g/mole, (b) 89,000-98,000 g/mole and (c) 146,000-186,000 g/mole; (a'-c') are higher magnification SEM images of (a-c). Circled areas show the fusion of PVA shells between fibres.

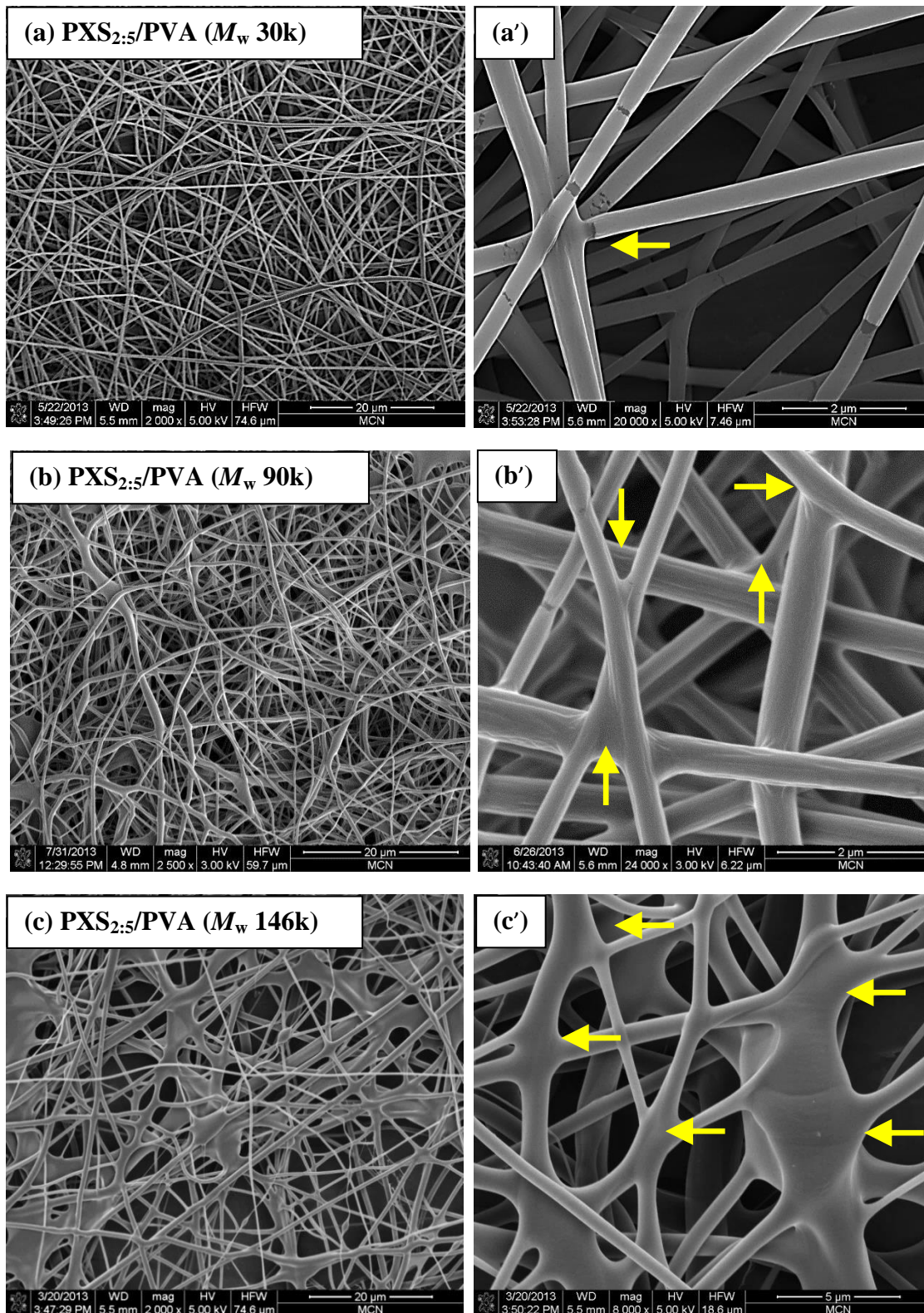


Fig. 7.2 SEM images of PXS/PVA core/shell fibre mats after curing at 130°C for 3 days. (a) PVA 31,000-50,000 g/mole, (b) 89,000-98,000 g/mole and (c) 146,000-186,000 g/mole, $[\eta]C$ value are about 9, 10, 9 respectively. (a'-c') are higher magnification SEM images of (a-c) which shows fusing occurred between fibres at contacting points which impede the sliding between fibres.

7.2.2. Removal of PVA shell from the PXS/PVA spun mats

Both electrospun PVA and PXS/PVA fibres, before and after curing, were white in colour because of the light scattering from the fibrous structure. When a PVA spun mat was immersed in water, the fibre mat immediately shrank and became transparent and gelatinous. After heating in water at 90°C for 1 h, the PVA fibres fully dissolved in water. In contrast, the PXS/PVA fibres did not shrink after immersion in water, but they became transparent as well. After washing in a stirring water bath at 90°C, the spun mats were taken out and vacuum dried. The final fibre mat was opaque, neither as white as the PXS/PVA fibres before washing nor as transparent as the PXS sheet, possibly due to residual PVA (Fig. 7.3).

Fig. 7.3 shows the SEM images of the spun PXS/PVA fibres after washing in hot water. As discussed above, when the PVA of a M_w of 31,000–50,000 g/mol was used as the shell material, a very small amount of PXS was spun out as a core fibre. As a result, after washing very thin PXS core material was left, with some PVA remaining in the final mat. The residual PVA was recrystallised and formed flakes on the surface (Fig. 7.3a and a'). The PVA with a M_w of 89,000–98,000g/mol was shown to produce the much improved PXS (with residual PVA) network (Fig. 7.3b and b'). Fibrous structure was observed in the washed spun mat, although most fibres were fused by the dissolved PVA remaining in the mat. In this porous material, the pore size ranged from 1 to 5 μm , as shown in Fig. 7.3b and b'. As mentioned above, among the three PVA polymers used in the work, the PVA of a molecular weight of 89,000–98,000 g/mol produced the most optimal PXS/PVA fibres and PXS fibres. Therefore, the subsequent studies were focused on the PXS/PVA core/shell spun mat fabricated with this medium molecular weight PVA.

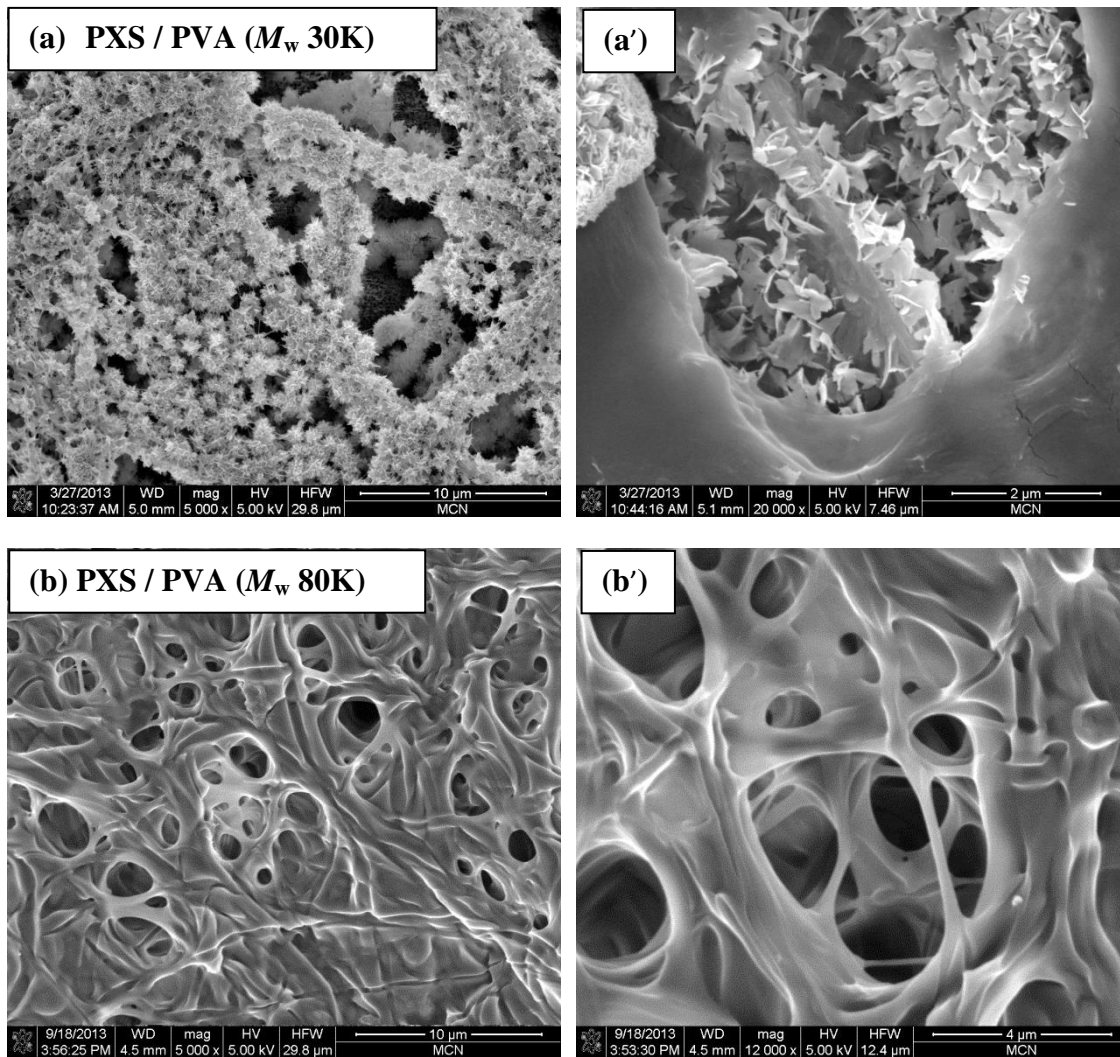


Fig. 7.3 SEM images of PXS/PVA core/shell fibre mats after curing then washed in distilled water (a) spun mat with PVA 31,000-50,000 g/mol washed at 80°C for 24h. (b) spun mat with PVA 89,000-98,000 g/mol washed at 90°C for 4h. (a') and (b') are higher magnification SEM images of (a) and (b).

7.2.3. Mechanical properties of core/shell spun mesh materials

The stress-strain curves of PXS sheet, PVA fibres, PXS/PVA core/shell fibres and washed PXS/PVA fibres are shown in Fig. 7.4. The stress-strain curve of the PXS sheet was approximately linear; whereas the curves of the spun PXS/PVA fibres showed an abrupt slope at small strains lower than 10 %, after which the slope became flat. The above mechanical behaviour could be explained by the SEM observation of fibre fusion between the PXS/PVA fibres at their contact points (Fig. 7.2a'-b'). A comparison of the stress-strain curves of PVA and PXS/PVA revealed that the plateau of stress-strain curve of PXS/PVA approximately started when the stress reached the UTS of PVA. Hence, it is possible that the junctions between the PVA shells detached when the stress reached the UTS of PVA, after which the fibres could easily slide relative to each other, demonstrating a plateau on the stress-strain curve.

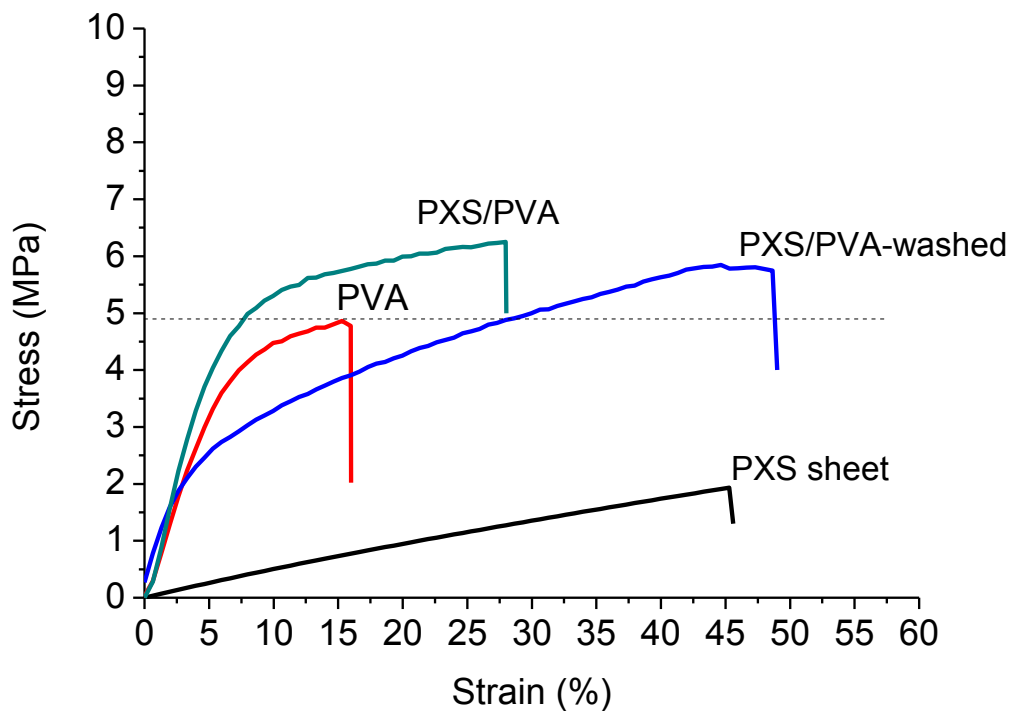


Fig. 7.4 Typical tensile stress-strain curves of PXS sheets, PVA fibre mats, PXS/PVA fibre mats and PXS/PVA-washed fibre mats.

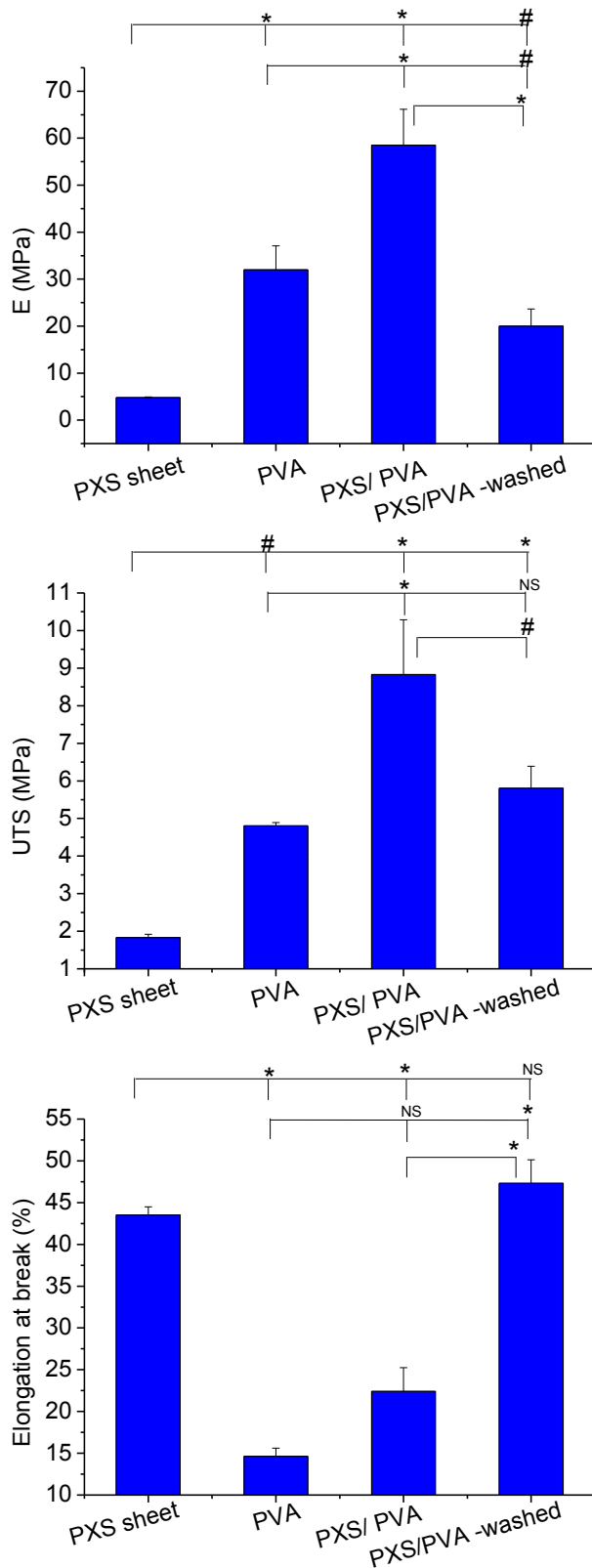


Fig. 7.5 Mechanical properties of PXS sheets, PVA fibre mast, PXS/PVA fibre mats and PXS/PVA-washed fibre mats. (a) Young's modulus (E), (b) Ultimate tensile strength (UTS) and (c) elongation at break. The error bars represent one standard error. * $p < 0.01$, # $p < 0.05$. NS stands for 'not significant'

Fig. 7.5 shows the mechanical properties of the PXS sheet, PVA fibres, PXS/PVA core/shell fibres and washed PXS/PVA core/shell fibres under the dry condition. Table 7.2 lists the Young's modulus E , UTS, rupture strain values of all the tested materials. The PXS/PVA core/shell fibrous mats exhibited a higher UTS (8.8 ± 1.5 MPa) and a higher E (58.5 ± 7.7 MPa) than the both PXS sheets (UTS = 1.8 ± 0.1 MPa, $E = 4.8 \pm 0.1$ MPa) and PVA fibrous mats (UTS = 4.8 ± 0.1 MPa, $E = 32 \pm 4.1$ MPa). However, the rupture elongation of the PXS/PVA (22 ± 3 %) was statistically similar to that of the PVA (14 ± 1 %). The rupture elongations of the fibrous materials were considerably smaller than that of the PXS solid sheet (44 ± 1 %), as shown in Fig. 7.5c and Table 7.2 After washing to remove the PVA shell, both UTS (5.8 ± 0.6 MPa) and E (20 ± 3.7 MPa) of the PXS/PVA core/shell fibre mats decreased, but they were still higher than those of the PXS sheets. The higher E and UTS of washed PXS/PVA mat could be attributed to the residual PVA in the fibrous network. The rupture elongation of the washed PXS/PVA fibrous mat was 47 ± 3 %, higher than that of the PXS sheet (44 ± 1 %), although the difference was not statistically significant.

Table 7.2 Mechanical properties PXS sheet, PVA fibres, PXS/PVA core-shell fibres and washed PXS/PVA core-shell fibres

Materials*	E (MPa)	UTS (MPa)	Elongation at break (%)
PXS sheet	4.8 ± 0.1	1.8 ± 0.1	44 ± 1
PVA	32 ± 4.1	4.8 ± 0.1	14 ± 1
PXS/PVA	58.5 ± 7.7	8.8 ± 1.5	22 ± 3
PXS/PVA- washed	20 ± 3.7	5.8 ± 0.6	47 ± 3
PVA -wet	1.9 ± 0.3	0.8 ± 0.2	59 ± 2
PXS/PVA -wet	3.3 ± 0.3	1.3 ± 0.3	55 ± 3
PXS/PVA -ww	1.1 ± 0.2	1.7 ± 0.1	76 ± 8

* The process of the samples are listed in table 3.2.

To study the performance of the fibre mats in preparation for physiological conditions, the mechanical properties of hydrated fibrous mats were tested (Fig. 7.6). Compared with the dried fibre mats, the UTS of the PVA-wet, PXS/PVA-wet and the PXS/PVA-washed and wet (PXS/PVA-ww) fibre mats significantly decreased to 0.8 ± 0.2 , 1.3 ± 0.3 and 1.7 ± 0.1 MPa, respectively under hydrated conditions (Fig. 7.7a). The Young's moduli of the PVA-wet, PXS/PVA-wet and the PXS/PVA-ww also significantly decreased to roughly one-twentieth of their dry counterparts, being 1.9 ± 0.3 , 3.3 ± 0.3 and 1.1 ± 0.2 MPa, respectively (Fig. 7.7b). The E value of the PXS/PVA-ww was similar to that of PXS mats. As described in a previous study[24], PXS shows little swelling in water.

The rupture elongation of the spun fibre mats all increased significantly compared to their dried counterparts, as shown in Fig. 7.7c. The increase in rupture elongation was largest with PVA-wet (59 ± 2 %), with the increase being about four times greater than that of the dried PVA fibrous mats. The low elongation of the PVA in the dry condition was apparently due to its thermoplasticity, which makes it brittle, whereas PVA forms a hydrogel in water. Among the hydrated fibre mats, the PXS/PVA-ww had the highest rupture elongation (76 ± 8 %), which was also significantly higher than that of the PXS sheet (44%, $p < 0.0001$). Under wet conditions, residual PVA on the washed PXS/PVA fibre mats is in the form of a hydrogel, thus the physical linkage with PVA would have been dissociated. Hence, the PXS fibres could slide over each other easily in wet conditions and exhibit larger rupture elongations than highly crosslinked PXS solid sheets.

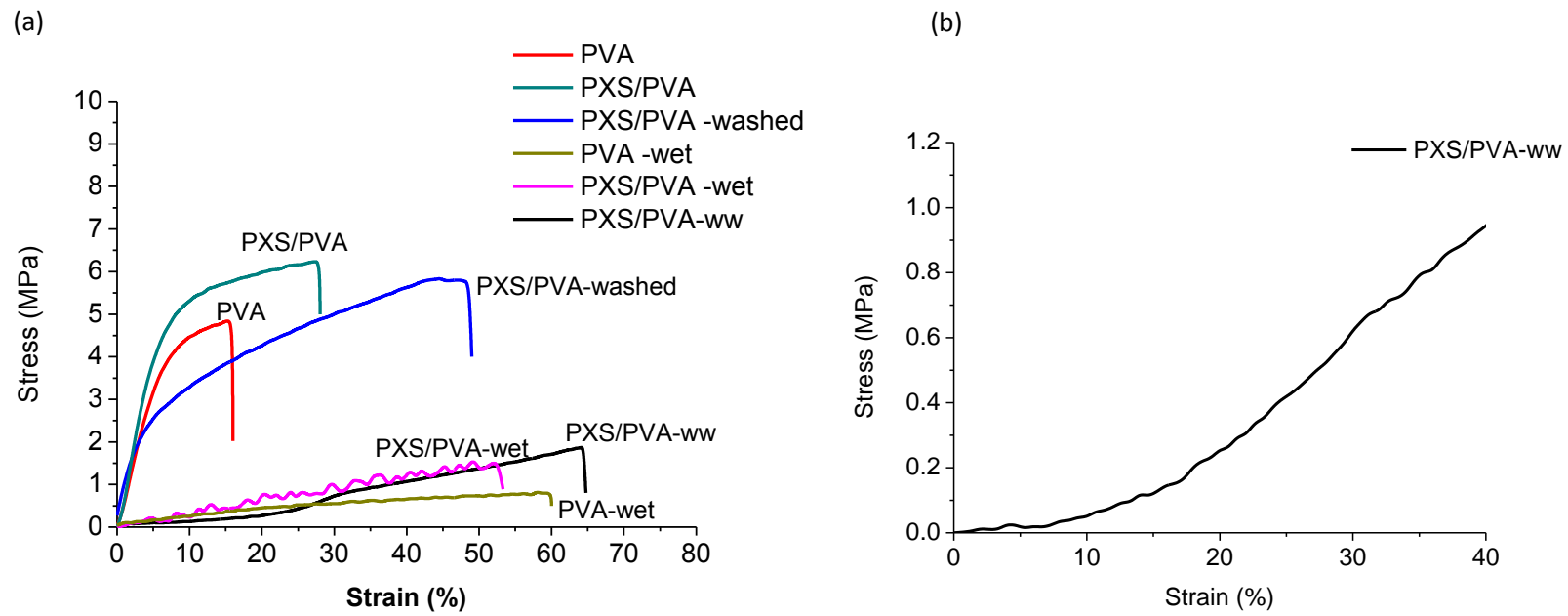


Fig. 7.6 (a) The typical tensile stress-strain curves for the materials which show the effect of water on the mechanical properties of PVA fibre mats, PXS/PVA fibre mats and PXS/PVA-washed fibre mats. The fibres were tested under dry and hydrated conditions after immersion of mats in water, (b) J-shaped tensile stress-strain curves of PXS/PVA-ww fibrous mats in wet conditions.

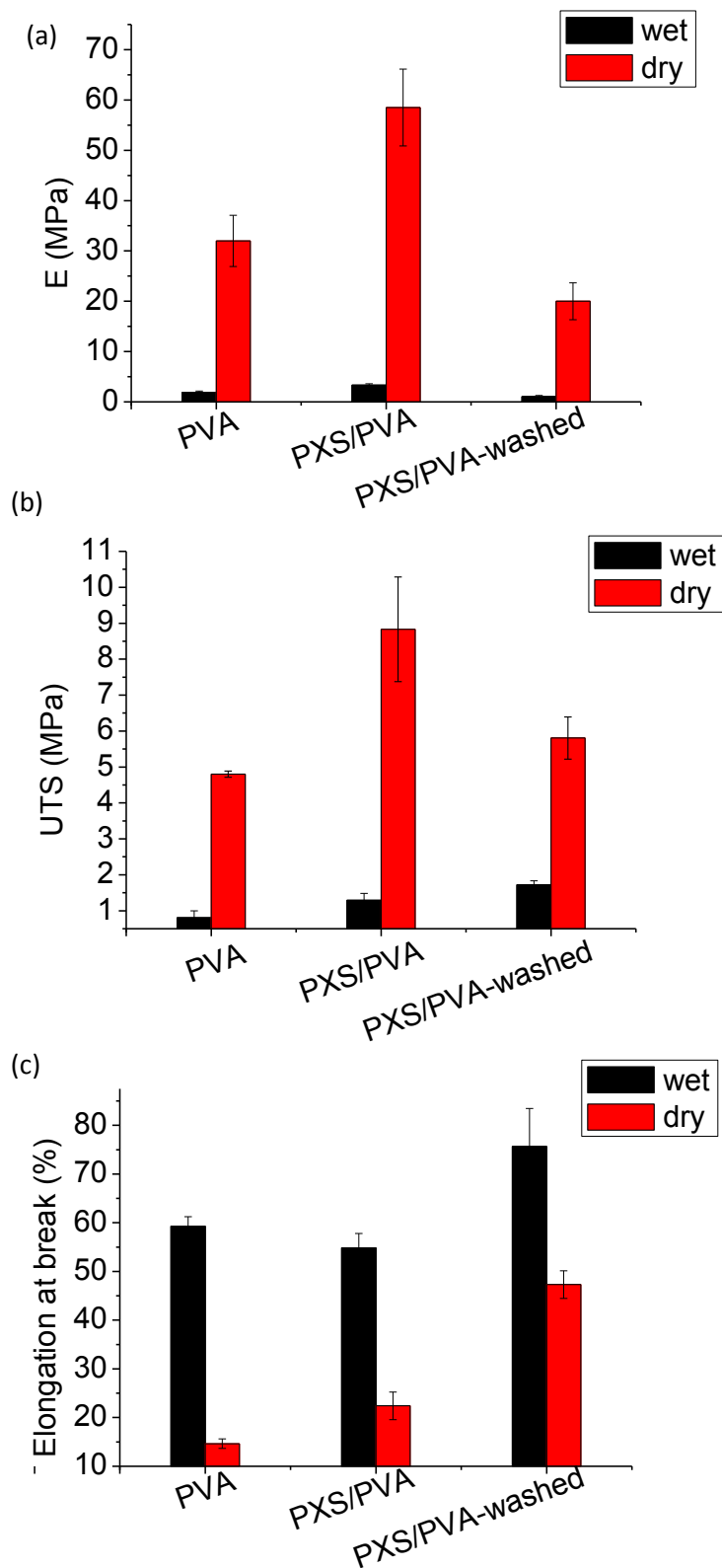


Fig. 7.7 The effect of water on the mechanical properties of fibre mats made from PVA, PXS/PVA and PXS/PVA-washed. The fibres were tested at dry condition and wet fibres after immersed in water, with values of (a) Young's modulus (E), (b) UTS and (c) elongation at break. The error bars represent one standard error. For those three materials the differences of all mechanical properties at dry and wet conditions are significant ($p < 0.01$).

To summarise, under wet conditions the PXS/PVA-ww fibrous mats had the lowest Young's moduli, but the highest UTS and rupture elongation among the three types of fibrous mats. The mechanical characteristics of PXS/PVA-ww fibrous meshes make them promising candidates for applications in soft tissue engineering, as the low Young's moduli are in the range of soft tissues, while their high UTS and rupture elongations offer mechanical safety and reliability.

Cyclic testing of the materials demonstrated that the PXS sheet, the PXS/PVA-washed and the hydrated counterpart PXS/PVA-ww had a resilience of 93%, 46% and 84%, respectively (Fig. 7.8). This is similar to that of elastic proteins, which have resilience ranging from 35 % (for partially hydrated elastin) to 90 % (for fully hydrated collagen and elastin) [60].

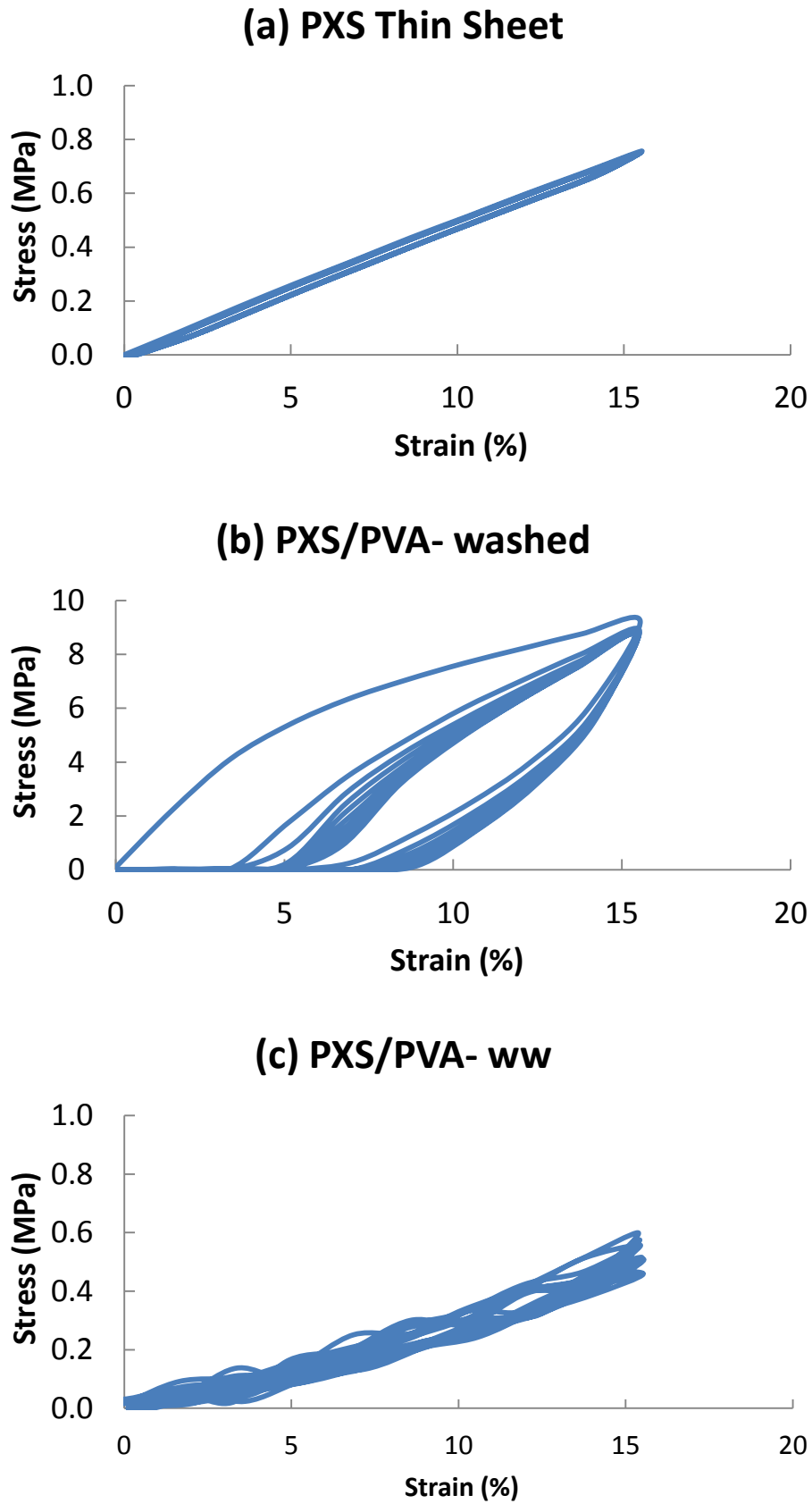


Fig. 7.8 A 50-cycle tensile stress-strain curve of (a) PXS sheet, (b) PXS/PVA-washed fibre mat and (c) PXS/PVA-ww fibre mat.

In the present work, the stress-strain curves of fibrous meshes exhibited different shapes under the dry and wet conditions. Under dry conditions, the stress-strain curves of PVA, PXS/PVA and PXS/PVA-washed fibrous networks exhibited an upward trajectory (Fig. 7.6a), whereas under the wet conditions, the stress-strain curves of the same fibrous mats were J-shaped (Fig. 7.6b and 7.8c). The upward trajectory shape of stress-strain curves can be attributed to the role of PVA in inter-fibre fusion (Fig. 7.1-7.3). It is well documented that the shape of stress-strain curves of crosslinked polymer chain networks are upward-trajectory at small strains, as represented by Eq. 3.4 [157]. One can envisage that when cross-links (i.e. physical barriers) are dissociated, the fibres can easily slide over each other under a very low stress, and thus produce a J-shaped stress-strain curve. This is the probable mechanism behind the J-shape of the stress-strain curves of the PVA, PXS/PVA and PXS/PVA-washed fibrous networks under wet conditions. The links between fibres in these three groups of fibrous networks were caused by the PVA. Because PVA is water soluble, the links due to PVA fusion are quickly dissociated once the fibrous mats are soaked in an aqueous environment. As a result, the non-fused fibrous network exhibited J-shaped stress-strain curve in the wet conditions.

The inter-fibre fusion caused by the PVA can also be dissociated by physical stretch. Once the fused PVA linkers of a network break, the network would produce J-shape stress-strain curves in the subsequent deformation cycles. This mechanism explains the upward-trajectory stress-strains curve of the first cycle and the J-shaped stress-strain curves of the subsequent deformation cycles in Fig. 7.8b.

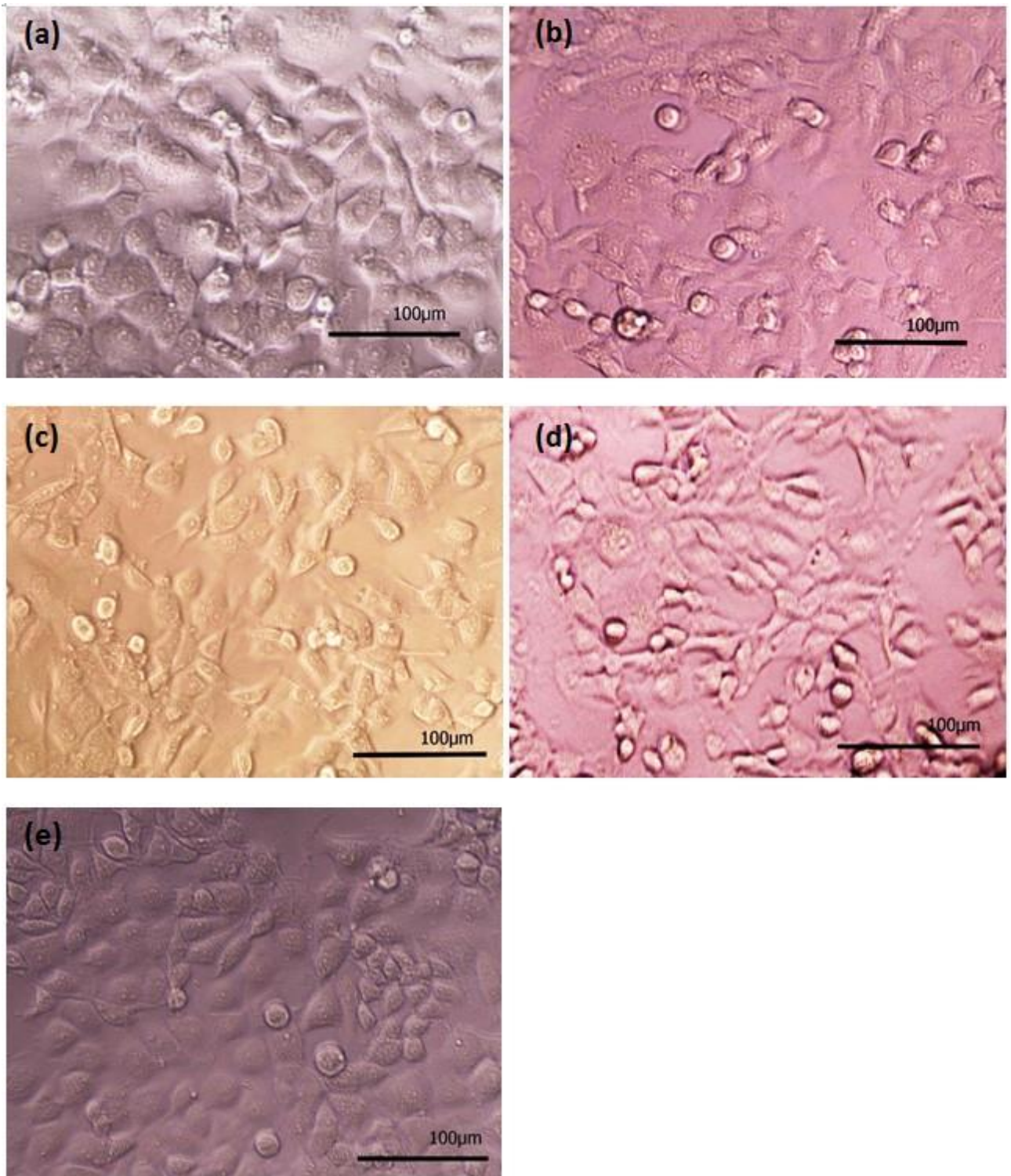


Fig. 7.9 Images of SNL cells cultured in media with evaluated materials direct placed in for 24 h. (a) Negative control (free culture medium); (b) positive control with PLLA fibre; (c) PXS sheet; (d) PXS/PVA core/shell fibrous mesh (e) electrospun fibre mat of PXS/PVA, with PVA being washed off.

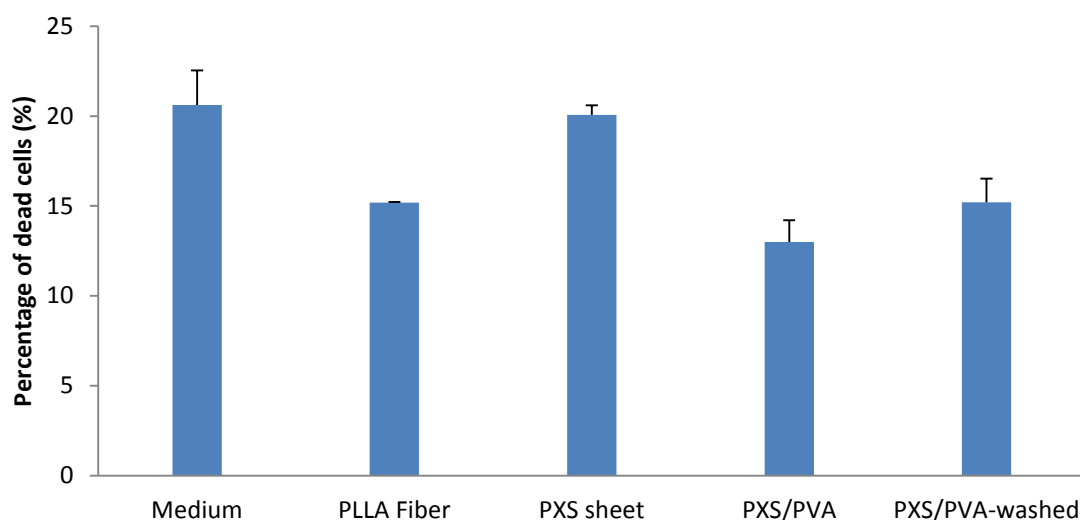


Fig. 7.10 Cytotoxicity of the PXS sheet, electrospun fibre mat PXS/PVA and PXS/PVA-washed, determined by measure the release of LDH after two days of culture. The positive control group was PLLA electrospun fibre. The percentages of dead cells in test material's group were not significantly different from either the negative control (medium alone) or positive control (PLLA) groups.

7.2.4. Cytocompatibility *in vitro*

In vitro cytocompatibility test were conducted through culturing SNL cells in culture medium with different test samples, visual examination did not show considerable cytotoxicity. Fig. 7.9 showed the healthy cell morphology in all test groups. After two days culture, the number of cells increased from 2,000 to over 4000 and almost covered the surfaces of each well. Quantitative LDH measurements confirmed that the cytocompatibility of test samples PXS sheet, PXS/PVA fibre mat and PXS/PVA-washed fibre mat were as good as the two control groups (free culture medium and PLLA fibre mat), with no significant differences detected in cell death percentage between the test sample groups with the two control groups (Fig. 7.10).

7.3. Conclusions

The fabrication process of elastic fibrous mats from PXS and PVA using the core/shell electrospinning technique has been established in this work. PVA with M_w of 89,000–98,000 g/mol was the best one to produce stable PXS/PVA core/shell fibres with the satisfactory characteristics. After crosslinking treatment of PXS core, the PVA shell could be washed off by water, resulting in a porous elastic scaffold of PXS. Under the dry testing condition, the resultant PXS/PVA fibrous scaffolds possessed a higher UTS value than both the PXS solid sheets and the PVA fibre mats, and

the rupture strain of PXS/PVA-washed fibre mat was similar to that of the PXS sheet but much higher than that of PVA fibre mat. The Young's modulus of the PXS/PVA-washed fibrous scaffolds was also higher than that of the PXS sheet but lower than that of the PVA fibre mat. Under the *in vivo* physiological conditions, the wet fibre mats were much softer and had remarkably higher rupture elongation than their dry counterparts. The washed PXS/PVA fibre mats had the lowest Young's modulus (1.1 ± 0.2 MPa) and the highest rupture elongation (76 ± 8 %), significantly higher than that of the PXS sheet. An *In vitro* evaluation has demonstrated that the cytocompatibility of PXS/PVA core/shell fibres with or without washing were similar to both negative and positive controls. Hence, the washed PXS/PVA electrospun porous mats offer an opportunity to develop new scaffolds for soft tissue engineering, especially for applications requiring high extensibility, such as neurological applications. For other applications, such as muscle tissue engineering, the same mats are also very suitable because they offer reliable performance with cyclic loading under hydrated conditions. This could be controlled by finer adjustments to PXS/PVA mole ratio or cross-link time

CHAPTER EIGHT

SUMMARY AND FUTURE WORK

The synthesis of two poly(polyol sebacate) members, PGS and PXS elastomers, has been thoroughly explored in this research. The microstructure, mechanical properties and degradation rates of the polymers have been thoroughly characterised. Most importantly, new elastomeric PXS/PVA fibrous scaffolds have been developed using the core/shell electrospinning technique, which have shown to be promising candidates for applications of soft tissue engineering. However, it is also clear that to achieve clinical applications of the PPS-based materials further work must be carried out.

This chapter first summaries the major results of this project described in Chapters 4-7. In the second part of this chapter, a series of recommended topics for future work is presented.

8.1. Summary

8.1.1. Synthesis, characterisation and properties of PGS

Some of the major drawbacks of PGS include poor reproducibility of properties and the unacceptable toxicity of very soft PGS elastomers. To identify the mechanism of these problems, PGS was synthesized at different temperatures and for varying times, and detail characterisation work (determination of carboxylic acid reaction percentages and carbon NMR analysis) was carried out for the first time with the PGS system. This helped to explain the intrinsic factors influence the material properties, so they can be controlled for various tissue engineering applications. The most important conclusions can be drawn from the work, as list as follows:

- 1) It was first time found that the co-evaporation of glycerol with water was a major cause of the loss of reproducibility of the elastomer synthesis and this was more significant at higher reaction temperatures.
- 2) The polymer microstructure was analysed by NMR and all twelve acylglyceride ¹³C-signals as well as two small extra peaks of the residual glycerol were observed in the prepolymer and for the PGS gel, with glyceride moieties characterized by NMR for the first time. This

characterisation work propels the understanding the polymer reaction in microstructure level and helps to control synthesis and develop the PGS-copolymer in future work.

- 3) The modulus and ultimate tensile strength of the gel increased with longer cure times and at higher cure temperatures while the elongation to break decreased, and this was successfully interpreted in terms of network theory.
- 4) The cell viability of mouse fibroblasts for PGS samples were significantly improved through increasing the reaction percentage of carboxylic acid in synthesised PGS.

This work has been published in Polymer International [217].

8.1.2. A comparative study of PXS and PGS: mechanical properties, biodegradation and cytocompatibility

Although a slow degradation and satisfactory cytocompatibility can be achieved in PGS by increasing the crosslink density of the network, this PGS is brittle with significantly compromised elasticity. Using longer polyol monomers xylitol could be a potential approach to develop degradable elastomers with a satisfactory combination of flexibility and degradation rate. However, the longer polyols monomers have more hydroxyl group and the effect of the extra hydroxyl groups on hydrolysis of the PPS network was an open question and worth to investigation.

Therefore, the mechanical properties, degradation kinetics and biocompatibility of PXS have been systematically investigated in comparison with those of PGS. Under the condition of the same crosslinked density, the PXS elastomer networks have approximately twice the extensibility (elongation at break) of PGS, whilst PXS maintained its degradation rate. The cell compatibility of PXS at higher reaction percentage of carboxylic acid groups was better and it is comparable to PGS and control materials. These observations were attributed to PXS has longer and more orientable xylitol monomers and a steric hindrance effect of the side chains, i.e. the large-sized hydroxyl groups can shield ester bonds from the attack of water molecules. Hence, increase chain length by using polyols of more than three hydroxyl groups is a feasible way to obtain PPPS elastomers with enhanced flexibility while slower degradation rate. This work has been published in Biomedical Materials [152].

8.1.3. Enzymatic and oxidative degradation of PPS

There is only limited knowledge of the degradation mechanisms of PPS elastomers and how the fast degradation rate can be controlled, especially no oxidative degradation study of PPS. Hence, Chapter 6 was devoted to explore the enzymatic and oxidative degradation mechanisms of these polyesters, using biochemical conditions similar to those occurring *in vivo*. To this end, PGS and PXS of different crosslink densities were incubated *in vitro* under physiological conditions in tissue culture media supplemented with either a biodegrading enzyme (esterase), an oxidant species ($\text{FeSO}_4/\text{H}_2\text{O}_2$), an oxidant generating enzyme (xanthine oxidase and xanthine (XO/X)), or combinations of these ($\text{FeSO}_4/\text{H}_2\text{O}_2$ and esterase, or (v) XO/X and esterase), based on their independent effects on polymer degradation.

It was found that degradation kinetics of both PGS and PXS samples were primarily determined by the degree of crosslink density. The new phenomena has been discovered for the first time in PPS system that esterase and $\text{FeSO}_4/\text{H}_2\text{O}_2$ accelerated the degradation of both polymers, by promoting hydrolysis and free radical degradation, although this action was not affected by the presence of XO/X. Degradation of PGS and PXS is primarily mediated by the action of esterase, with free radical oxidation playing a secondary role, suggesting that both could synergistically affect the biodegradability of biomaterial implants, under more complex biological conditions. Hence, we recommend that the crosslink density of PPS samples should be carefully considered when choosing alternative materials for mass loss analysis, if using this technique. In addition, both enzymatic and oxidative degradation tests are of value *in vitro* investigation to predict the degradation profile of a biomaterial *in vivo*. This work has been published in the Journal of biomaterials applications [218].

8.1.4. Elastomeric PXS/PVA fibrous sheets produced by core/shell electrospinning: fabrication, characterisation and properties

PXS elastomeric fibrous scaffold for soft tissue engineering has been successfully fabricated through a new process using the core/shell electrospinning technique. The water dissolvable PVA material was used for shell material for the first time and the optimal fabrication conditions were established, with PVA of an average molecular weight (M_w) of 89,000–98,000 g/mol producing the most satisfactory PXS/PVA core/shell fibres. After heat treatment to crosslink the PXS core, the PVA shell could be washed off with water, resulting in a porous elastomeric scaffold of PXS fibres. Unlike previous research using organic solvent to remove PLLA shell, this unique process design

has avoided that the organic solvent damaged the core polymer network and cause brittle fibre during PLLA shell removing [115]. The novel elastomeric fibrous sheets have demonstrated remarkable mechanical properties and biocompatibility:

1) Under aqueous conditions, both PXS/PVA and PXS fibre mats were very soft and had remarkably high rupture elongation which could indicate a good performance *in vivo* for soft tissue applications. The PXS fibre mats had very low Young's modulus (1.1 ± 0.2 MPa) and the high rupture elongation (76 ± 8 %), which was significantly higher than that of two dimensional PXS sheets.

2) Meanwhile, the materials showed good cytocompatibility (similar to control groups culture medium and PLLA material) in direct contact with cell monolayers, under tissue culture conditions.

The combined mechanical characteristics and cytocompatibility therefore make the newly developed porous PXS scaffolds very promising for application in soft tissue engineering. They are likely to be used as implants for lung and intestine repair.

8.2. Limitations

The Mass loss method was used to compare the degradation rate of the PPS materials; however the degradation rate is influenced by the crosslink density, original weight and surface area of the samples. Therefore, the degradation rate obtained in this study is difficult to exactly compare with the previous results produced by other research groups. Thus, it is recommended to set up a sample standard of PPS materials for mass loss analysis, to enable comparison of the results from different research groups in future.

Although the porous PXS network has been studied *in vitro* and presents good cytocompatibility, its performance *in vivo* has not yet been characterized, and is considered beyond the scope of this thesis. The source of material that we used for our applications is also considered only suitable for experimental applications, and would require further approval for animal studies. *In vivo* testing of the porous PXS networks remains an important step toward determining whether it is a good candidate for specific medical applications.

8.3. Future Work

8.3.1. Developing PPS-based copolymers

Although increasing the crosslink density can slow down the degradation rate and improve the cytocompatibility of PPS elastomers, the elasticity is always compromised at the same time. Designing and synthesising new PPS-based copolymers can be a feasible way to achieve a balance between degradation rate and elasticity, and synthesis with block copolymers of poly(ϵ -caprolactone), poly(lactic acid), and polyhydroxyalkanoates are recommended.

Previous research has involved development of poly(glycerol sebacate-co-lactic acid) (PGS-co-LA)[114], however the polymerization kinetics of lactic acid are relatively slow, and the crosslinking kinetics of PGS-co-LA copolymer are also markedly slower than PGS [209]. So, one interesting research direction would be to improve the efficiency of synthesis routes for PGS-co-LA. For example, PGS prepolymer (poly(sebacoyl diglyceride)) contains more free hydroxyl groups, so can be synthesised by an epoxide ring-opening reaction between diglycidyl and sebacic acid [180]. The PGS prepolymer can then be used to react with lactic acid to synthesis PGS-co-LA. Through this process, the reaction kinetics may be faster, achieving a lower crosslink density than PGS-co-LA synthesised from lactic acid reacting with traditional polymerized PGS, since this has many polymer branch chains [1]. In addition, it is also recommended to use catalyst in the synthesis procedure of PGS-LA such as tin(II) bis-2-ethylhexanoic acid, which has been used as catalyst in PLA synthesis due to its low toxicity, FDA approval, and high catalytic activity[219].

8.3.2. Surface modification of PPS

Surface chemistry of a biomaterial is important because it can significantly influence how cells attach and spread out on a substrate, before they start to proliferate. However, there is very little evidence of the surface interactions between the PPS and cells or tissue. While the mechanical properties of PPS are highly adjustable and potentially suitable for many soft tissue engineering applications, it is essential to conduct surface modification work for PPS to meet specific requirements of the cell-material interface. There are some surface modification techniques that can be used to modify the surface properties in PPS materials : (1) morphological modification (i.e. coatings to change the porosity, roughness and nano-structure of the surface and encourage tissue adhesion and ingrowth); (2) chemical modifications (such as grafting functional groups, to reduce protein adsorption and cell adhesion for vascular applications, or crosslinking polymeric surface to

decrease the surface permeability may decrease the degradation rate); (3) Bioactive modifications through immobilizing biomolecules (specific peptides or growth factors) on PPS surface to enhance cell adhesion, cell growth and signalling.

8.3.3. Improvement of the PVA/PXS electrospun scaffolds

In this project, core-shell electrospun PVA shells were rinsed in water, allowing it to fuse together after immersion in water. If PVA could be crosslinked, the PVA/PXS fibres could maintain better fibrous structures in wet conditions [220]. Researchers have developed many PVA crosslinking methods, including physical methods, such as heat and radiation, and treatment with chemical agents including glutaraldehyde, glyoxal and boric acid. Amongst these methods, glutaraldehyde vapour phase exposure to spun fibre mats has been a promising method because it has little or no cytotoxic effect, and crosslinking of PVA can be easily controlled by the exposure time [68]. Therefore, glutaraldehyde vapour treatment could be a possible step in future to develop PVA/PXS fibres which can maintain the structure in wet state. Unfortunately, glutaraldehyde is a potent carcinogen, so regulatory approval of materials treated with this method may be hard to get.

In addition, scaffolds should provide similar structures to natural tissue, to guide cells and tissue regeneration in three dimensions. Aligned textures are currently favoured in many tissue engineering applications for cell guidance, such as in myocardial and neural tissue [70]. Aligned nano-structure can be fabricated using modification of the same electrospinning technique. Therefore, it is necessary to fabricate aligned and random PVA/PXS fibre mats, and compare their mechanical properties, to see how they affect cell morphology and differentiation.

8.3.4. *In vitro* and *in vivo* studies

One vital goal of a scaffold is to support specific types of cells to proliferate on it, and assist the regeneration of impaired or injured tissues, thus it is important to conduct *in vitro* investigation with different cell types as the first step. This reduces the cost of clinical studies and decreasing the need for animal usage, although, clinical studies are still required for future medical applications.

From the research of this project, the fabricated PPS fibrous scaffold has potential to be applied to many soft tissue engineering applications. Therefore, it is necessary to investigate the ability of the scaffolds to support the adhesion and migration of specific cell types such as enteric neural crest

progenitor cells, Schwann cells and neural stem cell for neural tissue engineering [63, 70, 73] as well as cardiomyocytes, smooth muscle cells and endothelial progenitor cells for cardiac tissue engineering [18]. In addition, the scaffold should maintain porous structure and provide sufficient mechanical strength in short term to for cells to grow in and form their own matrix, which applies to all tissues. Thus, it is necessary to study the degradation of the scaffolds *in vitro* and test the changes of their structure and mechanical properties during degradation.

In vivo assessment of fabricated scaffolds is an important step toward medical applications. Compared to *in vitro* tests, scaffolds exposed to *in vivo* environments are subjected to much more complex mechanical stresses from around native tissue, and more influenced by tissue fluids and enzymes. Therefore, the kinetics of scaffold degradation *in vitro* and *in vivo* are likely different and it is important to study how the mechanical properties of the present scaffold changes *in vivo* during degradation.

8.4. Conclusions

This research work has explored the methods to optimize the properties of PPS materials, and newly fabricated electrospun PXS elastic scaffolds. It has proven that tuneable mechanical properties, better cytocompatibility and slower degradation rate of the materials are achievable by controlling synthetic conditions and modifying molecular structures (using different polyol monomers). The newly fabricated elastomeric PXS scaffold provides significantly improved mechanical properties and more favourable structure than two dimensional PXS sheet and this scaffold is a promising candidate to be applied in soft tissue engineering. Further work will likely focus on optimizing *in vitro* cell cultures on the scaffolds, for soft tissue types (e.g. neural progenitor cells), towards *in vivo* investigations of the material as an implantable material in soft tissue repair.

REFERENCES

- [1] Wang Y, Ameer GA, Sheppard BJ, Langer R. A tough biodegradable elastomer. *Nature biotechnology*. 2002;20:602-6.
- [2] Bettinger CJ. Biodegradable Elastomers for Tissue Engineering and Cell–Biomaterial Interactions. *Macromolecular Bioscience*. 2011;11:467-82.
- [3] Langer R, Vacanti J. Tissue engineering. *Science*. 1993;260:920-6.
- [4] Niklason LE, Gao J, Abbott WM, Hirschi KK, Houser S, Marini R, et al. Functional Arteries Grown in Vitro. *Science*. 1999;284:489-93.
- [5] Yang J, Webb AR, Pickerill SJ, Hageman G, Ameer GA. Synthesis and evaluation of poly(diols citrate) biodegradable elastomers. *Biomaterials*. 2006;27:1889-98.
- [6] Yang J, Webb A, Ameer G. Novel Citric Acid-Based Biodegradable Elastomers for Tissue Engineering. *Advanced Materials*. 2004;16:511-6.
- [7] Chen Q-Z, Bismarck A, Hansen U, Junaid S, Tran MQ, Harding SE, et al. Characterisation of a soft elastomer poly(glycerol sebacate) designed to match the mechanical properties of myocardial tissue. *Biomaterials*. 2008;29:47-57.
- [8] Bettinger C, Weinberg E, Kulig K, Vacanti J, Wang Y, Borenstein J, et al. Three-Dimensional Microfluidic Tissue-Engineering Scaffolds Using a Flexible Biodegradable Polymer. *Advanced Materials*. 2006;18:165-9.
- [9] Zhang L-Q, Shi R. Novel Elastomers for Biomedical Applications. *Current Topics in Elastomers Research*: CRC Press; 2008.
- [10] Stankus JJ, Guan J, Wagner WR. Elastomers, Biodegradable. *Encyclopedia of Biomaterials and Biomedical Engineering*. 2004:484 - 94.
- [11] Mark JE, Erman B, Eirich FR. *Science and Technology of Rubber*: San Diego : Academic Press 2005.
- [12] Webb AR, Yang J, Ameer GA. Biodegradable polyester elastomers in tissue engineering. *Expert Opinion on Biological Therapy*. 2004;4:801-12.
- [13] Zdrahala RJ, Zdrahala IJ. Biomedical Applications of Polyurethanes: A Review of Past Promises, Present Realities, and a Vibrant Future. *Journal of Biomaterials Applications*. 1999;14:67-90.
- [14] Martina M, Hutmacher DW. Biodegradable polymers applied in tissue engineering research: a review. *Polym Int*. 2007;56:145-57.
- [15] Nugent HM, Edelman ER. Tissue Engineering Therapy for Cardiovascular Disease. *Circ Res*. 2003;92:1068-78.
- [16] http://www.hopkinsmedicine.org/news/media/releases/rubber_gloves_born_and_now_banished_at_johns_hopkins. retrieved on 22 March 2011.
- [17] Yoda R. Elastomers for biomedical applications. *Journal of Biomaterials Science-Polymer Edition*. 1998;9:561-626.
- [18] Chen QZ, Harding SE, Ali NN, Lyon AR, Boccaccini AR. Biomaterials in cardiac tissue engineering: Ten years of research survey. *Mat Sci Eng R*. 2008;59:1-37.
- [19] Chen G-Q, Wu Q. The application of polyhydroxyalkanoates as tissue engineering materials. *Biomaterials*. 2005;26:6565-78.
- [20] Martin DP, Williams SF. Medical applications of poly-4-hydroxybutyrate: a strong flexible absorbable biomaterial. *Biochemical Engineering Journal*. 2003;16:97-105.
- [21] Shi R, Chen DF, Liu QY, Wu Y, Xu XC, Zhang LQ, et al. Recent Advances in Synthetic Bioelastomers. *International Journal of Molecular Sciences*. 2009;10:4223-56.
- [22] Lendlein A, Langer R. Biodegradable, Elastic Shape-Memory Polymers for Potential Biomedical Applications. *Science*. 2002;296:1673-6.
- [23] Bruggeman JP, de Bruin BJ, Bettinger CJ, Langer R. Biodegradable poly(polyol sebacate) polymers. *Biomaterials*. 2008;29:4726-35.
- [24] Bruggeman JP, Bettinger CJ, Nijst CL, Kohane DS, Langer R. Biodegradable Xylitol-Based Polymers. *Advanced Materials*. 2008;20:1922-7.

- [25] Nijst CLE, Bruggeman JP, Karp JM, Ferreira L, Zumbuehl A, Bettinger CJ, et al. Synthesis and Characterization of Photocurable Elastomers from Poly(glycerol-co-sebacate). *Biomacromolecules*. 2007;8:3067-73.
- [26] Yang J, Zhang Y, Gautam S, Liu L, Dey J, Chen W, et al. Development of aliphatic biodegradable photoluminescent polymers. *P Natl Acad Sci USA*. 2009;106:10086-91.
- [27] Lei LJ, Ding T, Shi R, Liu QY, Zhang LQ, Chen DF, et al. Synthesis, characterization and in vitro degradation of a novel degradable poly((1,2-propanediol-sebacate)-citrate) bioelastomer. *Polymer Degradation and Stability*. 2007;92:389-96.
- [28] Tran RT, Thevenot P, Gyawali D, Chiao J-C, Tang L, Yang J. Synthesis and characterization of a biodegradable elastomer featuring a dual crosslinking mechanism. *Soft Matter*. 2010;6:2449-61.
- [29] Gyawali D, Nair P, Zhang Y, Tran RT, Zhang C, Samchukov M, et al. Citric acid-derived in situ crosslinkable biodegradable polymers for cell delivery. *Biomaterials*. 2010;31:9092-105.
- [30] Younes HM, Bravo-Grimaldo E, Amsden BG. Synthesis, characterization and in vitro degradation of a biodegradable elastomer. *Biomaterials*. 2004;25:5261-9.
- [31] Amsden BG, Misra G, Gu F, Younes HM. Synthesis and characterization of a photo-cross-linked biodegradable elastomer. *Biomacromolecules*. 2004;5:2479-86.
- [32] Bettinger CJ, Bruggeman JP, Borenstein JT, Langer R. In vitro and in vivo degradation of poly(1,3-diamino-2-hydroxypropane-co-polyol sebacate) elastomers. *J Biomed Mater Res A*. 2009;91A:1077-88.
- [33] Dausse Y, Grossin L, Miralles G, Pelletier S, Mainard D, Hubert P, et al. Cartilage repair using new polysaccharidic biomaterials: macroscopic, histological and biochemical approaches in a rat model of cartilage defect. *Osteoarthritis and Cartilage*. 2003;11:16-28.
- [34] Augst AD, Kong HJ, Mooney DJ. Alginate Hydrogels as Biomaterials. *Macromolecular Bioscience*. 2006;6:623-33.
- [35] Seal BL, Otero TC, Panitch A. Polymeric biomaterials for tissue and organ regeneration. *Mat Sci Eng R*. 2001;34:147-230.
- [36] Grover CN, Cameron RE, Best SM. Investigating the morphological, mechanical and degradation properties of scaffolds comprising collagen, gelatin and elastin for use in soft tissue engineering. *Journal of the Mechanical Behavior of Biomedical Materials*. 2012;10:62-74.
- [37] William TB, Karthik N, Elliot LC. Elastin. In: Wnek GE, Bowlin GL, editors. *Encyclopedia of Biomaterials and Biomedical Engineering*. New York Informa Healthcare; 2008. p. 891-6.
- [38] Nettles DL, Chilkoti A, Setton LA. Applications of elastin-like polypeptides in tissue engineering. *Advanced Drug Delivery Reviews*. 2010;62:1479-85.
- [39] Dandu R, Von Cresce A, Briber R, Dowell P, Cappello J, Ghandehari H. Silk-elastinlike protein polymer hydrogels: Influence of monomer sequence on physicochemical properties. *Polymer*. 2009;50:366-74.
- [40] Freier T. Biopolyesters in tissue engineering applications. *Polymers for Regenerative Medicine* 2006. p. 1-61.
- [41] Lee HB, Quach H, Berry DB, Stith WJ. CHARACTERISTICS OF AN IMPLANTABLE ELASTOMER - FINGER JOINT PROSTHESIS APPLICATION. *Acs Symposium Series*. 1984;256:99-109.
- [42] Wang YD, Ameer GA, Sheppard BJ, Langer R. A tough biodegradable elastomer. *Nature Biotechnology*. 2002;20:602-6.
- [43] Shewry PR, Tatham AS, Bailey AJ, Ebooks Corporation. *Elastomeric proteins structures, biomechanical properties, and biological roles*. Cambridge, UK; New York, NY: Cambridge University Press; Royal Society; 2003.
- [44] Siriwardane ML, Pfister BJ. Engineering Three-dimensional Nervous Tissue Constructs Based on Fiber-Gel Substrates. 2010 IEEE 36th Annual Northeast Bioengineering Conference. 2010.
- [45] Du C, Cui FZ, Zhu XD, de Groot K. Three-dimensional nano-HAp/collagen matrix loading with osteogenic cells in organ culture. *Journal of Biomedical Materials Research*. 1999;44:407-15.
- [46] Sittlinger M, Huttmacher DW, Risbud MV. Current strategies for cell delivery in cartilage and bone regeneration. *Current Opinion in Biotechnology*. 2004;15:411-8.
- [47] Raghunath J, Rollo J, Sales KM, Butler PE, Seifalian AM. Biomaterials and scaffold design: key to tissue-engineering cartilage. *Biotechnology and Applied Biochemistry*. 2007;46:73-84.

- [48] Balakrishnan B, Mohanty M, Umashankar PR, Jayakrishnan A. Evaluation of an in situ forming hydrogel wound dressing based on oxidized alginate and gelatin. *Biomaterials*. 2005;26:6335-42.
- [49] Hunt N, Grover L. Cell encapsulation using biopolymer gels for regenerative medicine. *Biotechnology Letters*. 2010;32:733-42.
- [50] Yu J, Gu Y, Du KT, Mihardja S, Sievers RE, Lee RJ. The effect of injected RGD modified alginate on angiogenesis and left ventricular function in a chronic rat infarct model. *Biomaterials*. 2009;30:751-6.
- [51] Zimmermann W-H, Melnychenko I, Eschenhagen T. Engineered heart tissue for regeneration of diseased hearts. *Biomaterials*. 2004;25:1639-47.
- [52] Miura Y, Akimoto T, Yagi K. Liver Functions in Hepatocytes Entrapped within Calcium Alginate. *Annals of the New York Academy of Sciences*. 1988;542:521-32.
- [53] Hashimoto T, Suzuki Y, Kitada M, Kataoka K, Wu S, Suzuki K, et al. Peripheral nerve regeneration through alginate gel: analysis of early outgrowth and late increase in diameter of regenerating axons. *Experimental Brain Research*. 2002;146:356-68.
- [54] Vacanti. CA, Bonassar. LJ, J.P.Vacanti. In: Lanza. RP, Langer. R, Vacanti. JP, editors. *Principles of Tissue Engineering*. 2nd ed. California: Academic Press; 2000. p. 671–82.
- [55] Callister WD. *Materials science and engineering: an introduction*. 7th edn ed. New York: John Wiley and Sons; 2007.
- [56] Barrett DG, Yousaf MN. Design and Applications of Biodegradable Polyester Tissue Scaffolds Based on Endogenous Monomers Found in Human Metabolism. *Molecules*. 2009;14:4022-50.
- [57] Gorna K, Gogolewski S. novel biodegradable polyurethane for biomedical applications. In: Chandra Mauli Agrawal, Jack E. Parr, Lin ST, editors. *Synthetic bioabsorbable polymers for implants*. West Conshohochen, PA, USA: ASTM International; 2000. p. 39.
- [58] Zong X, Bien H, Chung C-Y, Yin L, Fang D, Hsiao BS, et al. Electrospun fine-textured scaffolds for heart tissue constructs. *Biomaterials*. 2005;26:5330-8.
- [59] Patel A, Gaharwar AK, Iviglia G, Zhang H, Mukundan S, Mihaila SM, et al. Highly elastomeric poly(glycerol sebacate)-co-poly(ethylene glycol) amphiphilic block copolymers. *Biomaterials*. 2013;34:3970-83.
- [60] Gosline J, Lillie M, Carrington E, Guerette P, Ortlepp C, Savage K. Elastic proteins: biological roles and mechanical properties. *Philosophical Transactions of the Royal Society of London Series B: Biological Sciences*. 2002;357:121-32.
- [61] Isenburg JC, Simionescu DT, Vyavahare NR. Elastin stabilization in cardiovascular implants: improved resistance to enzymatic degradation by treatment with tannic acid. *Biomaterials*. 2004;25:3293-302.
- [62] Freed LE, Engelmayr GC, Borenstein JT, Moutos FT, Guilak F. Advanced Material Strategies for Tissue Engineering Scaffolds. *Advanced Materials*. 2009;21:3410-8.
- [63] Xu B, Rollo B, Stamp LA, Zhang D, Fang X, Newgreen DF, et al. Non-linear elasticity of core/shell spun PGS/PLLA fibres and their effect on cell proliferation. *Biomaterials*. 2013;34:6306-17.
- [64] Sahu AK, Selvarani G, Pitchumani S, Sridhar P, Shukla AK, Narayanan N, et al. PVA-PSSA Membrane with Interpenetrating Networks and its Methanol Crossover Mitigating Effect in DMFCs. *Journal of The Electrochemical Society*. 2008;155:B686-B95.
- [65] Chiono V, Sartori S, Rechichi A, Tonda-Turo C, Vozzi G, Vozzi F, et al. Poly(ester urethane) Guides for Peripheral Nerve Regeneration. *Macromolecular Bioscience*. 2011;11:245-56.
- [66] Xiahong Wang, Tongkui Cui, Yongnian Yan, Renji Zhang. Peroneal Nerve Regeneration Using a Unique Bilayer Polyurethane-collagen Guide Conduit. *Journal of Bioactive and Compatible Polymers*. 2009;24:109-27.
- [67] Ratner BD, Hoffman AS, Schoen FJ, Lemons JE. *Biomaterials Science : An Introduction to Materials in Medicine*. 2 ed. Burlington: Elsevier Science; 2004.
- [68] Destaye AG, Lin C-K, Lee C-K. Glutaraldehyde Vapor Cross-linked Nanofibrous PVA Mat with in Situ Formed Silver Nanoparticles. *ACS Applied Materials & Interfaces*. 2013;5:4745-52.
- [69] Borkenhagen M, Stoll RC, Neuenschwander P, Suter UW, Aebischer P. In vivo performance of a new biodegradable polyester urethane system used as a nerve guidance channel. *Biomaterials*. 1998;19:2155-65.

- [70] Yang F, Murugan R, Wang S, Ramakrishna S. Electrospinning of nano/micro scale poly(l-lactic acid) aligned fibers and their potential in neural tissue engineering. *Biomaterials*. 2005;26:2603-10.
- [71] Roach P, Eglin D, Rohde K, Perry C. Modern biomaterials: a review—bulk properties and implications of surface modifications. *Journal of Materials Science: Materials in Medicine*. 2007;18:1263-77.
- [72] Yu TT, Shoichet MS. Guided cell adhesion and outgrowth in peptide-modified channels for neural tissue engineering. *Biomaterials*. 2005;26:1507-14.
- [73] Gupta D, Venugopal J, Prabhakaran MP, Dev VRG, Low S, Choon AT, et al. Aligned and random nanofibrous substrate for the in vitro culture of Schwann cells for neural tissue engineering. *Acta Biomater*. 2009;5:2560-9.
- [74] Jiao Y-P, Cui F-Z. Surface modification of polyester biomaterials for tissue engineering. *Biomedical Materials*. 2007;2:R24-R37.
- [75] Son WK, Youk JH, Lee TS, Park WH. The effects of solution properties and polyelectrolyte on electrospinning of ultrafine poly(ethylene oxide) fibers. *Polymer*. 2004;45:2959-66.
- [76] Zeng J, Chen X, Xu X, Liang Q, Bian X, Yang L, et al. Ultrafine fibers electrospun from biodegradable polymers. *Journal of Applied Polymer Science*. 2003;89:1085-92.
- [77] Gross JH. *Mass Spectrometry: A Textbook*. Second ed. Heidelberg: Springer; 2004. p. 466-7.
- [78] Terrier P, Desmazières B, Tortajada J, Buchmann W. APCI/APPI for synthetic polymer analysis. *Mass Spectrometry Reviews*. 2011;30:854-74.
- [79] Giorgio M, Robert L. *Mass Spectrometry of Polymers*. In: Giorgio M, Maurizio SM, Filippo S, editors. *Matrix-Assisted Laser Desorption Ionization/ Mass Spectrometry of Polymers (MALDI-MS)*. Boca Raton, Florida: CRC Press; 2002.
- [80] Rufino AR, Biaggio FC, Santos JC, de Castro HF. Chemoenzymatic synthesis: a strategy to obtain xylitol monoesters. *Journal of Chemical Technology & Biotechnology*. 2009;84:957-60.
- [81] Pouillart P, Douillet O, Scappini B, Antonella G, Santini V, Grossi A, et al. Regioselective synthesis and biological profiling of butyric and phenylalkylcarboxylic esters derived from D-mannose and xylitol: influence of alkyl chain length on acute toxicity. *European Journal of Pharmaceutical Sciences*. 1999;7:93-106.
- [82] Klompmaker J, Veth RPH, Jansen HWB, Nielsen HKL, De Groot JH, Pennings AJ. Meniscal replacement using a porous polymer prosthesis: a preliminary study in the dog. *Biomaterials*. 1996;17:1169-75.
- [83] Adnani A, Basri M, Chaibakhsh N, Ahangar HA, Salleh AB, Rahman RNZRA, et al. Chemometric analysis of lipase-catalyzed synthesis of xylitol esters in a solvent-free system. *Carbohydrate Research*. 2011;346:472-9.
- [84] Angyal SJ, Le Fur R. The ¹³C-N.M.R. spectra of alditols. *Carbohydrate Research*. 1980;84:201-9.
- [85] Klompmaker J, Jansen HWB, Veth RPH, de Groot JH, Nijenhuis AJ, Pennings AJ. Porous polymer implant for repair of meniscal lesions: a preliminary study in dogs. *Biomaterials*. 1991;12:810-6.
- [86] Cramer JF, Dueholm MS, Nielsen SB, Pedersen DS, Wimmer R, Pedersen LH. Controlling the degree of esterification in lipase catalysed synthesis of xylitol fatty acid esters. *Enzyme and Microbial Technology*. 2007;41:346-52.
- [87] Gusntone FD. ¹³C-NMR studies of mono-, di- and tri-acylglycerols leading to qualitative and semiquantitative information about mixtures of these glycerol esters. *Chemistry and Physics of Lipids*. 1991;58:219-24.
- [88] Schnarr GW, Vyas DM, Szarek WA. Carbon-13 nuclear magnetic resonance spectra of acyclic carbohydrate derivatives : alditols, 1,2-bis(phenylhydrazones), and dithioacetals. *Journal of the Chemical Society, Perkin Transactions 1*. 1979:496-503.
- [89] Yoshimoto H, Shin YM, Terai H, Vacanti JP. A biodegradable nanofiber scaffold by electrospinning and its potential for bone tissue engineering. *Biomaterials*. 2003;24:2077-82.
- [90] Boland ED, Wnek GE, Simpson DG, Pawlowski KJ, Bowlin GL. Tailoring tissue engineering scaffolds using electrostatic processing techniques: a study of poly(glycolic acid) electrospinning. *Journal of Macromolecular Science, Part A*. 2001;38:1231-43.

- [91] Xu B, Li Y, Fang X, Thouas GA, Cook WD, Newgreen DF, et al. Mechanically tissue-like elastomeric polymers and their potential as a vehicle to deliver functional cardiomyocytes. *Journal of the Mechanical Behavior of Biomedical Materials*. 2013;28:354-65.
- [92] Bruins AP. Atmospheric-pressure-ionization mass spectrometry: II. Applications in pharmacy, biochemistry and general chemistry. *TrAC Trends in Analytical Chemistry*. 1994;13:81-90.
- [93] Byrdwell W. Atmospheric pressure chemical ionization mass spectrometry for analysis of lipids. *Lipids*. 2001;36:327-46.
- [94] Storey RF, Hickey TP. Degradable polyurethane networks based on d,l-lactide, glycolide, ϵ -caprolactone, and trimethylene carbonate homopolyester and copolyester triols. *Polymer*. 1994;35:830-8.
- [95] Stuckey DJ, Ishii H, Chen Q-Z, Boccaccini AR, Hansen U, Carr CA, et al. Magnetic Resonance Imaging Evaluation of Remodeling by Cardiac Elastomeric Tissue Scaffold Biomaterials in a Rat Model of Myocardial Infarction. *Tissue Engineering Part A*. 2010;16:3395-402.
- [96] Townsend-Nicholson A, Jayasinghe SN. Cell Electrospinning: a Unique Biotechnique for Encapsulating Living Organisms for Generating Active Biological Microthreads/Scaffolds. *Biomacromolecules*. 2006;7:3364-9.
- [97] Lloyd JA, Harron AF, McEwen CN. Combination Atmospheric Pressure Solids Analysis Probe and Desorption Electrospray Ionization Mass Spectrometry Ion Source. *Analytical Chemistry*. 2009;81:9158-62.
- [98] Wang YD, Kim YM, Langer R. In vivo degradation characteristics of poly(glycerol sebacate). *Journal of Biomedical Materials Research Part A*. 2003;66A:192-7.
- [99] Sundback CA, Shyu JY, Wang YD, Faquin WC, Langer RS, Vacanti JP, et al. Biocompatibility analysis of poly(glycerol sebacate) as a nerve guide material. *Biomaterials*. 2005;26:5454-64.
- [100] Motlagh D, Yang J, Lui KY, Webb AR, Ameer GA. Hemocompatibility evaluation of poly(glycerol-sebacate) in vitro for vascular tissue engineering. *Biomaterials*. 2006;27:4315-24.
- [101] Bettinger CJ, Weinberg EJ, Kulig KM, Vacanti JP, Wang Y, Borenstein JT, et al. Three-Dimensional Microfluidic Tissue-Engineering Scaffolds Using a Flexible Biodegradable Polymer. *Adv Mater*. 2005;18:165-9.
- [102] Bettinger CJ, Orrick B, Misra A, Langer R, Borenstein JT. Microfabrication of poly (glycerol-sebacate) for contact guidance applications. *Biomaterials*. 2006;27:2558-65.
- [103] Kemppainen JM, Hollister SJ. Tailoring the mechanical properties of 3D-designed poly(glycerol sebacate) scaffolds for cartilage applications. *J Biomed Mater Res A*. 2010;94:9-18.
- [104] Liu G, Hinch B, Beavis AD. Mechanisms for the Transport of α,ω -Dicarboxylates through the Mitochondrial Inner Membrane. *Journal of Biological Chemistry*. 1996;271:25338-44.
- [105] Grego AV, Mingrone G. Dicarboxylic acids, an alternate fuel substrate in parenteral nutrition: an update. *Clinical Nutrition*. 1995;14:143-8.
- [106] Tamada J, Langer R. THE DEVELOPMENT OF POLYANHYDRIDES FOR DRUG DELIVERY APPLICATIONS. *J Biomater Sci-Polym Ed*. 1992;3:315-53.
- [107] Wang Y, Ameer GA, Sheppard BJ, Langer R. A tough biodegradable elastomer. *Nat Biotechnol*. 2002;20:602-6.
- [108] Chen QZ, Ishii H, Thouas GA, Lyon AR, Wright JS, Blaker JJ, et al. An elastomeric patch derived from poly(glycerol sebacate) for delivery of embryonic stem cells to the heart. *Biomaterials*. 2010;31:3885-93.
- [109] Stockmayer W. Advancing fronts in chemistry. In: Twist S, editor. *High Polymers*. New York: Reinhold, ; 1945. p. 70.
- [110] Gao J, Crapo PM, Wang YD. Macroporous elastomeric scaffolds with extensive micropores for soft tissue engineering. *Tissue Eng*. 2006;12:917-25.
- [111] Wang Y, Kim YM, Langer R. In vivo degradation characteristics of poly(glycerol sebacate). *Journal of Biomedical Materials Research Part A*. 2003;66A:192-7.
- [112] Engelmayr GC, Cheng M, Bettinger CJ, Borenstein JT, Langer R, Freed LE. Accordion-like honeycombs for tissue engineering of cardiac anisotropy. *Nat Mater*. 2008;7:1003-10.
- [113] Chen QZ, Bismarck A, Hansen U, Junaid S, Tran MQ, Harding SE, et al. Characterisation of a soft elastomer poly(glycerol sebacate) designed to match the mechanical properties of myocardial tissue. *Biomaterials*. 2008;29:47-57.

- [114] Chen Q, Liang S, Thouas GA. Synthesis and characterisation of poly(glycerol sebacate)-co-lactic acid as surgical sealants. *Soft Matter*. 2011;7:6484-92.
- [115] Yi F, Lavan DA. Poly(glycerol sebacate) nanofiber scaffolds by core/shell electrospinning. *Macromolecular Bioscience*. 2008;8:803-6.
- [116] Stuckey DJ, Ishii H, Chen QZ, Boccaccini AR, Hansen U, Carr CA, et al. Magnetic Resonance Imaging Evaluation of Remodeling by Cardiac Elastomeric Tissue Scaffold Biomaterials in a Rat Model of Myocardial Infarction. *Tissue Engineering Part A*. 2010;16:3395-402.
- [117] Chen QZ, Jin LY, Cook WD, Mohn D, Lagerqvist EL, Elliott DA, et al. Elastomeric nanocomposites as cell delivery vehicles and cardiac support devices. *Soft Matter*. 2010;6:4715-26.
- [118] Liang SL, Cook WD, Thouas GA, Chen QZ. The mechanical characteristics and in vitro biocompatibility of poly(glycerol sebacate)-Bioglass (R) elastomeric composites. *Biomaterials*. 2010;31:8516-29.
- [119] Liang S-L, Cook WD, Thouas GA, Chen Q-Z. The mechanical characteristics and in vitro biocompatibility of poly(glycerol sebacate)-Bioglass® elastomeric composites. *Biomaterials*. 2010;31:8516-29.
- [120] Pomerantseva I, Krebs N, Hart A, Neville CM, Huang AY, Sundback CA. Degradation behavior of poly(glycerol sebacate). *J Biomed Mater Res A*. 2009;91A:1038-47.
- [121] Liang S-L, Yang X-Y, Fang X-Y, Cook WD, Thouas GA, Chen Q-Z. *In vitro* enzymatic degradation of poly(glycerol sebacate)-based materials. *Biomaterials*. 2011;32:8486-96.
- [122] Göpferich A. Mechanisms of polymer degradation and erosion. *Biomaterials*. 1996;17:103-14.
- [123] Sun Z-J, Chen C, Sun M-Z, Ai C-H, Lu X-L, Zheng Y-F, et al. The application of poly (glycerol-sebacate) as biodegradable drug carrier. *Biomaterials*. 2009;30:5209-14.
- [124] Chen Q-Z, Ishii H, Thouas GA, Lyon AR, Wright JS, Blaker JJ, et al. An elastomeric patch derived from poly(glycerol sebacate) for delivery of embryonic stem cells to the heart. *Biomaterials*. 2010;31:3885-93.
- [125] Sundback CA, Shyu JY, Wang Y, Faquin WC, Langer RS, Vacanti JP, et al. Biocompatibility analysis of poly(glycerol sebacate) as a nerve guide material. *Biomaterials*. 2005;26:5454-64.
- [126] Gao J, Ensley AE, Nerem RM, Wang Y. Poly(glycerol sebacate) supports the proliferation and phenotypic protein expression of primary baboon vascular cells. *J Biomed Mater Res A*. 2007;83A:1070-5.
- [127] Kakar S, Einhorn TA. Biology and enhancement of skeletal repair. In: Browner BD, Levine AM, Jupiter JB, Trafton PG, Krettek C, editors. *Skeletal Trauma: Basic Science, Management, and Reconstruction*. 4 ed. Philadelphia: Saunders, Elsevier; 2008. p. 33-50.
- [128] Jaafar I, Ammar M, Jedlicka S, Pearson R, Coulter J. Spectroscopic evaluation, thermal, and thermomechanical characterization of poly(glycerol-sebacate) with variations in curing temperatures and durations. *J Mater Sci*. 2010;45:2525-9.
- [129] Barrett DG, Luo W, Yousaf MN. Aliphatic polyester elastomers derived from erythritol and [small alpha],[small omega]-diacids. *Polymer Chemistry*. 2010;1:296-302.
- [130] Chen QZ, Yang XY, Li Y. A comparative study of in vitro enzymatic degradation of PXS and PGS. *RSC Advances*. 2012;Accepted.
- [131] Ifkovits JL, Padera RF, Burdick JA. Biodegradable and radically polymerized elastomers with enhanced processing capabilities. *Biomedical Materials*. 2008;3.
- [132] Chen Q, Jin L, Cook WD, Mohn D, Lagerqvist EL, Elliott DA, et al. Elastomeric nanocomposites as cell delivery vehicles and cardiac support devices. *Soft Matter*. 2010;6:4715-26.
- [133] Liu Q, Wu J, Tan T, Zhang L, Chen D, Tian W. Preparation, properties and cytotoxicity evaluation of a biodegradable polyester elastomer composite. *Polymer Degradation and Stability*. 2009;94:1427-35.
- [134] Wang Y, Kim YM, Langer R. In vivo degradation characteristics of poly(glycerol sebacate). *J Biomed Mater Res A*. 2003;66:192-7.
- [135] Stuckey DJ, Ishii H, Chen QZ, Boccaccini AR, Hansen U, Carr CA, et al. Magnetic resonance imaging evaluation of remodeling by cardiac elastomeric tissue scaffold biomaterials in a rat model of myocardial infarction. *Tissue Eng Part A*. 2010;16:3395-402.
- [136] Yang J, Webb AR, Ameer GA. Novel Citric Acid-Based Biodegradable Elastomers for Tissue Engineering. *Advanced Materials*. 2004;16:511-6.

- [137] Roeder R, Wolfe J, Lianakis N, Hinson T, Geddes LA, Obermiller J. Compliance, elastic modulus, and burst pressure of small-intestine submucosa (SIS), small-diameter vascular grafts. *J Biomed Mater Res.* 1999;47:65-70.
- [138] Bettinger CJ, Bruggeman JP, Borenstein JT, Langer RS. Amino alcohol-based degradable poly(ester amide) elastomers. *Biomaterials.* 2008;29:2315-25.
- [139] Daniel KD, Kim GY, Vassiliou CC, Jalali-Yazdi F, Langer R, Cima MJ. Multi-reservoir device for detecting a soluble cancer biomarker. *Lab on a Chip.* 2007;7:1288-93.
- [140] Pêgo AP, Grijpma DW, Feijen J. Enhanced mechanical properties of 1,3-trimethylene carbonate polymers and networks. *Polymer.* 2003;44:6495-504.
- [141] Hutmacher DW. Scaffolds in tissue engineering bone and cartilage. *Biomaterials.* 2000;21:2529-43.
- [142] Widmer MS, Mikos AG. Fabrication of Biodegradable Polymer Scaffolds for Tissue Engineering. In: Charles WP, Jr, Antonios GM, Larry VM, Langer RS, editors. *Frontiers in Tissue Engineering.* Oxford: Pergamon; 1998. p. 107-20.
- [143] Murphy MB, Mikos AG. Polymer scaffold fabrication. In: Robert L, Robert L, Joseph V, editors. *Principles of Tissue Engineering (Third Edition).* Burlington: Academic Press; 2007. p. 309-21.
- [144] Borenstein JT, Terai H, King KR, Weinberg EJ, Kaazempur-Mofrad MR, Vacanti JP. Microfabrication technology for vascularized tissue engineering. *Biomed Microdevices.* 2002;4:167-75.
- [145] Xu B, Li Y, Fang X, Thouas GA, Cook WD, Chen Q. Mechanically tissue-like elastomeric polymers and their potential as a vehicle to deliver functional cardiomyocytes. *Journal of the Mechanical Behavior of Biomedical Materials.*
- [146] Ifkovits JL, Devlin JJ, Eng G, Martens TP, Vunjak-Novakovic G, Burdick JA. Biodegradable Fibrous Scaffolds with Tunable Properties Formed from Photo-Cross-Linkable Poly(glycerol sebacate). *ACS Applied Materials & Interfaces.* 2009;1:1878-86.
- [147] Leong KF, Cheah CM, Chua CK. Solid freeform fabrication of three-dimensional scaffolds for engineering replacement tissues and organs. *Biomaterials.* 2003;24:2363-78.
- [148] Kemppainen JM, Hollister SJ. Tailoring the mechanical properties of 3D-designed poly(glycerol sebacate) scaffolds for cartilage applications. *J Biomed Mater Res A.* 2010;94A:9-18.
- [149] Zein I, Hutmacher DW, Tan KC, Teoh SH. Fused deposition modeling of novel scaffold architectures for tissue engineering applications. *Biomaterials.* 2002;23:1169-85.
- [150] Pretsch E, Bühlmann P, Badertscher M. *Structure Determination of Organic Compounds.* Fourth ed: Springer; 2009.
- [151] Bruggeman JP, Bettinger CJ, Langer R. Biodegradable xylitol-based elastomers: In vivo behavior and biocompatibility. *J Biomed Mater Res A.* 2010;95A:92-104.
- [152] Li Y, Huang W, Cook WD, Chen Q. A comparative study on poly(xylitol sebacate) and poly(glycerol sebacate): mechanical properties, biodegradation and cytocompatibility. *Biomedical Materials.* 2013;8.
- [153] Pinner SH. *A Practical Course in Polymer Chemistry.* Pergamon Press; 1961. p. 70-2.
- [154] Claridge TDW. *High-resolution NMR techniques in organic chemistry.* 2nd ed 2009.
- [155] Lv S, Dudek DM, Cao Y, Balamurali MM, Gosline J, Li H. Designed biomaterials to mimic the mechanical properties of muscles. *Nature.* 2010;465:69-73.
- [156] Veress AI, Gullberg GT, Weiss JA. Measurement of strain in the left ventricle during diastole with cine-MRI and deformable image registration. *Journal of Biomechanical Engineering-Transactions of the Asme.* 2005;127:1195-207.
- [157] Flory PJ. *Principles of polymer chemistry.* New York: Cornell University Press; 1953.
- [158] Chen Q-Z, Li Y, Jin L-Y, Quinn JMW, Komesaroff PA. A new sol-gel process for producing Na₂O-containing bioactive glass ceramics. *Acta Biomater.* 2010;6:4143-53.
- [159] Liang S-L, Yang X-Y, Fang X-Y, Cook WD, Thouas GA, Chen Q-Z. In vitro enzymatic degradation of poly(glycerol sebacate)-based materials. *Biomaterials.* 2011;32:8486-96.
- [160] Chapanian R, Tse MY, Pang SC, Amsden BG. The role of oxidation and enzymatic hydrolysis on the in vivo degradation of trimethylene carbonate based photocrosslinkable elastomers. *Biomaterials.* 2009;30:295-306.

- [161] Yavuz Y, Savas Koparal A, Bakir Ögütveren Ü. Phenol Removal through Chemical Oxidation using Fenton Reagent. *Chemical Engineering & Technology*. 2007;30:583-6.
- [162] Labow RS, Meek E, Santerre JP. The biodegradation of poly(urethane)s by the esterolytic activity of serine proteases and oxidative enzyme systems. *Journal of Biomaterials Science, Polymer Edition*. 1999;10:699-713.
- [163] Chen Q, Yang X, Li Y. A comparative study on in vitro enzymatic degradation of poly(glycerol sebacate) and poly(xylitol sebacate). *RSC Advances*. 2012.
- [164] Granger DN. Role of xanthine oxidase and granulocytes in ischemia-reperfusion injury. *American Journal of Physiology - Heart and Circulatory Physiology*. 1988;255:H1269-H75.
- [165] Williams DF, Mort E. Enzyme-accelerate hydrolysis of Polyglycolic acid *J Bioeng*. 1977;1:231-8.
- [166] Williams DF. Enzymic hydrolysis of polylactic acid. *Engineering in Medicine*. 1981;10:5-7.
- [167] Vunjak-Novakovic G, Radisic M, Obradovic B. Cardiac tissue engineering: effects of bioreactor flow environment on tissue constructs. *Journal of Chemical Technology and Biotechnology*. 2006;81:485-90.
- [168] Stochmayer WH. *Advancing Fronts in Chemistry*. In: Twiss SB, editor. *High Polymers*. New York: Reinhold Publishing Company; 1945. p. 61-73.
- [169] Rowland SP, Brannan MAF, Janssen HJ, Pittman PF. A kinetic analysis of the reactivities of the hydroxyl groups in formylation of the D-glucopyranosyl residues in dextrin. *Carbohydrate Research*. 1967;3:361-8.
- [170] Virna L, Sales M, Engelmayr GC, John A, Johnson, Gao J, Wang Y, Sacks MS, et al. Protein Precoating of Elastomeric Tissue-Engineering Scaffolds Increased Cellularity, Enhanced Extracellular Matrix Protein Production, and Differentially Regulated the Phenotypes of Circulating Endothelial Progenitor Cells. *Circulation*. 2007;116:55-63.
- [171] Christina F, R M, Kaazempur-Mofrad, Jeffrey B, P J, Vacanti, et al. Endothelialized Microvasculature Based on a Biodegradable Elastomer. *Tissue Eng*. 2005;11:302-9.
- [172] Liu Q, Tian M, Ding T, Shi R, Feng Y, Zhang L, et al. Preparation and characterization of a thermoplastic poly(glycerol sebacate) elastomer by two-step method. *Journal of Applied Polymer Science*. 2007;103:1412-9.
- [173] Ravichandran R, Venugopal JR, Sundarajan S, Mukherjee S, Ramakrishna S. Poly(Glycerol Sebacate)/Gelatin Core/Shell Fibrous Structure for Regeneration of Myocardial Infarction. *Tissue Engineering Part A*. 2011;17:1363-73.
- [174] Weast RC. *CRC handbook of chemistry and physics*. 1st Student ed. Boca Raton, FL: CRC Press; 1988.
- [175] Jordan CB, Hatch VO. Determination of Water in Glycols and Glycerol. *Analytical Chemistry*. 1950;22:177-9.
- [176] Nagata M, Kiyotsukuri T, Ibuki H, Tsutsumi N, Sakai W. Synthesis and enzymatic degradation of regular network aliphatic polyesters. *Reactive and Functional Polymers*. 1996;30:165-71.
- [177] Nagata M, Machida T, Sakai W, Tsutsumi N. Synthesis, characterization, and enzymatic degradation of network aliphatic copolyesters. *Journal of Polymer Science Part A: Polymer Chemistry*. 1999;37:2005-11.
- [178] Uyama H, Inada K, Kobayashi S. Regioselective polymerization of divinyl sebacate and triols using lipase catalyst. *Macromol Rapid Commun*. 1999;20:171-4.
- [179] Uyama H, Inada K, Kobayashi S. Regioselectivity Control in Lipase-Catalyzed Polymerization of Divinyl Sebacate and Triols. *Macromolecular Bioscience*. 2001;1:40-4.
- [180] You Z, Cao H, Gao J, Shin PH, Day BW, Wang Y. A functionalizable polyester with free hydroxyl groups and tunable physicochemical and biological properties. *Biomaterials*. 2010;31:3129-38.
- [181] Miller DR, Macosko CW. A New Derivation of Post Gel Properties of Network Polymers. *Macromolecules*. 1976;9:206-11.
- [182] Gunstone FD. ¹³C-NMR spectra of some synthetic glycerol esters alone and as mixtures. *Chemistry and Physics of Lipids*. 1990;56:195-9.
- [183] Gunstone FD. High-resolution ¹³C NMR spectra of long-chain acids, methyl esters, glycerol esters, wax esters, nitriles, amides, alcohols and acetates. *Chemistry and Physics of Lipids*. 1993;66:189-93.

- [184] Vlahov G. Improved quantitative ^{13}C nuclear magnetic resonance criteria for determination of grades of virgin olive oils. The normal ranges for diglycerides in olive oil. *Journal of the American Oil Chemists' Society*. 1996;73:1201-3.
- [185] Bain AD, Eaton DR, Hamielec AE, Mlekuz M, Sayer BG. Line broadening in the carbon-13 NMR spectra of crosslinked polymers. *Macromolecules*. 1989;22:3561-4.
- [186] Taylor GR, Darin SR. The tensile strength of elastomers. *Journal of Polymer Science*. 1955;17:511-25.
- [187] Chen QZ, Liang SL, Thouas GA. Synthesis and characterisation of poly(glycerol sebacate)-co-lactic acid as surgical sealants. *Soft Matter*. 2011;7:6484-92.
- [188] Chen Q-Z, Liang S-L, Wang J, Simon GP. Manipulation of mechanical compliance of elastomeric PGS by incorporation of halloysite nanotubes for soft tissue engineering applications. *Journal of the mechanical behavior of biomedical materials*. 2011;4:1805-18.
- [189] Bruggeman JP, de Bruin B-J, Bettinger CJ, Langer R. Biodegradable poly(polyol sebacate) polymers. *Biomaterials*. 2008;29:4726-35.
- [190] Koshy KT. Comparative stability of benzamide, salicylamide, and some N-substituted derivatives. *Journal of Pharmaceutical Sciences*. 1959;58:560-3.
- [191] Detar DF, Tenpas CJ. Calculations of steric hindrance in ester hydrolysis based on estimation of vanderwaals strain energies of alkanes. *Journal of the American Chemical Society*. 1976;98:4567-71.
- [192] Chen Q, Liang S, Thouas GA. Elastomeric biomaterials for tissue engineering. *Prog Polym Sci*. 2013;38:584-671.
- [193] Williams DF, Zhong SP. Biodeterioration/biodegradation of polymeric medical devices in situ. *International Biodeterioration & Biodegradation*. 1994;34:95-130.
- [194] Williams DF. Polymer Degradation in Biological Environments *Comprehensive Polymer Science*. 1989;6.
- [195] Schakenraad JM, Hardonk MJ, Feijen J, Molenaar I, Nieuwenhuis P. Enzymatic-activity toward poly(L-lactic acid) implants *Journal of Biomedical Materials Research*. 1990;24:529-45.
- [196] Smith R, Oliver C, Williams DF. The enzymatic degradation of polymers in vitro. *Journal of Biomedical Materials Research*. 1987;21:991-1003.
- [197] Smith R, Williams DF, Oliver C. The biodegradation of poly(ether urethanes). *Journal of Biomedical Materials Research*. 1987;21:1149-65.
- [198] Coleman JW. Nitric oxide in immunity and inflammation. *International Immunopharmacology*. 2001;1:1397-406.
- [199] Labow RS, Tang YW, McCloskey CB, Santerre JP. The effect of oxidation on the enzyme-catalyzed hydrolytic biodegradation of poly(urethane)s. *J Biomater Sci-Polym Ed*. 2002;13:651-65.
- [200] Ali SAM, Doherty PJ, Williams DF. The mechanisms of oxidative degradation of biomedical polymers by free radicals. *Journal of Applied Polymer Science*. 1994;51:1389-98.
- [201] Lee KH, Won CY, Chu CC, Gitsov I. Hydrolysis of biodegradable polymers by superoxide ions. *Journal of Polymer Science Part A: Polymer Chemistry*. 1999;37:3558-67.
- [202] McCord JM. Free radicals and inflammation: protection of synovial fluid by superoxide dismutase. *Science*. 1974;185:529-31.
- [203] Ali SAM, Doherty PJ, Williams DF. Mechanisms of polymer degradation in implantable devices. 2. Poly(DL-lactic acid). *Journal of Biomedical Materials Research*. 1993;27:1409-18.
- [204] Santerre JP, Labow RS, Duguay DG, Erfle D, Adams GA. Biodegradation evaluation of polyether and polyester-urethanes with oxidative and hydrolytic enzymes. *Journal of Biomedical Materials Research*. 1994;28:1187-99.
- [205] Bergmann F, Rimon S, Segal R. Effect of pH on the activity of eel esterase towards different substrates *Biochemical Journal*. 1958;68:493-9.
- [206] Ivanova T, Panaiotov I, Boury F, Proust JE, Benoit JP, Verger R. Hydrolysis kinetics of poly(D,L-lactide) monolayers spread on basic or acidic aqueous subphases. *Colloid Surf B-Biointerfaces*. 1997;8:217-25.
- [207] Li W-J, Laurencin CT, Cateson EJ, Tuan RS, Ko FK. Electrospun nanofibrous structure: A novel scaffold for tissue engineering. *Journal of Biomedical Materials Research*. 2002;60:613-21.

- [208] Pham QP, Sharma U, Mikos AG. Electrospinning of polymeric nanofibers for tissue engineering applications: A review. *Tissue Eng.* 2006;12:1197-211.
- [209] Chen Q, Liang S, Thouas GA. Elastomeric biomaterials for tissue engineering. *Prog Polym Sci.* 2013;38:581-671.
- [210] Yao L, Haas TW, Guiseppi-Elie A, Bowlin GL, Simpson DG, Wnek GE. Electrospinning and Stabilization of Fully Hydrolyzed Poly(Vinyl Alcohol) Fibers. *Chemistry of Materials.* 2003;15:1860-4.
- [211] Zhang C, Yuan X, Wu L, Han Y, Sheng J. Study on morphology of electrospun poly(vinyl alcohol) mats. *Eur Polym J.* 2005;41:423-32.
- [212] Zeng J, Aigner A, Czubyko F, Kissel T, Wendorff JH, Greiner A. Poly(vinyl alcohol) Nanofibers by Electrospinning as a Protein Delivery System and the Retardation of Enzyme Release by Additional Polymer Coatings. *Biomacromolecules.* 2005;6:1484-8.
- [213] Slaughter BV, Khurshid SS, Fisher OZ, Khademhosseini A, Peppas NA. Hydrogels in Regenerative Medicine. *Advanced Materials.* 2009;21:3307-29.
- [214] Kobayashi M, Toguchida J, Oka M. Development of poly(vinyl alcohol)-hydrogel (PVA-H) with a high water content for tendon injury repair. *The Journal of Hand Surgery: British & European Volume.* 2001;26:436-40.
- [215] Koski A, Yim K, Shivkumar S. Effect of molecular weight on fibrous PVA produced by electrospinning. *Mater Lett.* 2004;58:493-7.
- [216] Tacx JCJF, Schoffeleers HM, Brands AGM, Teuwen L. Dissolution behavior and solution properties of polyvinylalcohol as determined by viscometry and light scattering in DMSO, ethyleneglycol and water. *Polymer.* 2000;41:947-57.
- [217] Li Y, Cook WD, Moorhoff C, Huang W-C, Chen Q-Z. Synthesis, characterization and properties of biocompatible poly(glycerol sebacate) pre-polymer and gel. *Polym Int.* 2012;62:534-47.
- [218] Li Y, Thouas GA, Shi H, Chen Q. Enzymatic and oxidative degradation of poly(polyol sebacate). *Journal of Biomaterials Applications.* 2014;28:1138-50.
- [219] Garlotta D. A Literature Review of Poly(Lactic Acid). *Journal of Polymers and the Environment.* 2001;9:63-84.
- [220] Wang X, Chen X, Yoon K, Fang D, Hsiao BS, Chu B. High Flux Filtration Medium Based on Nanofibrous Substrate with Hydrophilic Nanocomposite Coating. *Environmental Science & Technology.* 2005;39:7684-91.

LIST OF PUBLICATIONS

1. Yuan Li, George A Thouas, Qizhi Chen, Biodegradable soft elastomers: synthesis/properties of materials and fabrication of scaffolds, RSC Advance, 2012, 2: 8229-8242
2. Yuan Li, Wayne D Cook, Cornelis Moorhoff, Wen-Chao Huang, Qi-Zhi Chen, Synthesis, characterization and properties of biocompatible poly(glycerol sebacate) pre-polymer and gel, Polymer International, 2012, 62:534-547
3. Yuan Li, Wen-Chao. Huang, Wayne D Cook, Qizhi Chen, A comparative study on poly (xylitol sebacate) and poly (glycerol sebacate): mechanical properties, biodegradation and cytocompatibility, Biomedical Materials, 2013, 8:035006.
4. Yuan Li, George A Thouas, Hanning Shi, Qizhi. Chen, Enzymatic and oxidative degradation of poly (polyol sebacate), Journal of biomaterials applications, 2013, 28, 1138-1150.
5. Bing. Xu, Yuan. Li, XiYa. Fang, George. A. Thouas, Wayne. D. Cook, Qizhi. Chen, Mechanically tissue-like elastomeric polymers and their potential as a vehicle to deliver functional cardiomyocytes. Journal of the Mechanical Behavior of Biomedical Materials, 2013, 28: 354-365.
6. Qizhi. Chen, XueYuan. Yang, Yuan. Li, A comparative study on in vitro enzymatic degradation of poly(glycerol sebacate) and poly(xylitol sebacate), RSC Advances, 2012, 2,4125-4134.